COPOLYMER HYDROGELS AS FULLY IMPLANTABLE OPTICAL BIOSENSORS: INVESTIGATING DESIGN PARADIGMS TO ACHIEVE LONG-TERM PRECLINICAL FUNCTION

A Dissertation

by

RACHEL MICHELLE UNRUH

Submitted to the Office of Graduate and Professional Studies of
Texas A&M University
in partial fulfillment of the requirements for the degree of

DOCTOR OF PHILOSOPHY

Chair of Committee,	Michael J. McShane
Committee Members,	Melissa A. Grunlan
	Daniel L. Alge
	David E. Bergbreiter
Head of Department,	Michael J. McShane

December 2017

Major Subject: Biomedical Engineering

ABSTRACT

Many diagnostic tests for disease management and overall health monitoring provide only an instantaneous measurement of the patient's state of health, leaving intermediate fluctuations in biochemistry levels undisclosed. Often, fluid samples are collected periodically and analyzed using *ex vivo* assays. Diabetes is a prime example of this enigma where knowledge of blood biochemistry fluctuation patterns in real time could allow patients to make more informed treatment and lifestyle decisions.

In recent years, hydrogels have been investigated as fully implantable biosensors by functionalizing them with enzymes and long-lifetime phosphors. However, maintaining a proper balance between enzyme stability and substrate transport when implanted has prevented preclinical proof of concept using this enzyme/phosphor sensing platform. This work explores the effect of matrix chemistry on enzyme stability and substrate transport and demonstrates the first noninvasive glucose tracking in porcine models by measuring luminescence lifetime instead of intensity.

The first aim of this work focuses on poly(HEMA-co-AAm) matrices, characterizing them as glucose sensors *in vitro* and *in vivo*. A copolymer hydrogel containing 75:25 HEMA:AAm responded to up to 167 mg/dL of glucose *in vitro* and tracked real-time porcine blood glucose levels two hours after implantation, the first-reported real-time glucose tracking measuring phosphorescence lifetime using a noninvasive interrogation method. The second aim of this work employs alternative monomers such as dimethylacrylamide, N-vinyl pyrrolidone, and a 3-

[Tris(trimethylsiloxy)silyl]propyl methacrylate to investigate enzyme stability and optimize substrate transport. These studies revealed that gels containing dimethylacrylamide and N-vinyl pyrrolidone provide the most enzyme stability, preserving between 60 and 93% of the original apparent activity after one week of incubation, but matrix inhomogeneities from adding silicone monomers can decrease sensor dynamic range by 56%. Finally, hybrid inorganic-organic interpenetrating network hydrogels were developed to prevent silicone phase separation in the hydrogels. These materials increased oxygen transport by up to 256% *in vitro* compared to pHEMA-based oxygen sensors and responded to modulated inspired oxygen in porcine models over 72 days. Hybrid sensors made with tissue-integrating inverted colloidal crystal architectures revealed minimal fibrosis *in vivo* with loosely woven collagen surrounding the implants, demonstrating promise for these hybrid materials as long-term implantable biosensors.

DEDICATION

This dissertation is dedicated to my friend Dr. Anita V. Mantri, PhD (Aggie class of 2017). While I will never understand why you were taken from this earth less than a year ago, I have faith that you are soaring across the heavens overlooking your beloved space flight missions from an entirely new perspective. Although you were one year away from earning your second doctorate, your MD degree, your care and compassion for your friends, your family, and the greater Space Life Science community are paralleled by no one and continue to bring us all closer together in spite of your passing. Thank you for the countless encouraging conversations and cups of coffee that helped fuel this research.

ACKNOWLEDGEMENTS

First, I would like to thank my committee chair, Dr. Michael McShane, for challenging me to be a better researcher and grow as a person professionally for the past six years, continually pushing the boundaries of my scientific reasoning skills and technical writing skills. The goal-oriented mindset I have developed during my time in his lab will carry me through the rest of my career. A big thank you to all of my other committee members, Dr. Melissa Grunlan, Dr. Daniel Alge, and Dr. David Bergbreiter, for their continual inspiration, guidance, and support throughout this journey. In particular, I would like to thank Dr. Grunlan for playing a pivotal part in my decision to attend graduate school through her role as my undergraduate research mentor through the USRG program. She has continued to serve as a mentor for me throughout my years of graduate school, including as a teaching mentor during the fall 2016 semester, my first semester as a Graduate Teaching Fellow. Additionally, I am grateful to Dr. Alge for his guidance and support for my research during the past three years and most recently as an additional teaching mentor to me during my second semester as a Graduate Teaching Fellow. Last but not least, thanks to the rest of the faculty and staff of the Biomedical Engineering Department.

I've had the opportunity to work alongside many great researchers over the past seven years, both as an undergraduate and graduate student. As an undergraduate student, I worked in Dr. Grunlan's lab under the mentorship of Dr. Brennan Bailey; this early experience was my first foray in research and heavily influenced my decision to

pursue a doctoral degree. During my first few years of graduate school, I continued to learn from the more-senior students of the McShane lab, particularly Dr. Dustin Ritter, Dr. Jason Roberts, and Dr. Ashvin Nagaraja. However, all of the members of the McShane group—past and present—are acknowledged for enriching my experience at Texas A&M University. In particular, I would like to thank Lindsey Bornhoeft, who has made significant contributions toward the completion of the interpenetrating network hydrogel characterization.

Dr. Natalie Wisniewski and Dr. Scott Nichols of PROFUSA are gratefully acknowledged for providing technical expertise, perspective, and suggestions on experimental design and the trajectory of my research throughout my time developing sensors for *in vivo* testing in porcine models. Dr. Soya Gamsey is acknowledged for her guidance on various hydrogel formulation development, synthesizing, and donating the benzoporphyrin dye and the beadcakes for creating the tissue-integrating implants.

I would like to extend my heartfelt gratitude to the Dwight Look College of Engineering at Texas A&M University for two semesters of support through the Graduate Teaching Fellowship program.

Finally, I could not have made it to this point without a strong support system of family and friends. In particular, I would like to thank my mother and father for their guidance, support, and encouragement in everything I have done. They have supported my dreams throughout my entire time in school, believing in me often more than I believe in myself. Dad, thank you for sparking my interest in science and engineering during my junior high and high school years via dinnertime thermodynamics

conversations and many late night debates about how to derive the quadratic equation. My brother Kyle was and still is my first and closest friend in life and has served as a voice of reason throughout our whole engineering journey inside the classroom and out. Kyle, I look forward to continuing my career as an engineer with you alongside. Mom, thank you for sharing your passion for communications and teaching with me. Your work as a preschool teacher has reminded me that no matter how much potential impact my research may have on the scientific community, if it can't be explained to a child, I don't understand it well enough. In your words, thank you for "feeding and watering" me for 28 years and allowing me to grow and blossom into the engineer and woman I am today.

NOMENCLATURE

AAm	Acrylamide
BSA	Bovine serum albumin
$CaCO_3$	Calcium carbonate (vaterite polymorph)
CAT	Catalase
CGM	Continuous glucose monitoring
CLSM	Confocal Laser Scanning Microscopy
DCM	Dichloromethane
DMA	Dimethylacrylamide
DMSO	Dimethyl sulfoxide
DSC	Differential scanning calorimetry
EDS	Energy-dispersive spectroscopy
EGDMA	Ethylene glycol dimethacrylate
EtOH	Ethanol
EWC	Equilibrium water content
FRET	Förster resonance energy transfer
GGG	Gadolinium-gallium-garnet
GOx	Glucose oxidase
HEMA	2-hydroxyethyl methacrylate
IPA	Isopropanol
IPN	Interpenetrating network

LbL	Layer by layer
MEHQ	Hydroquinone monomethyl ether
NaOAc	Sodium acetate
PBS	Phosphate-buffered saline
PMMA	Poly(methyl methacrylate)
NVP	N-vinylpyrrolidone
PdBP	Tetramethacrylated Pd(II) benzoporphyrin
PdBP-acid	Tetracarboxylated Pd(II) benzoporphyrin
PDMS	Poly(dimethylsiloxane)
PEG	Poly(ethylene glycol)
pHEMA	Poly(2-hydroxyethyl methacrylate)
RITC	Rhodamine isothiocyanate
SEM	Scanning electron microscopy
SERS	Surface-enhanced Raman spectroscopy
TEGDMA	Tetraethylene glycol dimethacrylate
T_g	Glass transition temperature
TRIS	3-[Tris(trimethylsiloxy)silyl]propyl methacrylate
λ_{ex}	Excitation wavelength
λ_{em}	Emission wavelength

CONTRIBUTORS AND FUNDING SOURCES

Contributors

This work was supervised by a dissertation committee consisting of Professors Michael J. McShane, Melissa A. Grunlan, and Daniel L. Alge of the Department of Biomedical Engineering and Professor David E. Bergbreiter of the Department of Chemistry.

In vivo oxygen sensor and GGG reference data were provided by Drs. Natalie A. Wisniewski and Scott P. Nichols of PROFUSA, Inc. The *in vivo* analyses depicted in Chapter 3 were conducted in part by Professor Michael J. McShane of the Department of Biomedical Engineering and were published in 2015. The Stern-Volmer analyses depicted in Chapter 4 were conducted in part by Jenna L. Weaver of the Department of Biomedical Engineering and were published in 2015. The rheometry data and histology images in Chapter 5 were provided by Lindsey R. Bornhoeft of the Department of Biomedical Engineering.

All other work conducted for the dissertation was completed by the student independently.

Funding Sources

Graduate study was supported for two semesters (fall 2016 and spring 2017) by a Graduate Teaching Fellowship from the Dwight Look College of Engineering.

This work was made possible in part by the National Institutes of Health under Grant Numbers 1R43DK093139 and 1R01EB016414. Its contents are solely the

responsibility of the author and does not necessarily represent the official views of the National Institutes of Health.

TABLE OF CONTENTS

Page

LIST OF FIGURES

LIST OF TABLES

1. INTRODUCTION

1.1. Current Standard of Healthcare—Diagnostics and Disease Management

Traditionally, the standard of healthcare in the US has been one of a highly centralized structure, requiring many patients to travel long distances to receive information about their state of health and to receive treatment. High costs, fragmented health status information, and delayed treatment are associated with such a healthcare structure [1]. Recently, efforts have placed emphasis on a paradigm shift from a highly centralized standard of care in the clinic to a highly networked structure, placing the patient at the center and connecting the patient and healthcare provider in an on-demand fashion [2-4]. Researchers are utilizing remote healthcare and telemedicine to pave the way for personalized medicine, a field that has been deemed the "Holy Grail" of revolutionized healthcare [5]. Biosensors capable of rapid, on-demand analyte detection are essential to realizing this healthcare shift, allowing real-time tracking of biomarker concentrations in order to take therapeutic action in a timely manner.

To manage many chronic diseases, fluid samples are collected periodically and analyzed using *ex vivo* assays. There are clinical assays for diagnosing and managing numerous chronic diseases such as hypothyroidism, cardiac disease, and cancer, among others [6]. Assays to detect numerous biomarkers have been developed for use in the clinic by sampling biological fluid (e.g., urine, saliva, or blood). These methods use assays such as Reverse Transcriptase Polymerase Chain Reaction (RT-PCR) and Enzyme-Linked Immunosorbent Assay (ELISA). Biomarkers are detected, and signal

levels are correlated to a biomarker concentration predictive of the patient's state of health [7]. Based on these readings, the patient can then take corrective action to manage his or her disease, if necessary.

While many assay methods have been developed to detect biomolecules for a variety of diseases, the aforementioned methods are often confined to clinical settings. Not only does this restrict disease diagnosis and management to highly developed areas of society, but it also requires time to process the biological samples, sometimes on the order of days to a week, delaying transfer of knowledge to the patient to take corrective action. Some diseases benefit from more frequent testing, causing the rise of point-of-care devices such as the glucometer and pregnancy test, which are the two most common and commercially available. Point-of-care devices offer the patient more control over managing his or her disease by preventing the management method from being restricted solely to a clinical setting [8].

1.2. Point-of-Care Disease Management and Continuous Glucose Monitoring

Efforts are being made to deliver chronic disease management at the point of care [9, 10], but some chronic diseases are more effectively managed by continuously monitoring biochemistry. Diabetes mellitus affects nearly 30 million children and adults in the US, with 1.7 million Americans being diagnosed each year. At this rate, it is estimated that one in every three adults will have diabetes by the year 2050 [11-14]. Additionally, $200 billion is spent annually on diabetes healthcare management. A long-lasting, continuous glucose monitoring (CGM) system is needed to better the welfare of individuals affected by this chronic disease through improving the precision of glycemic

control and patient compliance [15, 16]. Currently, a few CGM models are commercially available but contain rigid electrochemical probes that are easily recognized as foreign material by the body and cause significant inflammatory responses, despite efforts to make these devices more flexible [17-19]. Additionally, inserting these devices requires creating a percutaneous wound, which provides a pathway to infection throughout the entire time the device remains *in vivo*. Because of dynamic tissue environments surrounding the sensor, the percutaneous nature of these CGMs requires frequent probe calibration (up to four times daily) throughout the device's operational lifetime [20, 21]. Although made to be relatively small, commercially available CGMs all require an external transmitter that sits on the surface of the skin, subjecting the sensor to micromovements that cause more tissue trauma, discomfort, and infection. The cumulative effect of these factors leaves patients with a very narrow window within which they can obtain reliable real-time blood glucose concentration measurements and real-time profiles. Hydrogels have been investigated for long-term implantable biosensing applications by functionalizing them with enzymes and luminescent dyes to create a softer, fully implantable alternative to the commercially available electrochemical CGMs [22-27].

1.2.1. Mobile Healthcare and Personalized Medicine

With the advent of mobile technology, one rising field called mobile health (mHealth) has grown in the last decade [6]. In principle, incorporating mobile devices into a disease management regimen could allow for even more frequent and seamless testing of biomarker levels by allowing data transfer to a smartphone, requiring even less

hands-on time from the patient; however, unless a sensor is continually present in the body, this vision of seamless integration is still somewhat curtailed. Even with the advent of portable, handheld, and point-of-care devices, patients endure painful, repeated fingersticks, and the limitations of discrete time-point analysis do not provide caregivers or patients the ability to monitor systemic fluctuations over time [5, 24]. A prime example of this is diabetes, where knowledge of blood glucose dynamics helps inform decisions about treatment and lifestyle; yet, there are other situations where tracking biochemistry may also lead to improved outcomes [21, 28-32].

1.2.2. Factors Affecting Continuous Monitoring Device Operational Lifetime

Several methods of blood glucose detection employ the enzyme glucose oxidase (GOx) to catalyze the reaction of glucose in the presence of oxygen and water into gluconic acid, producing hydrogen peroxide as a byproduct. Often, GOx is immobilized on a solid substrate, polymer film, or gel to enhance stabilization. Based on the method of immobilization, several factors could play a role in sensor performance longevity, including enzyme deactivation and the substrate (oxygen and glucose) diffusion balance through the immobilization platform [17, 22, 27, 33, 34]. Therefore, both substrate transport and the ability of GOx to catalyze the reaction converting glucose into its oxidized form gluconic acid (i.e., the “apparent enzyme activity”) can affect sensor readings.

Causes for enzyme deactivation include prolonged exposure to both glucose and oxygen, which produce peroxide and acid. Hydrogen peroxide has been shown to irreversibly deactivate GOx, especially when GOx is in its reduced form [35-43]. In

addition, acid production can affect the apparent activity of the enzyme, even without denaturing it [44, 45]. If overall substrate transport is high, GOx will turn over both substrates quicker, leading to quicker GOx deactivation and potentially ultimately decreasing the device longevity. The *in vivo* environment presents additional hurdles to sensor performance longevity because of the elevated temperature of the body (37°C vs. 25°C at room temperature), reactive oxygen species (ROS) such as hydrogen peroxide secreted by macrophages, and end-stage fibrosis around the implant, providing an additional diffusion barrier to oxygen and glucose [24].

However, different reaction-diffusion balances yield different sensor response profiles, depicted by hypothetical data in Figure 1-1. For example, if sufficient enzyme apparent activity exists but the glucose transport is too low relative to oxygen, the signal sensitivity is diminished because there is not enough access to glucose to drive the reaction, as depicted in Figure 1-1A. On the other hand, if enzyme activity is sufficient but glucose transport is too high relative to oxygen transport, the signal level will increase rapidly, and high glucose levels will be undetectable because the optical

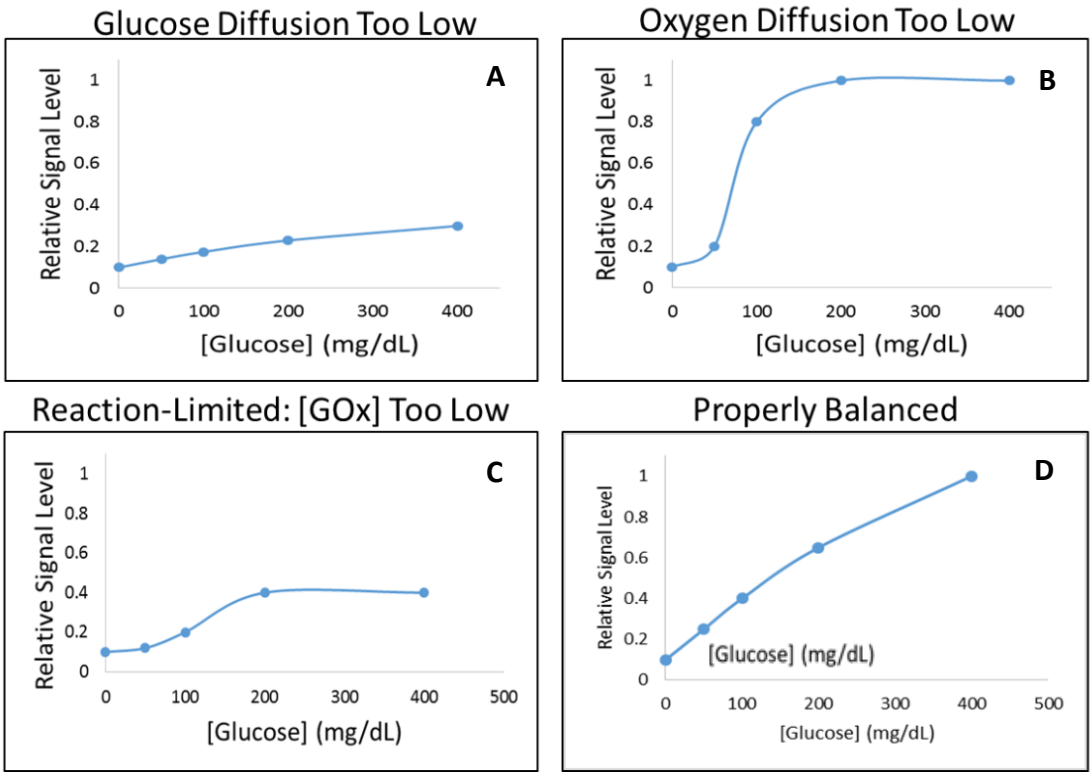

Figure 1-1: Various scenarios of sensor responses over the physiologically relevant glucose ranges with different reaction/diffusion balances. Responses are based on normalized signal levels of hypothetical data.

range of the dye will be saturated quickly (i.e., local oxygen levels depleting faster than they can be replenished, rendering oxygen the limiting substrate of the GOx-catalyzed reaction, Figure 1-1B). Thirdly, if substrate diffusion is balanced but too little active enzyme is present, the enzyme will react at its maximum velocity in the middle of the glucose challenge, and insufficient catalysis will be present to transduce signal levels for the entire range (hypo-, eu-, and hyperglycemic levels), depicted in Figure 1-1C. Moreover, a properly balanced diffusion and reaction system (Figure 1-1D) is necessary to optimize the sensor dynamic range and sensitivity across all glucose levels (0 to 400 mg/dL).

1.3. Criteria for Long-Term Fully Implantable Continuous Monitoring Devices

Therefore, to realize a long-term fully implantable optical glucose biosensor, each component of sensor performance (diffusion and reaction) must be considered. In order to improve device operational lifetime *in vivo*, a need exists for a hydrogel that imparts long-term enzyme stability as well as provides adequate substrate transport balance, even when accounting for end-stage foreign body response (FBR). There are two potential approaches to this problem: 1) rational design and 2) combinatorial, brute force. The former method requires knowledge of fundamental properties of enzymes and their interaction with different solvents and solutes, as well as mechanisms of deactivation following immobilization and substrate transport. The latter does not require any *a priori* understanding of enzyme-material interactions and substrate transport, but is a time-consuming and expensive affair involving screening of a large number of material candidates to search for a global or local optimum. Unfortunately, there is a dearth of knowledge on enzyme-hydrogel interactions, described in further detail in later chapters, from which to directly draw conclusions that could lead to optimal material selection for this application. Thus, there is a need to generate better understanding of these fundamental effects as well as develop efficient methods of evaluating candidate materials for their suitability as an enzyme-encapsulating matrix.

The experiments described herein are designed to quantify substrate diffusion and apparent enzymatic activity/stability, identifying relationships between each parameter to identify promising formulations *in vitro*. Additionally, formulations are challenged in porcine models to determine the effectiveness of translating rational sensor

designs on the benchtop to an *in vivo* environment to further refine the design of hydrogel matrices for long-term sensor function.

The following chapters of this dissertation are organized to present results of studies in a logical progression. Several of the studies presented herein have been submitted for publication or are available online and in print. In Chapter 2, the background for this work is provided, portraying prior work on using polymeric biomaterials in biosensor design. Chapters 3 to 5 describe the characterization and preclinical evaluation of a pHEMA-co-AAm phosphorescent glucose sensor (Section 3.3), chemically modified pHEMA copolymers and the physicochemical characterization thereof (Section 4.3), and hybrid materials to optimize oxygen transport (Section 5.3). Some of the results and associated methods presented in Chapter 3 were published in the *Journal of Diabetes Science and Technology* and in Chapter 4 were published in *IEEE Sensors Proceedings.* The results and associated methods presented in Chapter 5 have been submitted for publication. Finally, Chapter 6 presents the conclusions drawn from this work, and future directions are proposed.

2. BACKGROUND

2.1. Traditional Materials in Continuous Monitoring Devices

Research and development efforts in implantable device design involve making the device "biocompatible," a term generally accepted as a device that encompasses materials that are not just cytocompatible (i.e., not cytotoxic) but that also retain biofunctionality of the device in the specific anatomical location where the device is applied [46]. This includes not only alleviating or mitigating the body's response to the implant, but also eliciting the proper host response to maintain function of the device in its intended biological application [47].

In the realm of biosensing, the operational lifetime of a biosensor is an indicator of the stability of its sensing components in its intended environment and the device's ability to transduce analyte signals over time. When considering biocompatibility of implantable biosensors specifically, the reported predominant biological events altering sensor functionality and preventing sustained device operational lifetime *in vivo* are (1) biofouling and (2) fibrosis. In both cases, signal attenuation and diminished signal reliability are fundamentally altered on the molecular level due to decreased substrate transport to the device. The following section provides a summary of the current state-of-the-art of transcutaneous sensors and the polymeric materials used in these devices.

2.1.1. Transcutaneous Sensors

The oldest types of commercial continuous biochemistry monitors contain electrochemical sensors. These devices require an electrode that punctures the abdomen

and is connected to an external transmitter to convert electrical signals to analyte concentrations [15, 16, 19, 29, 48]. While wearable devices (e.g, step counters and heart rate monitors) have been adopted by many people into their everyday lifestyles, they do not directly measure actual blood biochemistry fluctuations, but rather externally measured physiological phenomena. However, perhaps the most ubiquitously used device for monitoring real-time biochemistry on a daily basis is the CGM, given the worldwide prevalence of diabetes. Various polymeric materials have been used to create films, gels, and other coatings for these electrodes to increase their biocompatibility *in vivo* [48]. Most commonly, these sensors have a membrane composed of polyurethane or a pyridine copolymer such as those used in the Medtronic MiniMed and Abbott FreeStyle Navigator commercial models, often entrapping GOx within the membrane by both chemical and physical means [49, 50].

One completely non-invasive CGM, the GlucoWatch, became commercially available in the early 2000s. The GlucoWatch used reverse iontophoresis to attract ions to the electrode and subsequently bring interstitial fluid to the skin surface; it consisted of a hydrogel containing poly(ethylene glycol) (PEG) and poly(acrylic acid) containing GOx. The hydrogel served as a selectively permeable membrane allowing glucose, ions, water, and other small molecules to pass through to the device to produce peroxide and amperometrically determine glucose concentrations [51]. Despite the attractiveness of a completely non-invasive CGM, patient reports of severe rashes and blistering, as well as reports of highly unreliable glucose readings during times of intense exercise and perspiration, led to the removal of this device from the market in 2007 [52, 53].

The GlucoDay was created in Florence, Italy and combines amperometry with microdialysis [51]. GlucoDay contains a platinum electrode covered with three membranes: 1) cellulose acetate, 2) GOx, and 3) poly(carbonate) [51]. However, this electrode is external to the body and does not puncture the abdomen; this is currently the only CGM on the market that does not use an implanted sensor [53]. The GlucoDay extracts glucose via microdialysis and measures the effluent glucose concentration amperometrically. Because this device requires the patient to wear perfusion bags around the abdomen and the dialysis fiber must be replaced every 48 hours, the GlucoDay is limited to measuring blood glucose in clinical settings [51, 53].

Fluorinated polymers and siloxanes have been used in CGM research due to their anti-fouling nature and high oxygen permeability, respectively [48]. Specifically, Nafion is a sulfonated tetrafluoroethylene that is known for its excellent electrical conductivity and resistance to biofouling. One study showed that heat curing Nafion on the outer surface of the electrode showed resistance to degradation and sensor sensitivity in dogs for 10 days *in vivo* [54]. Another fluoroethylene, Teflon, has been used as well in CGMs because of its anti-fouling nature. Specifically, Blubaugh and Brunsman developed a CGM electrode that uses a membrane with a semi-interpenetrating network (semi-IPN) morphology consisting of Teflon and poly(dimethylsiloxane) (PDMS) as a way to compensate for oxygen deficits and biofouling simultaneously *in vivo* [55]. Certain merits of this design (i.e., selectively increasing oxygen permeability and using higher-order architectures within the polymer matrix) serve as the inspiration behind certain matrix designs for fully implantable biosensors described in Chapters 5 and 6 of this

work. As a segue into using such polymer matrices (i.e., hydrogels) in fully implantable optical biosensors, an overview of optical assays used in hydrogels for implantable biosensors is presented in Section 2.2.

2.2. Fully Implantable Biosensing Platforms

Transitioning to a fully implantable sensing platform opens the door to utilizing classes of biomaterials and transduction assays in unique ways beyond those of transcutaneous electrochemical biosensors. Using materials that more closely resemble the physical and chemical properties of human skin may allow researchers to utilize unique material properties, refining sensor performance and device operational lifetime *in vivo*.

Hydrogels are a class of biomaterials made of crosslinked polymer networks that swell in water without dissolving, allowing them to retain properties of solids [56-61]. Furthermore, hydrogels can have physical and chemical properties that match those of human skin, as well as other native tissues, and have been used in various biomedical device applications including contact lenses, microcantilevers (MEMS), drug delivery vehicles, prophylactic devices, and tissue engineering scaffolds [56, 57, 60-62]. Demonstrations of potential hydrogel sensor formats over the years have included PEG-based microspheres and fibers and include a variety of hollow polymeric capsules and various nanocomposite particulate systems using other encapsulating materials [22, 24-27, 63-65]. Utilizing these unique properties of hydrogels in a fully implantable CGM may circumvent repetitive tissue trauma and infection associated with the percutaneous nature of traditional CGM devices *in vivo* [17, 18, 66].

Used in medical devices for decades, one of the most widely studied and well-characterized hydrogels for biomedical applications is poly(2-hydroxyethyl methacrylate) (pHEMA) [58, 67]. Initially, pHEMA was primarily used in soft contact lenses, but it has also been exploited for a wide variety of biomedical applications including drug delivery, tissue engineering, drug delivery, and blood-contacting devices [58, 60, 61, 68-73]. Recent work has shown that pHEMA-based hydrogels can be functionalized with enzymes and phosphorescent dyes to be used as luminescence-based glucose sensors [24]. The same study illustrated the ability to tune sensor behavior by the composition of the hydrogels, which influences the glucose and oxygen diffusion rate. *In vitro* and *in vivo* biofouling of sensors was characterized, and the effects on substrate transport and overall sensor performance *in vitro* were determined for pHEMA, polyacrylamide (pAAm), and pHEMA-co-AAm copolymer hydrogels [24]. This study revealed that matrix chemistry can significantly impact the extent of biofouling on the matrix material, altering the diffusivity of glucose through the sensor and the sensor's overall dynamic range and sensitivity, decreasing maximum sensitivity by up to 35%. Additionally, this work established serum exposure as a good predictor of *in vivo* biofouling behavior and that using serum exposure to predict biofouling and changes in glucose transport could accelerate the translation of this optical enzymatic glucose-sensing platform to preclinical *in vivo* testing [24].

Various methods have been investigated in recent years to transduce biochemistry levels in hydrogels by functionalizing them with optical assays. The following presents a brief summary of three approaches, focusing on glucose-sensing

assays due to the prevalence of diabetes worldwide, the abundance of glucose in the body as an analyte, and the fact that these two premises drive many researchers to use glucose as a proof-of-concept analyte when developing optical biosensors and a personalized healthcare monitor. Additionally, it is worth mentioning that the creation of a personalized health monitor for chronic disease management may require multiplexing two or more of these assays together. While this section delineates fundamentals of these three assays, the key principle is that using various non-interfering modalities will allow temporal, spectral, or other optical separation (e.g., fluorescence vs. Raman scattering) necessary to multiplex several assays together.

2.2.1. Competitive Binding Assays

One class of assays used for the purpose of continuous and on-demand biochemistry monitoring is a competitive binding assay. These assays contain a luminophore and quencher (i.e., quantum dots or a fluorescent dye), a binding ligand (e.g., dextran or another polysaccharide), and an analyte receptor (i.e., concanavalin A (ConA)) [63, 74-79]. Competitive binding affinity sensors offer the potential for long-term, real-time sensing capabilities without reagent consumption or formation of harmful byproducts, such as hydrogen peroxide or acid, and are not affected by diffusional changes of any substrate besides glucose. They rely on energy transfer between optically tagged donor and acceptor components in order to transduce binding events, which can then be correlated to analyte concentrations. A commonly used affinity assay is the glucose assay based on a competitive binding scheme where saccharide receptors such as ConA bind to ligands (e.g., dextran or trimannose), competing with ConA for glucose

[64, 76, 79-86]. While sensitive Förster resonance energy transfer (FRET)–based glucose sensors have been developed, this assay is based on luminescence intensity measurements, and the signal level is highly affected by the light scattering milieu of the skin, which could complicate optical interrogation of the sensors [78]. Other factors plaguing the feasibility of many FRET assays include systems being excited by wavelengths of light that is highly absorbed or scattered by the skin (e.g., green light, blue light, etc.), spectral overlap of the two fluorophores, low molar absorbtivity, low quantum yield, small Stokes shifts, and photobleaching [87]. Recent efforts have developed chromophores that address some of the aforementioned drawbacks of optical probes used in FRET systems, including molecules excited in the near-infrared region. In particular, porphyrins have been emphasized as a class of organic chromophores having high photostability and large Stokes shifts [88]. These two properties make them attractive for optical biosensing and the eventual design of an implantable personal health monitor. Applications of these porphyrins in biosensing are described in detail in Section 2.2.2.

2.2.2 Phosphorescence Lifetime Assays

As an alternative to competitive binding assays, the McShane group has investigated biosensing platforms based on the coupling of oxidoreductase enzymes and oxygen-quenched phosphors (metalloporphyrin dyes) to detect glucose levels indirectly through detecting oxygen levels [22-24, 26-28, 34, 35]. One advantage of these assays over the previously mentioned competitive binding assays is that these dyes have luminescence lifetimes on the order of microseconds, rather than nanosecond lifetimes

characteristic of naturally occurring chromophores found in blood and proteins (e.g., heme groups) [89-91]. This means that the lifetimes of these metalloporphyrin dyes are temporally separate from those of native proteins, mitigating background signal due to skin autofluorescence when porphyrin emission light is collected after the time of fluorescence decay. Time-resolved measurements of phosphorescent lifetimes can be accomplished by using custom-designed hardware containing a pulsed light source and software consisting of algorithms that delay emission collection until the background fluorescence has decayed to zero [28, 65, 92-94]. Coupling oxygen-quenched phosphors with oxidoreductase enzymes such as GOx presents many advantages for long-term biosensing as there are numerous oxidoreductase enzymes commercially available, and enzymes are used throughout biomedical, biochemical, analytical chemistry, and various industrial fields due to their notorious specificity/selectivity for unique chemical substrates and their ability to catalyze chemical reactions involving those substrates with high efficiency [95]. Mathematical description of these porphyrin/enzyme diffusion-reaction systems is found in Chapters 3 and 4.

Despite their effectiveness as molecular catalysts, enzyme performance and functional longevity is often limited due to the strong influence of environmental conditions including pH, salt concentration, and temperature [96]. To improve performance stability, enzymes are often modified directly or immobilized in or on various structures to prolong their catalytic function [95-106]. In the case of immobilized enzymes, primary or secondary bonding with the immobilization substrate can cause steric hindrance or blockage of the enzyme's active and/or deactivation. The

immobilized enzyme's performance may decrease due to inability to chemically catalyze a reaction because of a physical constraint (confinement or blockage to enzyme's active site). It is often difficult to determine the absolute activity of immobilized enzymes because changes in catalysis can be due to deactivation of the enzyme itself, physical constraint (steric hindrance), and/or increased diffusion barrier provided by the immobilization substrate (e.g., polymer films and hydrogels).

Fortunately, GOx is one of the most versatile enzymes and is used in numerous biotechnology, nutritional, and consumer industries in applications ranging from bioreactors to biomedical devices and food/drink additives [101, 107]. Researchers have worked on immobilizing GOx on various substrates including polymer films, glass substrates, micro- and nanoparticles, and hydrogels [22, 95, 97, 99-101, 103, 105, 108-115]. Numerous combinations of materials and immobilization strategies are used to incorporate enzymes into structures for various applications, including hydrogel matrices with phosphors to develop fully implantable biosensors [24, 28, 65]. Phosphorescence assays will be the focus of later chapters in this work.

2.2.3 Plasmonic Assays Based on Surface-Enhanced Raman Spectroscopy

While competitive binding assays and phosphorescence lifetime assays both offer advantages in transducing biomolecule levels in real time with high specificity, they both have disadvantages. Often, competitive binding and phosphorescence assays contain proteins that can denature or deactivate, causing the assay to lose its sensitivity or even its overall function. On the device level, loss in sensitivity translates to decreased signal

levels, resulting in frequent recalibration, decreased signal-to-noise ratio (SNR), and eventual sensor replacement.

Plasmonic nanoparticles have gained interest in biosensing because of their potential to detect molecular binding events with high sensitivity and their ability to be excited at a particular wavelength without the risk of photobleaching like some of the fluorophores used in competitive binding assays [116, 117]. Metallic nanomaterials (i.e., gold and silver) have been exploited for this biosensing application by investigating optical phenomena such as localized surface plasmon resonance and surface-enhanced Raman spectroscopy (SERS) [116].

Specifically, SERS assays have been exploited in biosensor design because of their ability to increase Raman scattering intensity up to eight orders of magnitude versus traditional Raman scattering interactions. SERS substrates often consist of metallic nanoparticles made of bioinert metals such as gold or silver [117, 118]. SERS harnesses the power of surface plasmon resonance (SPR), which occurs in metallic structures at the nanoscale, to selectively interact with certain molecules and amplify Raman scattering signals. Although they do not provide the same type of temporal separation of luminescence lifetime as long-lifetime phosphors mentioned in Section 2.2.2, their photostability, spectral tunability, and ability to be made from bioinert materials (i.e., gold) still render them attractive from a biosensing standpoint, especially when functionalized with moieties to selectively amplify signals of biomolecules via SERS [119].

The Van Duyne group has made significant strides in establishing proof of concept of monitoring biomolecules with SERS substrates both *in vitro* and *in vivo.* In recent work from the Van Duyne group, nanoparticles (usually silica) are immobilized on a flat titanium substrate and coated with a silver or gold coating to impart Raman scattering ability to the particles; they are then functionalized with a self-assembled monolayer to impart selectivity to glucose [120, 121]. In fact, one study demonstrated that these materials, when planted subcutaneously in rats, can respond to glucose for over 17 days [121]. In comparison, commercially available CGMs only last up to seven days [16, 50, 122]. However, only 17 days of *in vivo* function for a fully implantable device is not ideal, as it is much more difficult to remove than current transcutaneous CGMs on the market. One factor hindering the long-term function of these implants (i.e., on the order of months) could be the interference of other biological molecules, such as proteins, with the glucose-sensitive ligand on the particles. Although the authors chose titanium as a substrate based on its FDA approval in other medical devices such as hip replacements, studies have shown that surface morphology can influence the inflammatory phenotype of immune cells and, ultimately, the severity of the FBR (i.e., fibrosis) [123, 124]. Presence of fibrosis could wall off the implant from the rest of the body, restricting bloodflow to the sensors and restricting access to glucose as described in other work with electrochemical glucose sensors containing metal components [125, 126]. Immobilizing the SERS assay in or on an implantable substrate that better mimics the chemical and physical properties of subcutaneous tissue may extend the operational lifetime of subcutaneous SERS sensors *in vivo*.

Recently, SERS-based plasmonic assays have been encapsulated in hydrogels and have been shown to measure pH and glucose in real time. A response to glucose was shown by encapsulating GOx and mercaptobenzoic acid (MBA)–tagged gold nanoparticles, measuring gluconic acid production from GOx [127]. However, only benchtop proof of concept has been demonstrated with this system in a 96-well plate. Additionally, because the body is a buffered environment, time-delayed response is a prominent hurdle for these systems (governed by substrate diffusion and conversion of glucose to gluconic acid) because of the interaction of MBA with ions in the surrounding interstitial fluid. This implantable sensing platform shows potential for real-time monitoring of substrates for personalized healthcare, but is still in early developmental stages and has not been shown to rapidly transduce clinically relevant biomarkers (i.e., glucose) in real time *in vivo*. Refinement of the system design (hardware and glucose response time) must be accomplished before practical *in vivo* measurements can be made. For this purpose, the rest of this work will focus on phosphorescence lifetime assays due to the fully characterized figures of merit in previous work.

3. PRECLINICAL PERFORMANCE OF PHEMA COPOLYMER HYDROGELS AS GLUCOSE SENSORS[*]

3.1. Introduction

As discussed in Section 2.2.2, phosphorescence-based assays have been encapsulated inside various hydrogel materials, both synthetic and natural, for minimally invasive glucose monitoring [22, 24-27]. These sensor designs have consisted of nanofilm-coated alginate microspheres and injectable pHEMA-based discs both comprising green-excitable oxygen-quenched phosphors and, in some cases, an additional reference fluorophore [22-24, 26, 27]. Previously, hydrogel-based sensing platforms have been evaluated through various avenues: modeling, *in vitro* characterization, and implantation into rats to test *ex vivo* [24]. While these studies helped pave the way for *in vivo* proof of concept, one main hurdle to observing a successful real-time response to glucose is the green excitation of the PtOEP and PdTCPP phosphors, as green light is strongly absorbed by the skin [22, 26].

Biocompatibility of pHEMA-co-AAm copolymer gels has been studied in detail with green-excitable phosphors. Prior work investigated glucose transport properties of three gel formulations: pHEMA and pAAm homopolymer gels and a 50:50 HEMA:AAm copolymer. These studies investigated the effect of adding matrix

---

[*] Parts of this section are reprinted with permission from R. M. Unruh, J. R. Roberts, S. P. Nichols, S. Gamsey, N. A. Wisniewski, and M. J. McShane, "Preclinical Evaluation of Poly(HEMA-co-acrylamide) Hydrogels Encapsulating Glucose Oxidase and Palladium Benzoporphyrin as Fully Implantable Glucose Sensors," *Journal of Diabetes Science and Technology,* vol. 9, no. 5, pp. 985-992, 2015. Copyright © 2015 by SAGE Publishing Inc. Reprinted by permission of SAGE Publications.

chemistry on glucose transport as well as impacts of *in vitro* biofouling (exposure to rat serum) and *in vivo* implantation on sensor response over a one-month time period. This study found that adding pAAm to the pHEMA gels increased glucose transport over 30-fold (regardless of 50 or 100% AAm), translating to a 496% increase in maximum sensitivity. However, while both the pHEMA homopolymer and the 50:50 HEMA:AAm were found to have lower limits of detection well in the hypoglycemic range (4.2 and 17.6 mg/dL for pHEMA and p(HEMA-co-AAm), respectively), a 286 mg/dL decrease in the upper limit of detection was observed with the 50:50 HEMA:AAm compared to the pHEMA homopoymer, rendering the upper limit of detection at only 70.5 mg/dL for 50:50 HEMA:AAm versus 356 mg/dL for the pHEMA homopolymer. In other words, the 50:50 HEMA:AAm sensor's dynamic range was confined to detect only hypoglycemic levels and could not detect euglycemic or hyperglycemic levels, whereas the dynamic range of the pHEMA sensors encompassed the hypo-, eu-, and hyperglycemic ranges. Stable signal levels could not be established with 100% acrylamide (AAm) hydrogel sensors, and these sensors were not tested for optical response to glucose. This suggests that some HEMA content could be necessary to ensure sensor stability, even though experiments showed that more HEMA results in decreased sensitivity to glucose.

Interestingly, serum exposure experiments indicated that all three formulations showed a significant (t-test, $\alpha = 0.05$) drop in glucose permeability after one week of serum exposure or one week of implantation, but little change in glucose diffusivity was observed from one week to one month of exposure or implantation, indicating that acute

nonspecific protein adsorption accounts for most of the changes in analyte permeability through these devices (as opposed to severe analyte occlusion), despite long-term fibrotic encapsulation. Although glucose diffusion experiments reported analyte accessibility to the sensor after one month of implantation, glucose sensors were not transdermally interrogated *in vivo*, and the rats were not challenged with glucose in order to measure real-time response to glucose [24].

The present work aimed to (1) extend the operating wavelength range for *in vivo*

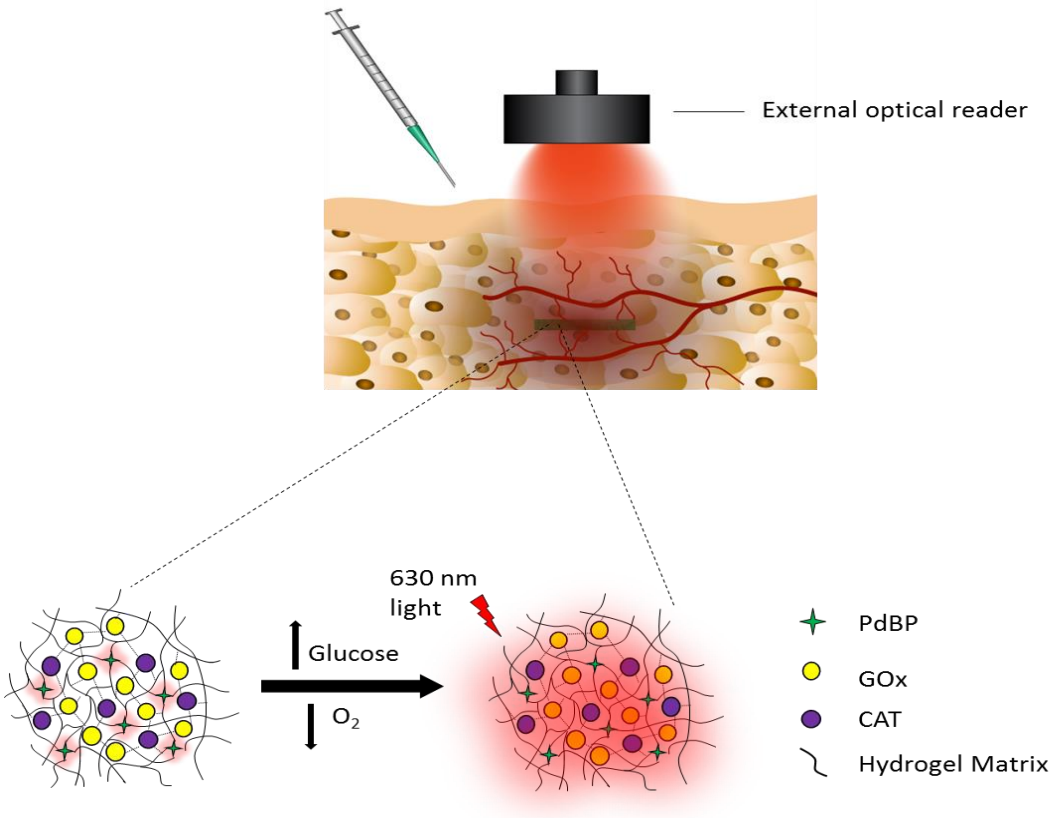

Figure 3-1: Illustration of transdermal optical interrogation of a subcutaneous sensor implant; left illustrates illumination, right illustrates implant emission. Image is only for understanding of system, and does not represent actual beam shape. Adapted with permission from SAGE Publications. © 2015 by SAGE Publications.

use by incorporating an alternative long-lifetime phosphor (Figure 3-1); (2) further characterize the *in vitro* glucose response characteristics of similar pHEMA-co-AAm hydrogels to more fully understand how to adjust their response properties to achieve an upper limit of detection in the hyperglycemic range without sacrificing sensitivity; and (3) perform proof-of-concept *in vivo* testing to evaluate its potential for use as implantable biosensors by tracking rising and falling glucose levels in real time.

This approach includes replacing the aforementioned phenyl porphyrin dyes with a benzoporphyrin dye. The literature has highlighted the potential of similar benzoporphyrin dyes—modified with moieties such as sulfonate groups and PEG chains, complexed with other metals such as Pt(II) and Zn(II), and encapsulated in various materials such as poly(styrene-block-pyrrolidone) and poly(sulfone)—as nanobeads to monitor subcutaneous tissue oxygen levels due to their NIR emission wavelength [90, 91]. These studies demonstrated several variations of benzoporphyrins with Q-bands near 630 nm and quantum yields 16 to 18% higher (in dimethylformamide, DMF) than the PdTCPP dyes used in previous green-excitable glucose sensors, suggesting that glucose sensors made with Pd(II) benzoporphyrins could be brighter and have a higher SNR than the same sensor made with PdTCPP [65, 90]. In addition, the highest-reported natural lifetime, τ_0, of these benzoporphyrins is 363 µs (room temperature, encapsulated in polystyrene) [91], whereas lifetimes for PdTCPP over 600 µs have been reported in pHEMA hydrogels [24]. This means that while the benzoporphyrins may better suited for *in vivo* transdermal optical interrogation (red excitation and higher quantum yield), the absolute microsecond resolution for a given change in oxygen concentrations will be

less than for PdTCPP, making a glucose sensor in pHEMA-based materials less sensitive than the equivalent sensor made with the PdTCPP phosphor.

In the present work, glucose sensors were synthesized with tetramethacrylated Pd(II) benzoporphyrin (PdBP) phosphors. Sensor behavior was investigated in various pHEMA-co-AAm formulations, allowing the dye to act as a covalently attached four-arm crosslinker in the matrix (Figure 3-2). In addition, solubility of the sensing assay was investigated. Finally and importantly, this work demonstrates the first successful transdermal optical interrogation and glucose challenge in a porcine model.

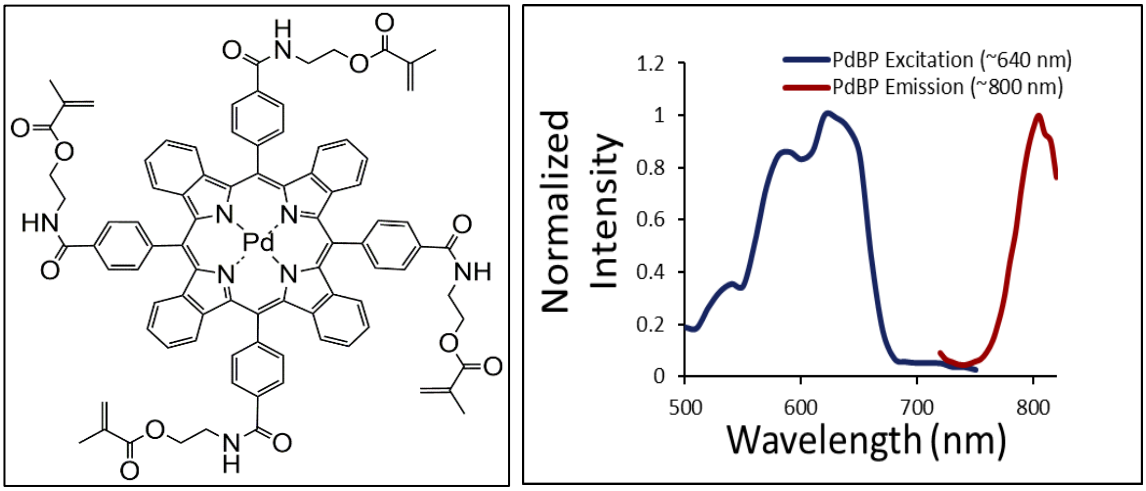

Figure 3-2: Structure and excitation/emission spectra of the PdBP dye

3.2. Theory and Methods

It is noteworthy that the benzoporphyrin dyes are oxygen-quenched; thus, in this enzyme-porphyrin platform, sensor response depends on the rate of glucose and oxygen consumption by GOx and the extent of local oxygen depletion near the dye. Hence, sensor response depends on the availability of the substrates glucose and oxygen to the enzyme (governed by mass transport), as well as the affinity of the enzyme for both substrates [22-24, 26-28].

Luminescence lifetimes of the benzoporphyrin dye in these sensors depend on the local oxygen concentration around the dye, governed by oxygen flux into the sensor. The Stern-Volmer relationship illustrates the behavior of collisional quenching of dye phosphorescence by oxygen which can be related to the diffusion kinetics underlying the glucose response according to the Stern-Volmer quenching relationship, illustrated by the following equation [90, 91, 128].

$$\tau_0/\tau = I_0/I = 1 + K_{SV}[O_2]$$

In the above relationship, τ_0 and I_0 are the luminescence lifetime and intensity in the absence of oxygen, respectively; τ and I are the luminescence lifetime and intensity at a particular oxygen concentration, $[O_2]$; and K_{SV} is the Stern-Volmer constant representing the linear relationship between the ratio τ_0/τ and $[O_2]$.

The following experimental methods have been designed to characterize more fully pHEMA-co-AAm glucose sensors from the standpoint of sensor homogeneity, underlying oxygen response, and overall glucose response. Figures of merit are obtained

from *in vitro* experiments and pave the way for more robust sensor preparation for preclinical evaluation, *in vivo* transdermal optical interrogation, and real-time tracking of blood glucose.

Firstly, three pHEMA-co-AAm formulations were fabricated with GOx and the PdBP phosphor. These formulations were investigated qualitatively for homogeneity and solubility of the sensing chemistry. Additionally, the gels were subjected to a screening test, where the thermostability of GOx was evaluated over a two-week period as a first-pass test for sensor functionality and stability. Results from the screening were reconciled with the observations of homogeneity in order to lay the groundwork for refining the sensor formulation.

Secondly, *in vitro* sensor response was investigated to observe real-time response of the sensors to both oxygen and glucose. Data were collected for both Stern-Volmer oxygen-quenching kinetics and optical response to glucose at ambient oxygen concentration in order to determine how the glucose response relates to the underlying oxygen response. Steady-state response plateaus at each oxygen concentration were used to generate Stern-Volmer quenching plots and a glucose calibration curve (a plot of steady-state lifetime versus glucose concentration). Stern-Volmer constants (K_{sv}) and bimolecular quenching constants (k_q) were calculated from the oxygen diffusion data and compared to previously reported immobilized benzoporphyrins. Similarly, glucose calibration curves were used to determine the analytical range and sensitivity of sensors and allow a method to compare this red-excitable platform with previously-used green-excitable sensing platforms.

Finally, the sensors were injected into a porcine model to investigate preliminary preclinical performance of this benzoporphyrin-based sensing platform. While previous studies indicated promising biocompatibility in rats based on the extent of biofouling and its effect on glucose transport through the sensor matrix, the sensors were neither interrogated transdermally nor tracked during a glucose challenge. The experiments in this chapter introduce three major advances from previous *in vivo* studies: (1) fabricating benzoporphyrin sensors as injectable strips for evaluation in porcine models, (2) interrogating the sensors and measuring phosphorescence lifetime transdermally using a portable red-excitation luminescence lifetime hardware system, and (3) monitoring sensor response in real-time to rising and falling glucose levels *in vivo*.

3.2.1. Materials

Tetraethylene glycol dimethacrylate (TEGDMA) and 2-hydroxyethyl methacrylate (HEMA, ophthalmic grade) and were purchased from Polysciences, Inc. (Warrington, PA). Ethylene glycol, 2,2-dimethoxy-2-phenyl-acetophenone (DMPAP), 1-Ethyl-3-[3-dimethylaminopropyl]carbodiimide hydrochloride (EDC), sterile phosphate-buffered saline (PBS, 0.01M phosphate buffer, 0.154M sodium chloride), *o*-dianisidine, horseradish peroxidase, and catalase (CAT) were obtained from Sigma-Aldrich® (St. Louis, MO). GOx was obtained from BBI™ Solutions (Cardiff, UK). Sodium chloride, potassium chloride, potassium phosphate (dibasic), sulfo-N-hydroxysuccinimide (sulfo-NHS), and dimethyl sulfoxide (DMSO) were purchased from VWR® (Radnor, PA). Sodium phosphate (monobasic) and glucose were purchased from ACROS Organics (ThermoFisher Scientific Inc., Waltham, MA) and Macron Fine Chemicals™

(Avantor™ Performance Materials, Inc., Center Valley, PA), respectively. Acrylamide and sterile DI water were purchased from AMRESCO® (Solon, OH) and Invitrogen™ (Life Technologies™, Grand Island, NY), respectively. Sterile 50% (w/w) dextrose was obtained from Cardinal Health (Dublin, OH). The red-excitable luminescent dye, a methacrylated PdBP (Figure 3-2), was custom-synthesized and donated by PROFUSA, Inc. (San Francisco, CA). The UV Lamp (Blak-Ray B-100SP) was purchased from UVP, LLC (Upland, CA).

3.2.2. Hydrogel-Based Glucose Sensor Fabrication

Three formulations were chosen to investigate based on prior work: a pHEMA homopolymer, a 75:25 HEMA:AAm copolymer, and a 50:50 HEMA:AAm copolymer [24]. Hydrogels for injection were fabricated similarly as described previously [24] with a few changes (exchanging the green-excitable phenyl porphyrin with the red-excitable PdBP, Figure 3-2).

3.2.2.1. Screening by Glucose Oxidase Activity Assays

To evaluate the feasibility of the formulations to house the sensing chemistry for the biosensing platform, gels of different compositions were evaluated for enzyme activity and stability with pure HEMA and AAm (40.2 w/w% in DI water). Gels of pHEMA (no AAm), 75:25 HEMA:AAm, and 50:50 HEMA:AAm were fabricated. To fabricate the hydrogels, the photoinitiator DMPA (2.5 mg) was weighed in a 2 mL microcentrifuge tube, to which was added 250 µL of the monomer(s) (appropriate v/v% ratio of AAm solution and HEMA), 5 µL of TEGDMA crosslinker, 90 µL of ethylene glycol, and 50 µL of a 10 mM PdBP solution in DMSO (or 50 µL of pure DMSO for

screening gels without dye) were added and mixed by vortexing. The enzyme component (107.5 µL in PBS) was added and mixed via pipette to avoid enzyme denaturation or deactivation from the shear force of vortexing. Gels with GOx only (2.3 µM in PBS, pure DMSO), as well as with GOx and the PdBP dye (2.3 µM GOx in PBS, 10 mM PdBP in DMSO) were prepared.

It is worth noting that the GOx concentration (2.3 µM or 0.4 mg/mL in PBS) is 100 times less than the GOx concentration used in glucose sensor implants [24, 65]. This was done due to the small volume of the assay cocktail used in each well of the well plate (200 µL), as well as the static test nature of the assay. In other words, the gel discs were exposed to a stagnant fluid for the duration of the experiment (due to the nature of the well plate structure) as opposed to the continuous flow experienced by the sensors when immobilized in the sample chamber, described in Section 3.2.3.2.

When the sensors are immersed in a small volume of stagnant fluid in the well, the substrate levels are not replenished in the same manner as in a continuous flow system. Therefore, it is necessary to avoid saturating the assay (i.e., depleting one or more substrates necessary to catalyze the assay reaction); this will result in a rapid increase in absorbance signal change and then a distinct plateau due to insufficient substrate levels to transduce a subsequent absorbance signal change. Ideally, the enzyme level should be high enough to provide a sensitive absorbance change over the experimental time window (i.e., 30 minutes), but low enough so that the enzyme can be saturated by the substrates and operate at its maximum velocity throughout the duration of the experiment (i.e., saturating the enzyme versus saturating the assay).

Gels with the full concentration of the enzyme (232.5 µM or 40.0 mg/mL) were found to saturate the assay within a matter of a few seconds; no change in absorbance could be observed in the plate reader due to nearly instantaneous depletion of the dissolved oxygen in the reaction cocktail. A 100× dilution of GOx from standard levels (denoted in Chapter 3) allowed the enzyme to operate at V_{max} throughout the duration of the screening experiments while transducing a distinct change in absorbance by o-dianisidine at 495 nm (Figure 3-3).

Precursor solutions were injected via syringes fitted with 26-gauge needles into glass molds with 0.01-in.-thick Teflon spacers secured with clips. Gels were photopolymerized with UV light (365 nm, 140 watts, three minutes per side). The

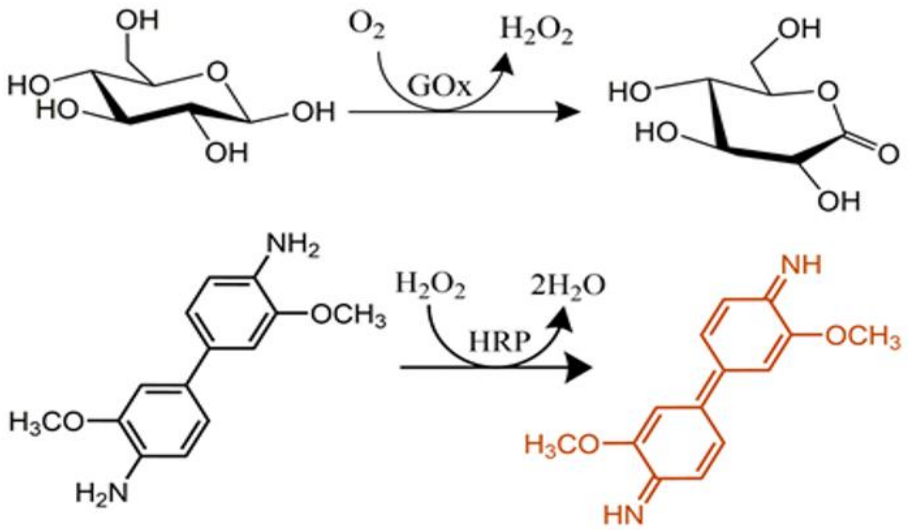

Figure 3-3: Illustration of the coupled redox reactions involved in the glucose oxidase activity assay. The first reaction (top) involves the oxidation of glucose into glucono-δ-lactone (quickly hydrolyzed into gluconic acid in aqueous environments), catalyzed by GOx, producing hydrogen peroxide. The second reaction (bottom) illustrates the reduction of hydrogen peroxide and the oxidation of o-dianisidine, inducing a visual color change in solution from colorless to burnt orange.

resulting crosslinked gels were removed from the mold, rinsed with DI water, and placed in 40 mL PBS with 0.056 mg EDC and 0.16 mg sulfo-NHS to crosslink enzymes and prevent enzyme leaching. After equilibration in PBS, 5-mm-diameter hydrogel discs were punched with a biopsy punch (for the purpose of lining a 96-well plate to perform the activity assays) and were placed in fresh PBS in a 15 mL centrifuge tube. The tubes were placed in an incubator at 37 °C in PBS for two weeks. The apparent activity of the GOx-only gels were tested initially and weekly after incubation using a colorimetric *o*-dianisidine absorbance-based activity assay, measuring absorbance at 492 nm versus time [129]. Activity measurements were also performed on GOx dissolved in phosphate buffer (pH 7.4) and were stored under the same conditions for comparison.

3.2.2.2. Injectable Glucose Sensor Fabrication

For implantation, a different hydrogel shape was chosen: 5-mm-long strips with a ~750 µm × 750 µm square cross section). This shape was selected for ease of insertion through a needle. The enzyme component in PBS contained 232.5 µM GOx and 25 µM CAT; CAT acts as a peroxide scavenger that aids in preserving GOx activity. The PdBP was dissolved in DMSO at a concentration of 10 mM (1 mM in the final gel).

Precursors containing the enzymes and PdBP dye were injected into glass slide molds, each with a 0.03-in.-thick Teflon spacer secured with clips. Gels were photopolymerized with UV light (365 nm, 140 watts, three minutes per side). Finally, the gels were removed from the mold, rinsed with deionized water, and placed in 40 mL of PBS with 5.6 mg of EDC and 16 mg of sulfo-NHS and were allowed to equilibrate in this solution overnight to crosslink enzymes and prevent enzyme leaching. Oxygen-

sensitive reference sensors (O2 Ref) were fabricated with the same parameters as described, except PBS replaced the enzyme solution and strips were not exposed to EDC/NHS. Materials for injection were cut to the same final dimensions described above.

3.2.3. In Vitro Sensor Response

3.2.3.1. Lifetime Measurements: Optical Interrogation and Data Collection

Sensors were monitored with a custom luminescent measurement system through a LabVIEW interface. The measurement system uses LEDs (Philips Lumileds Luxeon Rebel Red λ_{ex} = 630 nm) driven at ~200 mA (typical) for ~40 mW output during ON cycles. LEDs are typically pulsed ON for 250 µs and then held OFF for 5000 µs while the emission decay is monitored. Emission intensity is monitored with silicon PMTs (SensL) after collecting emission through a lens and filter (λ_{em} = 809 ± 40 nm, Semrock). The excitation source (LED) and detector (silicon photomultiplier) are housed in a 1.5-in. diameter puck where the 1 mm apertures for the excitation and emission are spaced at 6 mm. The puck is placed in contact with the flow cell (*in vitro*) or animal skin (*in vivo*). Emission decay curves are processed using nonlinear least-squares regression (Levenburg-Marquardt algorithm) using a mono-exponential decay to calculate the lifetime (τ) and intensity of the long-lived component (phosphorescence); the baseline background intensity resulting from scattered excitation light bleeding through the filter is then calculated as the residual of the difference between the fitted curve and the actual decay. In this experiment, the instrument was configured to measure the luminescent lifetime on each channel once every five seconds. Due to limited implantation space,

three sensors were monitored simultaneously in both the *in vitro* and *in vivo* experiments. Limited implantation space arose from testing these glucose sensors in parallel with other sensor formulations, including controls, standards, and shams. Some of those sensors were used in this study (controls), but others were used in separate experiments conducted by PROFUSA, Inc. which are not detailed in this work.

3.2.3.2. Glucose Response

To test the *in vitro* optical response of the sensors to glucose, sensor strips were immobilized in a sample chamber adapted from a previously described glucose flow-through apparatus (Figure 3-4) [24]. Briefly, two reservoirs (one containing PBS and the other containing 400 mg/dL glucose in PBS) were connected to two separate pumps controlled by a LabVIEW program. Combined pump effluents flowed directly to the sample chamber housing the immobilized sensing strips. The sample chamber consisted of a Teflon spacer with slots for samples to lie, housed between an acrylic base and top plate and secured with screws in an acrylic top plate. Chamber effluent drained directly into a waste tank. During the glucose experiment, sensors were exposed to six

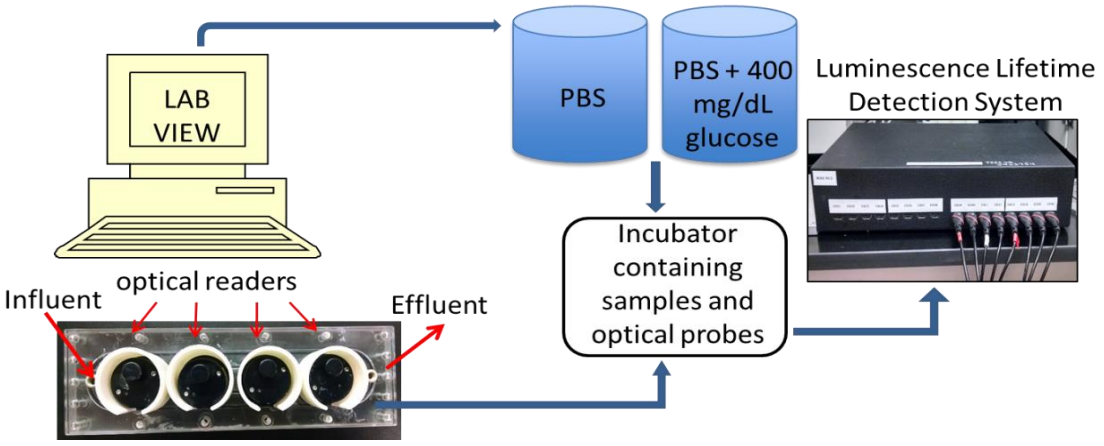

Figure 3-4: *In vitro* glucose response benchtop testing system

concentrations of glucose (0, 50, 100, 200, 300, and 400 mg/dL) in an incubator at 37 °C. These parameters were chosen based on relevant physiological concentrations of blood glucose and physiological temperature. After the final glucose concentration was reached (400 mg/dL), PBS (0 mg/dL glucose) was flowed over the sensors to test sensor reversibility.

Raw data (phosphorescent lifetime and timepoints) were plotted in MATLAB to generate a step response curve (lifetime versus time). To calculate the sensor calibration curves, 10 data points in each steady-state response region were averaged and their standard deviations calculated. The average and standard deviations in steady-state responses for each glucose concentration tested were plotted against the glucose concentrations to calculate dynamic range and sensitivity. The dynamic range and linear sensitivity of the sensor implants were calculated by fitting a curve to the data using a nonlinear least squares regression method. The upper and lower limits of detection were calculated using the 3σ approach: the lower limit was defined as the baseline lifetime plus three times the standard deviation, whereas the upper limit was defined as the saturation lifetime minus three times the standard deviation. The linear sensitivity was calculated as the slope of the line connecting the upper and lower limits of the analytical range.

3.2.3.3. Oxygen Response

For oxygen diffusion experiments, a similar setup was used, except a single recirculating system containing PBS was used (Figure 3-5). Mass flow controllers purged the PBS with nitrogen gas to vary oxygen levels, monitored with a calibrated

picoammeter (Unisense, Denmark). In both oxygen and glucose experiments, three strips were run simultaneously, and their luminescence lifetime responses to various glucose or oxygen concentrations were measured with the custom optical interrogation unit. For the oxygen diffusion experiment, sensors were exposed to five concentrations of oxygen in the physiological oxygen range: 50.22, 40.17, 30.13, 20.09, and 0 µM. The luminescence lifetime ratios were calculated and plotted against oxygen concentrations according to the Stern-Volmer equation in Section 0. Data were fit with a linear curve ($R^2 > 0.99$) to determine the Stern-Volmer quenching constant.

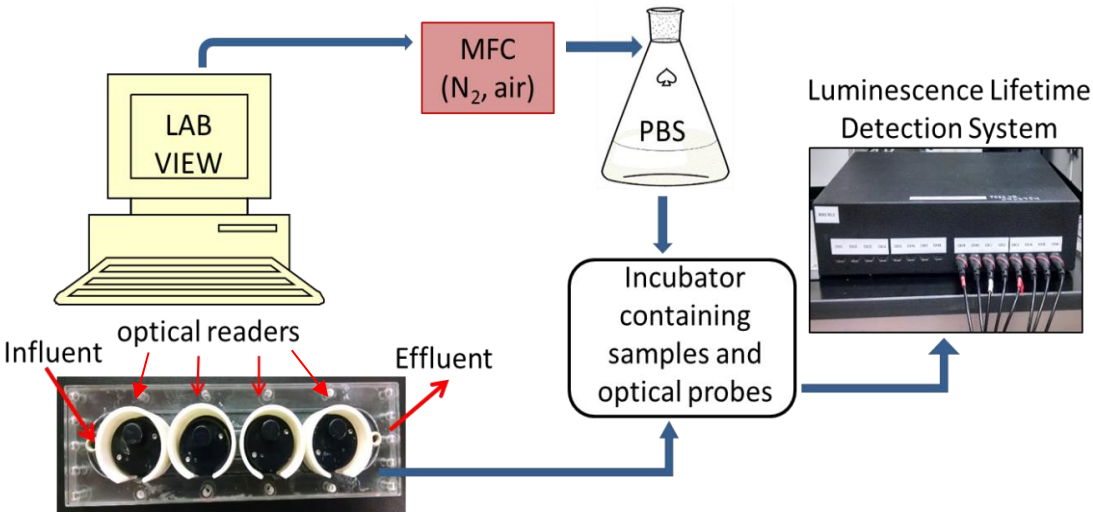

Figure 3-5: Stern-Volmer oxygen diffusion benchtop apparatus

3.2.4. In Vivo Sample Preparation

All utensils were autoclaved prior to use. Glucose sensing hydrogel slab strips (~0.75 × 0.75 × 5 mm) were suspended in 70% ethanol in a sterile 50 mL centrifuge tube for 10 minutes in a biosafety cabinet. One-third of the total volume was poured into a waste beaker and replaced with sterile DI water three times, allowing the sensors to equilibrate for 30 minutes between each solvent exchange. This gradual equilibration process was repeated but by (1) pouring off one-half of the total ethanol/water solution volume three times and filling with water, (2) pouring off the entire volume three times and filling with water, and (3) filling the entire tube with sterile PBS to equilibrate overnight prior to *in vivo* insertion.

3.2.5. In Vivo Injection

The animal protocol used in this study was approved by an IACUC committee at Texas A&M University. A female Sinclair mini-pig was obtained from Sinclair Bio-Resources (Columbia, MO). The pig was initially anesthetized with an injection of telazol (5 mg/kg) and buprenorphine (0.01 mg/kg). The pig was sedated, intubated, and anesthetized, and then dorsal hair was shaved and skin was thoroughly cleaned. Anesthesia was maintained with 1.5 to 2.0% isoflurane (v/v in O_2) to effect during sensor injections and blood glucose modulation. Skin was prepared for injections by scrubbing with ChloraPrep applicators (CareFusion, San Diego, CA). Sensors were injected subcutaneously into the dorsum of the pig (42.0 kg, one year old) from an 18-gauge cannula with a reverse-action plunger.

3.2.6. Glucose Challenge

The blood glucose of the pig was modulated between 40 and 235 mg/dL via continuous intravenous (IV) infusion of 20% dextrose in sterile saline (diluted from sterile 50% dextrose), followed by IV bolus infusions of Humalog insulin (Eli Lilly, Indianapolis, IN) (Figure 3-6). Sensors were optically interrogated transdermally and non-invasively with the same external optical reader puck described previously. Luminescence lifetimes were recorded for two glucose-sensitive implants, an oxygen-sensitive (but glucose-insensitive) reference implant, and a reference implant insensitive to both oxygen and glucose. The glucose- and oxygen-insensitive reference was

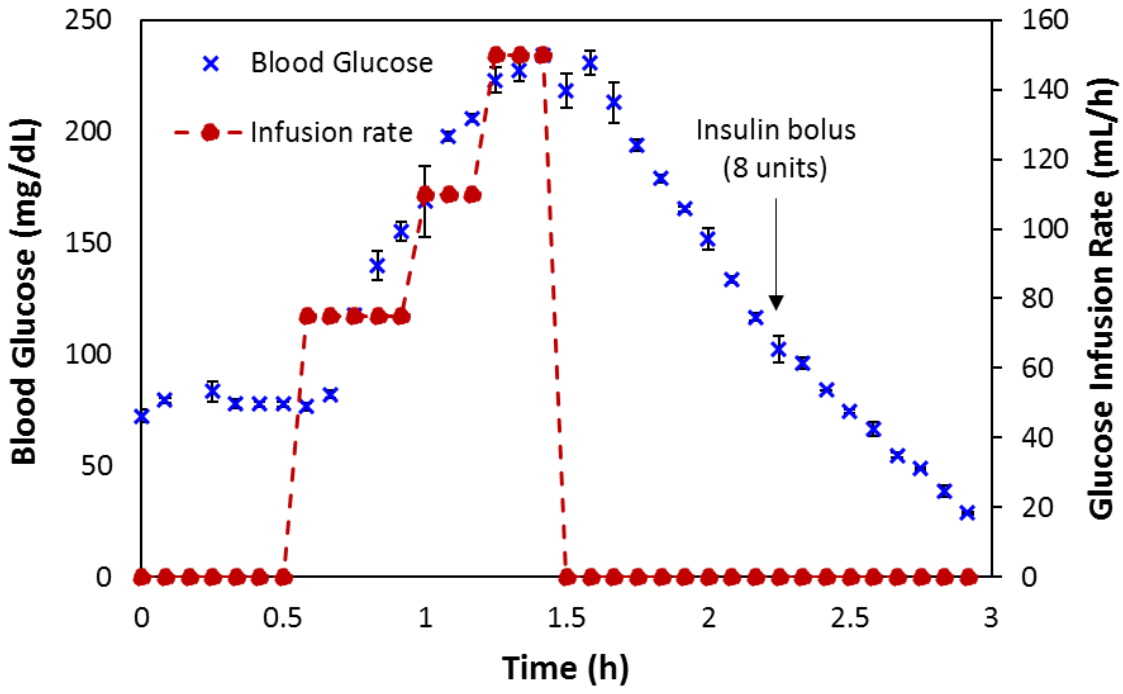

Figure 3-6: Glucose infusion profile versus measured blood glucose values. Dashed red lines serve as visual guides and do not necessarily convey mathematical trends between data points**.**

fabricated by encapsulating gadolinium-gallium-garnet crystals (GGG) in a pHEMA matrix. Capillary blood glucose was measured every 5 to 10 minutes in triplicate with three separate Accu-Check Nano glucometers (Roche, Indianapolis, IN).

3.3. Results and Discussion

3.3.1. Hydrogel Screening and Material Selection

Previous studies with similar glucose-sensitive hydrogel materials focused on evaluating the effects of serum proteins and *in vivo* biofouling on glucose diffusion through the materials and corresponding sensor response characteristics [24]. Their results showed that the change in glucose diffusivity from one week to one month is lowest among materials containing AAm That is, biofouling seems to have the least influence on the sensors made with AAm. Therefore, pHEMA-co-AAm copolymers could be promising for developing a stable and accurate long-term, fully implantable CGM system, which sparked the rationale for using a pHEMA-co-AAm copolymer for the present study. It was hypothesized that adding AAm to the precursor formulation would increase the hydrophilicity of the precursor solution and water content in the polymerized hydrogel (after PBS equilibration), yielding better

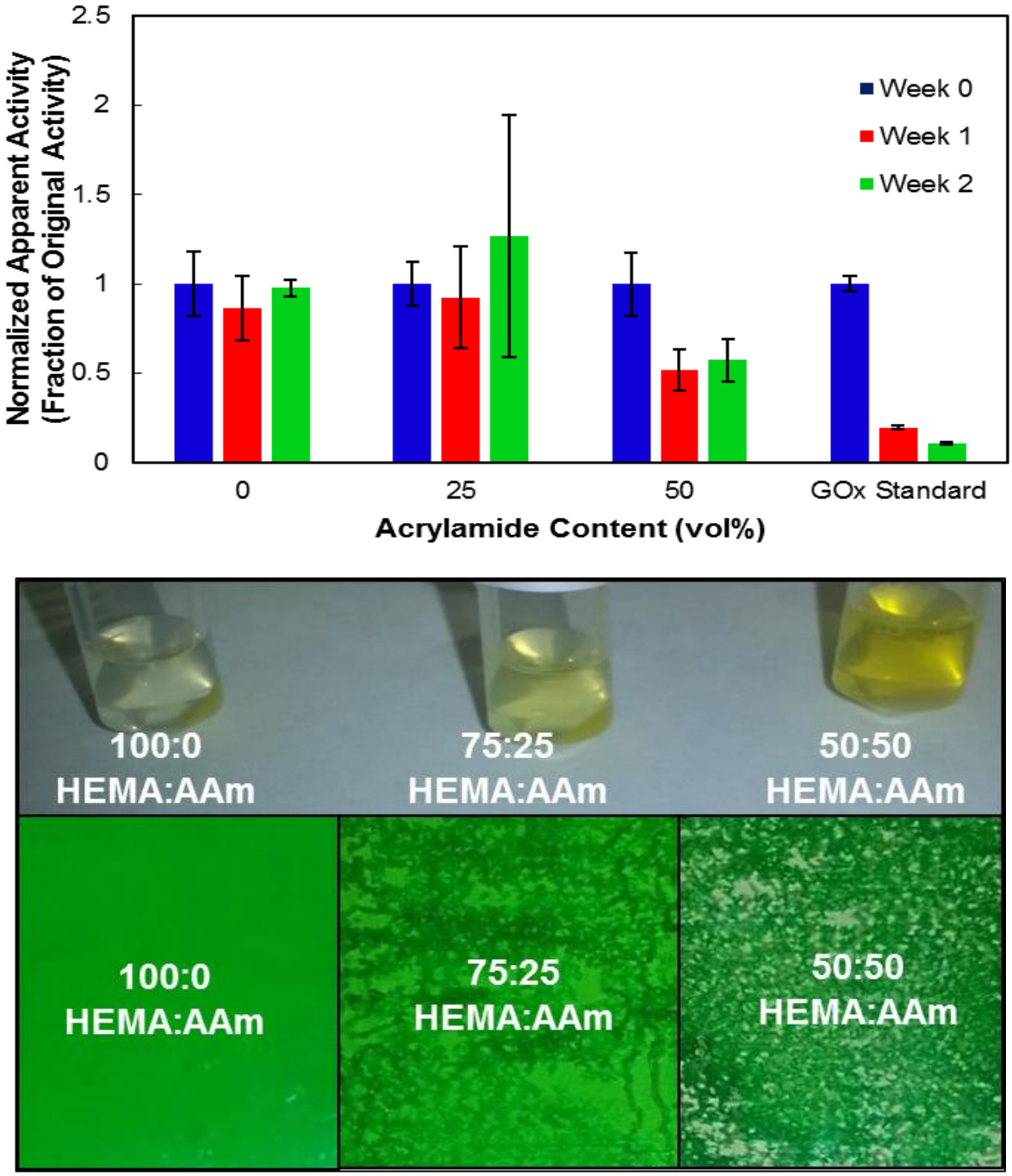

Figure 3-7: Photographs show the solubility of both sensing chemistry components—the GOx enzyme and PdBP dye—in all three hydrogel precursor formulations investigated in this study. Images reveal that an intermediate concentration of acrylamide provides a common middle ground for both sensing chemistry components.

enzyme dispersion throughout the precursor solution and improving thermostability by the polymerized matrix. Interestingly though, incubation of the 50:50 copolymer blend at 37 °C resulted in a statistically significant (t-test, $\alpha = 0.05$) decrease in apparent activity after one and two weeks (Figure 3-7, top), whereas the enzyme activity of the pure pHEMA and the 75:25 copolymer did not significantly change over time. It is known that pAAm gels swell more in water than pHEMA gels [130-132]; for this reason, 50:50 HEMA:AAm may have induced more strain on the enzyme due to swelling rather than protecting its native conformation and preserving activity. It should be noted that sensors were incubated in only PBS between *in vitro* tests to exclusively examine the thermostability of the GOx in the hydrogel matrix. Due to the consumptive nature and production of hydrogen peroxide by the GOx enzyme within the hydrogels, glucose was not added to incubating sensors.

3.3.2. In Vitro Performance

Based on the findings from the screening experiments and prior work, the 75:25 HEMA:AAm hydrogels were chosen for further investigation as a host matrix for this sensing platform [24]. Highly sensitive responses were observed for the glucose range of 0 to 200 mg/dL, as evidenced by the distinct stair-step curve in the raw data during the first four hours of the experiment (Figure 3-8, left). Sensors were exposed to each concentration for one hour and reached a steady-state response (lifetime plateau) within 20 minutes. Overall, at 0 mg/dL and 50 mg/dL glucose, all three sensor response curves appeared very smooth and trended closely with one another with some slight, but negligible, difference in the steady-state response lifetime at 50 mg/dL. More disparity

among the sensors' steady-state response lifetimes is noticeable in the range of 100 to 400 mg/dL glucose. This disparity may result from slight inhomogeneities in gels, as well as variations in sensor strip widths due to manual cutting procedures. These different surface-area-to-volume ratios as well as diffusion kinetics ultimately arrive at a different diffusion-reaction balance and, hence, different steady-state lifetimes [22]. Sensors were determined to have a dynamic range of 12 to 167 mg/dL with a linearized sensitivity of 1.44 ± 0.46 µs/(mg/dL). At the upper limit of the dynamic range, the lifetime of all three sensors was below the natural lifetime of the PdBP dye in this matrix (260.1 ± 4.3 µs) determined from Stern-Volmer experiments (Figure 3-8, inset). This suggests that the upper limit of detection is reached because of flux limitations of the substrates glucose and oxygen rather than complete consumption of oxygen throughout

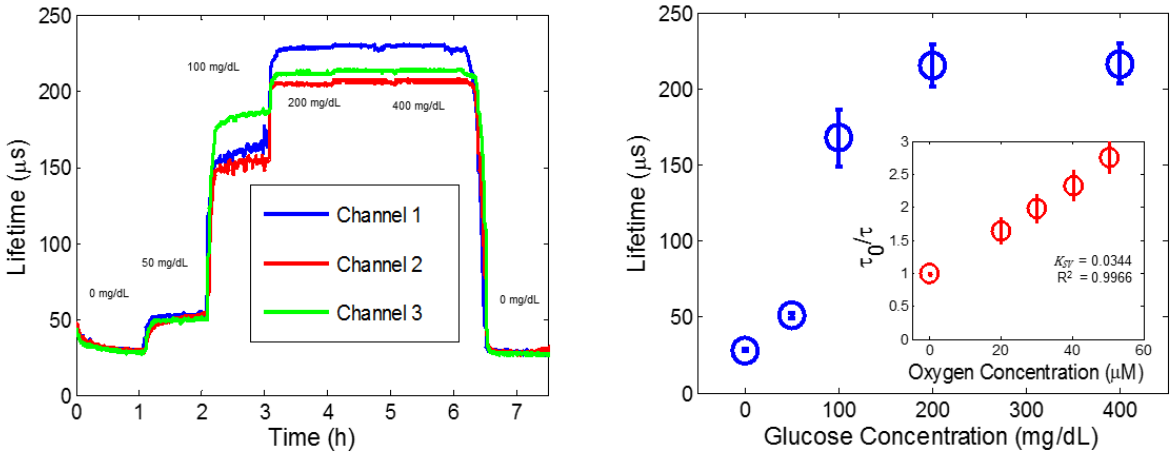

Figure 3-8: (Left) Response of the 75:25 HEMA:AAm copolymer to various glucose concentrations. (Right) Steady-state calibration curves for the 75:25 HEMA:AAm copolymer formulation (n=3, error bars represent 95% confidence intervals). Inset on right graph shows Stern-Volmer oxygen diffusion kinetics underlying the overall glucose response (n=3, error bars represent 95% confidence intervals). Reprinted with permission from SAGE Publications. © 2015 by SAGE Publications.

the entire sensor matrix. In other words, while both substrates are being consumed by GOx, the reaction may not be occurring throughout the entire volume of the sensor, but rather is being limited to the sensor surface due to the rate of substrate replenishment via diffusion into the sensor and the concentration of GOx in the sensor. If the rate of glucose replenishment at the site of the reaction is too high relative to that of oxygen, continued influx of glucose will not result in any further signal change. The system could be in an oxygen-limited state, despite the possibility of oxygen residing in deeper regions of the bulk matrix, resulting in a saturated sensor response before the natural lifetime of the dye is reached. In fact, wider dynamic ranges have been reported in hydrogels with greater pHEMA content when using similar sensing chemistry, further supporting this claim [24].

After exposure to all of the glucose concentrations (50 to 400 mg/dL), the sensors were again exposed to 0 mg/dL glucose (Figure 3-8). The consistent lifetime measurements at 0 mg/dL before (28.7 ± 0.9 μs) and after exposure to various glucose concentrations (27.9 ± 0.9 μs) prove the full reversibility of the sensing system.

3.3.3. In Vivo Performance

Three glucose-sensitive implants were injected into porcine dorsal subcutaneous tissue, and two were successfully located and interrogated transdermally two hours after implantation with the same optical system used for *in vitro* analysis (Section 3.2.3). During the glucose challenge, the oxygen-sensitive control (O2 Ref) and the oxygen-insensitive reference (GGG Ref) implants showed no response to changes in blood glucose levels (Figure 3-9). A drift downward in the O2 Ref lifetime was observed

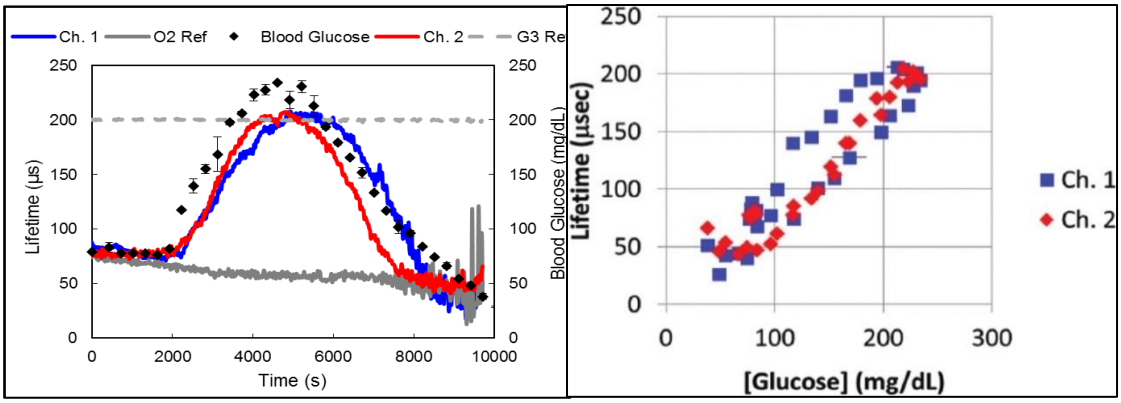

Figure 3-9: *In vivo* responses of subcutaneous sensor implants in the dorsum of a female Sinclair pigs. (Left) Sensor responses 2.5 hours (0 days) after implantation. Adapted with permission from SAGE Publications. © 2015 by SAGE Publications.

throughout the experiment, which is believed to be the result of slow tissue re-oxygenation following a test under hypoxic conditions that was conducted immediately preceding the glucose challenge. The downward-sloping lifetime trend observed during the experiment is likely due to local temperature changes around the sensor due to the electronic puck slightly warming the skin (Figure 3-10).

This downward trend was observed with both oxygen sensors and glucose sensors. The collisional quenching of porphyrins by oxygen is described by the bimolecular quenching coefficient, k_q, by the following relationship

$$k_q = {}^{(4r\pi RDN)}/_{10^3}$$

where r is the quenching efficiency (assumed to be 1), R is the radius of interaction between PdBP and oxygen, D is the sum of the diffusion coefficients of both PdPB and oxygen, and N is Avogadro's number [133]. Because PdBP is immobilized in the hydrogel and all other terms are constant in this application, the only term affecting the

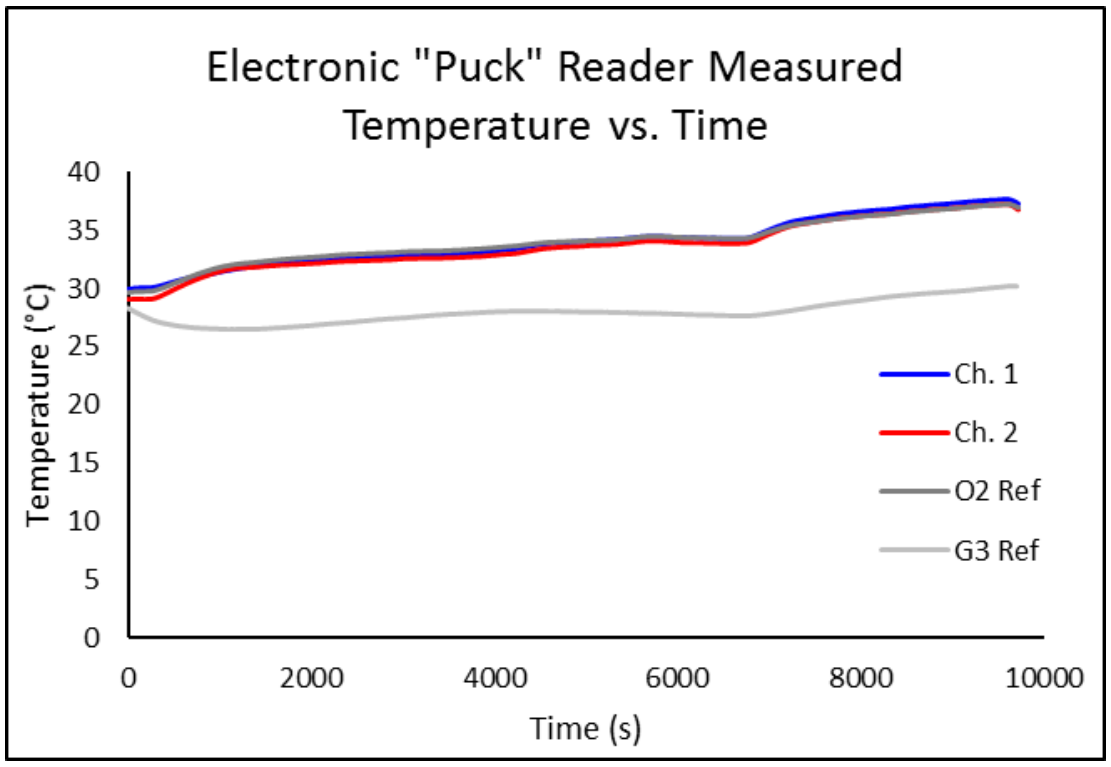

Figure 3-10: Temperature fluctuations for all four reported *in vivo* sensors as measured by the electronic puck readers during *in vivo* glucose modulation.

value of k_q is the diffusion coefficient of oxygen. Further, the diffusion of oxygen is governed by Brownian motion, described by the Stokes-Einstein equation

$$D = {k_B T}/{6\pi\eta d_h}$$

where D is the diffusion coefficient of oxygen, k_B is Boltzmann's constant, T is the absolute temperature, η is the solvent viscosity, and d_h is the hydrodynamic diameter of the Brownian particle (oxygen).

Because changes in the solvent viscosity, hydrodynamic diameter of oxygen are infinitesimally small with the temperature changes observed in this experiment, it can be said that D is directly proportional to T, and k_q is directly proportional to D. Therefore,

the change in k_q is directly proportional to the change in T. Based on experimental data provided by Sinaasappel and Ince, k_q increases linearly with increasing temperature, as expected from the previous equations [134]. Using this experimental data, a proportionality constant relating k_q and T was calculated to be 5.71×10^{-6} μM^{-1}-K^{-1} and was used to predict the change in k_q based on the change in temperature observed in the *in vivo* experiment (from 30 °C to 37 °C, Figure 3-10). Using this model, a predicted lifetime decrease of 84 µs was calculated for the 7 °C increase in temperature; however, a lifetime decrease of only 25 µs was observed. The discrepancy between predicted and observed lifetime decreases can be attributed to using experimental data for PdTCPP to calculate the proportionality constant between k_q and T. It is recommended that temperature calibration experiments be conducted to develop a more accurate model to predict the change in lifetime with fluctuating *in vivo* temperatures. Nevertheless, the mathematical equations and experimental data for PdTCPP agree that the effect of temperature on lifetime arises from a change in the quenching kinetics, governed by Brownian motion, for a given oxygen concentration.

Focusing specifically on the response to glucose, the two glucose-sensitive implants tracked closely with measured blood glucose levels. The peak lifetime was around 200 µs, which is similar to the saturation lifetime seen during the *in vitro* glucose challenge. Additionally, these *in vivo* lifetimes and measured blood glucose values follow closely with observed trends *in vitro* based on the calibration curve data. However, the lifetime curves did not appear to reach a plateau despite the glucose levels rising above the *in vitro* saturation concentration of 200 mg/dL. The extended analytical

range suggests that the subcutaneous sensors did not experience the exact same glucose concentration as was present in blood. Many factors may influence the different behavior observed *in vivo*, including glucose consumption by inflammatory cells during the acute immune response window [135]. Since in this study the sensors were monitored only two hours after implantation, the difference seen here is most likely due to the slower diffusion of glucose *in vivo* in the short time following the insertion wound and the consumptive nature of the sensors [136, 137].

Finally, the different apparent response rate/lag time of the two glucose sensors is attributed to differences in anatomical sensor placement on the pig dorsum, the positioning of the pig during the procedure, and potentially different degrees of tissue trauma caused by sensor insertion. Although sensor-to-sensor variations observed *in vitro* could theoretically affect the *in vivo* response, *in vitro* variability was primarily manifested in different steady-state lifetimes, not response times (i.e., lag time or time to reach steady-state). Since sensor response variations seen *in vivo* are exhibited in time delays, local physiological differences are likely the primary cause of variability here.

Anatomical locations combined with the pig's bodily position during the experiment can affect blood perfusion and, hence, glucose delivery to the sensor. Nevertheless, both glucose-sensitive implants returned to baseline values matching the O2 Ref after the blood glucose levels dropped below about 80 mg/dL. This flattening of the low-glucose response is also consistent with the *in vitro* data, where there is a decrease in sensitivity as glucose falls to lower levels, especially when considering that

the diffusion coefficient of glucose is likely substantially lower in subcutaneous tissue compared to the *in vitro* flow cell setup.

Pertaining to the scatter plot (Figure 3-9, right), measured real-time, uncorrected single-point lifetime values are plotted against the average blood glucose values obtained from the same blood droplet using three glucometers (horizontal error bars indicate one standard deviation in blood glucose). Channel 2 shows consistent clustering of lifetime values for similar glucose values, whereas channel 1 exhibits significant hysteresis in the measurements indicating a less reversible sensor response. This difference results from a different delay period observed for rising versus falling glucose levels (the higher levels represent measurements made on the falling edge). These differences are attributed to the local tissue environment, which will have unique characteristics related to the specific short-term host response to each implant. In practice, this may result in the need to calibrate the device more frequently throughout the day, as trends predicted as the glucose is rising may not accurately predict the rate at which glucose decreases. Errors in predicted blood glucose changes could result in under correction or over correction of rising and falling blood glucose levels, causing the patient to administer improper insulin dosages.

Because the study mentioned above was conducted on the sacrifice day of the pig, longer-term studies with the 75:25 HEMA:AAm formulation were conducted in a subsequent pig. In Figure 3-11, glucose challenge data are shown after seven days of implantation. Although the baseline lifetime (~1500 seconds) starts around 60 microseconds (similar to the day 0 timepoint presented in Figure 3-8), there is a more pronounced time lag throughout the duration of the glucose challenge. Furthermore, while the "fresh" implants (day 0) exhibited a uniform bell-shaped curve that closely followed the measured blood glucose levels in real-time and promptly declined after the administration of glucose, the response at day 7 assumed more of a plateau shape starting around 4000 seconds into the glucose challenge while the measured blood glucose levels continued to rise. While the blood glucose began declining shortly after

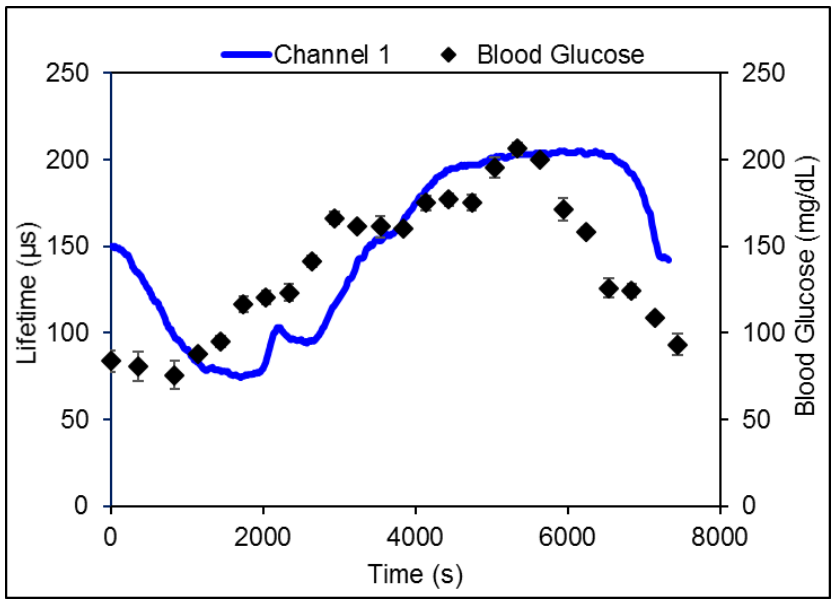

Figure 3-11: *In vivo* responses of a pHEMA-co-AAm hydrogel subcutaneous sensor seven days after implantation.

5000 seconds, the measured sensor lifetime did not reflect this change until ~1500 seconds later. These differences can be attributed to the foreign body response around the implant which is known to involve highly metabolic cells such as macrophages, and the formation of granular tissue on the order of days once a material is implanted in the body. Not only could the presence of cells and granulation tissue affect the diffusion of glucose and oxygen to the sensor by physical means, the immune cells could also consume both substrates in an effort to carry out their natural immune response cascades and ultimately resume homeostasis [33, 38, 125, 126].

It is also worth mentioning that no glucose modulation was observed past seven days of implantation. Starting baseline luminescence lifetimes of glucose sensors were over 200 µs (Figure 3-12), indicating extremely low oxygen concentrations near the sensor. A starting luminescence lifetime of ~200 µs indicates extremely low oxygen concentrations, as this signal level is close to the natural lifetime of the dye (lifetime in

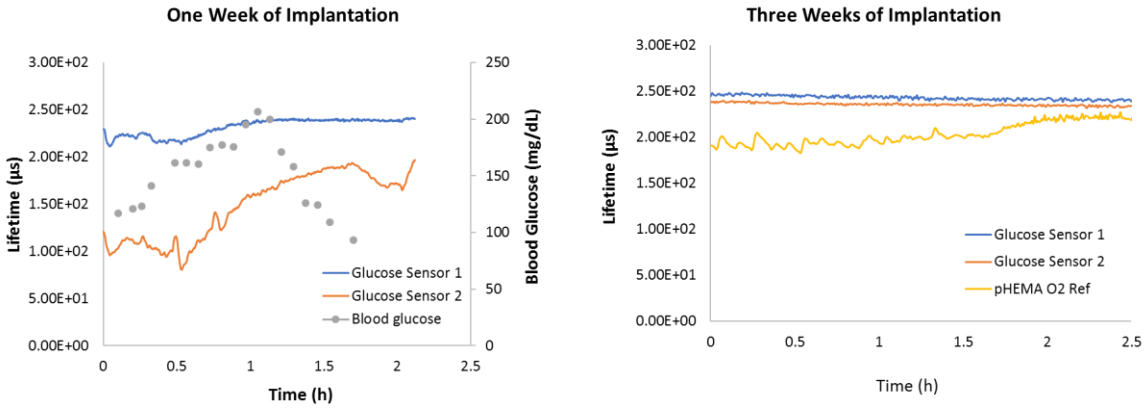

Figure 3-12: Comparison of glucose responses of the same sensors in the same pig one week and three weeks after implantation

the absence of oxygen). Representative results showing decrease in response to glucose from one to three weeks of implantation can be seen in Figure 3-12 below; week one and week three sensors are identical in formulation and from the same pig. Because of this drastic loss in sensor response at three weeks, these experiments highlight the need to investigate and refine substrate transport balance throughout the matrix.

3.4. Conclusions

This chapter shows that enzymatic sensors based on monitoring phosphorescence lifetime in copolymer hydrogels can be designed to respond to glucose concentrations *in vitro* up to 200 mg/dL. These materials also demonstrated the ability to monitor blood glucose levels over hyperglycemic, euglycemic, and slightly hyperglycemic blood glucose concentrations *in vivo* using a porcine model. This study demonstrates the first successful tracking of real-time *in vivo* glucose response from a fully implantable enzymatic glucose sensor measuring luminescence lifetime instead of intensity [77]. Therefore, this work represents an important advance toward non-invasive monitoring of injected sensor devices for chronic disease and personal health management. It is important to note that these data involve only the response of freshly implanted sensors. Long-term foreign body response effects (i.e., on the order of months) are not considered here. However, the fully-implantable nature of these systems reduces the chances of infection and physical stresses that can cause chronic tissue irritation. Furthermore, advances in specialized materials (e.g., microporous structures) provide promise that such hydrogels could meet the requirements for safe, effective, and minimally invasive long-term monitoring. Future work will involve conducting long-term stability tests *in*

vivo in porcine models and *in vitro* under physiological storage conditions for this particular copolymer/enzyme/porphyrin sensor formulation as well as other promising candidate materials. Additionally, the hydrogel chemical properties will be tailored to increase the analytical range measured *in vitro* with the ultimate goal of extending the device's *in vivo* functional lifetime.

4. INVESTIGATING OXYGEN TRANSPORT AND ENZYME STABILITY[*]

4.1. Introduction

As discussed in Chapters 2 and 3, development of a biocompatible glucose sensor requires the device to function in its application long-term, despite any FBR effects that may alter the ability of substrates to diffuse throughout the sensor and/or the substrate oxidation reaction to catalyze. Because of drastically fluctuating physiological conditions around the sensor implants during the wound healing phase, extending the operational lifetime of a fully implantable sensing platform long-term *in vivo* has yet to be realized. To optimize the *in vivo* operational lifetime of these devices, an *a priori* understanding of the relationship between matrix chemistry and device performance metrics must be established. Detailed study of the impact of hydrogel matrix properties on substrate diffusion and overall sensor response should impart knowledge necessary for improved rational sensor design and optimized function.

Loss of enzymatic activity affects overall device performance. With multicomponent systems such as these flux-based sensors, it is difficult to troubleshoot changes in overall device performance among formulations without foreknowledge of enzyme-matrix interactions and how a particular hydrogel formulation may stunt or accelerate enzyme activity loss. By the same token, designing a device without such a

[*] Parts of this section are reprinted with permission from R. M. Unruh, J. L. Weaver, and M. J. McShane, "Hydrogel matrix effects on oxygen diffusion: Controlling properties for biosensor applications," in *2015 IEEE SENSORS*, Busan, South Korea, 2015, pp. 1-4: IEEE Xplore, 2015. © 2015 by IEEE.

knowledge base can prove to be a time-consuming and expensive affair. With the vast material combinations and immobilization techniques, a method to rapidly screen enzyme/material combinations is necessary to build an adequate library of *a priori* knowledge for rational device design.

Some efforts have been made to quantify apparent activity of GOx immobilized in hydrogels. The Peppas group has monitored apparent activity of immobilized GOx by measuring the pH drop over time in a GOx microparticle suspension [115]. However, the efficacy of this method could be hindered in buffered solutions designed to resist pH change. Additionally, the reaction rate of GOx itself is pH-dependent, changing the apparent activity as an effect of changing pH levels. The Ratner group has developed a method for measuring apparent GOx activity assay whereby acid production levels are monitored and the pH is maintained by titration of sodium hydroxide; GOx apparent activity can be measured by measuring total volume of sodium hydroxide added [138]. However, this method requires relatively large volumes of assay liquid, and its throughput is low since only a single gel sample can be tested at a time with standard titration devices. Liu *et al*. have employed an endpoint assay to assess the bioactivity of GOx-loaded alginate microbeads based on the Trinder method, which uses 4-aminophenazone as a colorimetric indicator of peroxide production [139]. Brahim *et al*. used an endpoint method for GOx-loaded pHEMA gels to spectrophotometrically detect peroxide levels with dimethylaminobenzoic acid [109]. The nature of these endpoint assays is that they only provide discrete measurements of peroxide level within a sample, preventing observance of real-time peroxide production. Sensors with

functionalized with GOx and a porphyrin dye operate under diffusion-reaction balance, proving difficult to determine steady-state behavior without real-time monitoring [22, 24, 28, 65, 140]. When determining apparent activity of enzyme-loaded gels, a method to observe the peroxide production profile is helpful to ensure that the assay is run long enough to achieve the reaction-diffusion equilibrium (i.e., linear peroxide production versus time). The goal for the present study were to (1) increase throughput of the number of hydrogels tested at a given time, (2) avoid dependency on pH changes to detect GOx apparent activity, and (3) maintain the ability to monitor the GOx reaction in real time while minimizing reagent volume.

In this study, a term coined the "apparent enzymatic activity," a term assimilating diffusivity and reactivity of immobilized enzyme/substrate platforms into one metric, is applied and quantified. pHEMA and poly(acrylamide) hydrogels were chosen as the immobilization substrate based on their optical clarity abundant use in chemical and biomedical applications [28, 65, 95, 108, 109, 111, 138, 140-147].

A series of pHEMA copolymer formulations were fabricated with equivalent amounts of total protein, but with varying amounts of GOx enzyme, and tested for apparent activity using an absorbance-based assay and a plate reader. The scope of this section is to outline the methodology used to quantify apparent GOx activity and set the stage for developing the aforementioned library of *a priori* knowledge of GOx/material interactions as a segue for optimized material selection for enzyme-containing devices. Detailed study of the impact of hydrogel matrix properties on substrate diffusion and

overall sensor response will impart knowledge necessary for improved rational sensor design and optimized function.

Toward this aim, a series of experiments are designed to investigate how matrix chemistry affects glucose and oxygen transport, GOx stability, and the overall sensor performance. These experiments are organized into several overarching thrusts: (1) identify an array of promising alternative hydrogel materials to pHEMA-co-AAm and screen these materials in a high-throughput manner to hone in on promising material candidates for enzyme stability over a one-month timeframe, (2) filter out the most promising material candidates from thrust 1 to quantify substrate diffusion, and (3) test the overall sensor response profile on the formulations from thrust 2 and relate the response to the various sensor metrics and figures of merit.

4.2. Experimental Methods

4.2.1. Materials

GOx was purchased from BBI Enzymes (Cardiff, UK). TEGDMA and HEMA were purchased from Polysciences (Warrington, PA). Sodium acetate trihydrate, horseradish peroxidase (HRP), *o*-dianisidine, 2,2-dimethoxy-2-phenyl-acetophenone (DMAP), ethylene glycol, and 1-Ethyl-3-[3-dimethylaminopropyl]carbodiimide hydrochloride (EDC) were purchased from Sigma (St. Louis, MO). Sodium chloride, potassium chloride, potassium phosphate (dibasic), sulfo-N-hydroxysuccinimide (sulfo-NHS), and DMSO were purchased from VWR® (Radnor, PA). Sodium phosphate (monobasic) was purchased from ACROS Organics (ThermoFisher Scientific, Waltham,

MA). Acrylamide was purchased from AMRESCO (Solon, OH), and glucose was purchased from Macron Fine Chemicals (Center Valley, PA).

4.2.2. Hydrogel Fabrication

Hydrogels were fabricated according to previously described methods (Section 3.2.2) with a few slight changes [65]. In some formulations, the type of comonomer(s) was changed. Comonomers investigated here include AAm, N, N-dimethylacrylamide (DMA), N-vinylpyrrolidone (NVP), and 3-[Tris(trimethylsiloxy)silyl] propyl methacrylate (TRIS), with each formulation

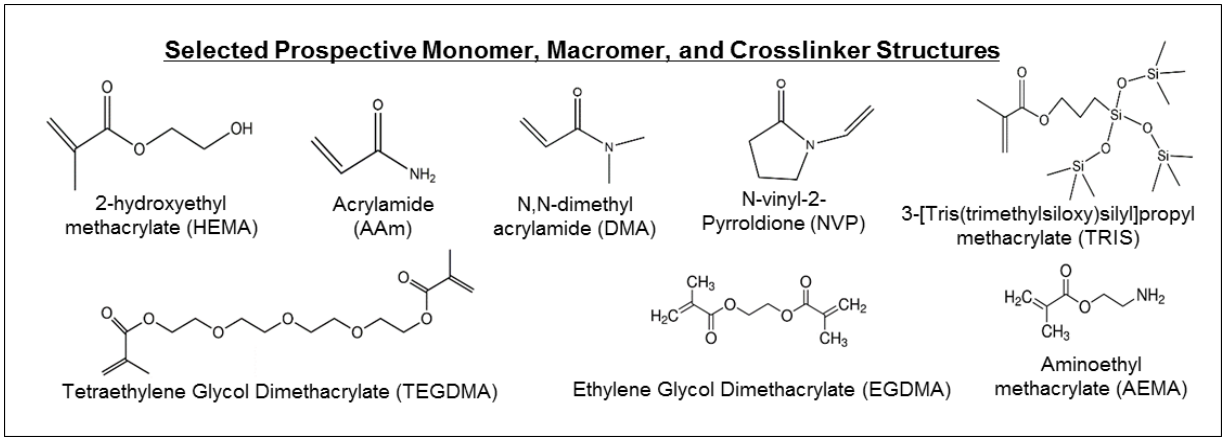

Figure 4-1: Structures of selected hydrogel matrix components (monomers and crosslinkers)

Table 4-1: Table of monomer combinations. Both 75:25 and 50:50 HEMA:comonomer ratios were tested for each formulation (with the exception of the pHEMA homopolymer).

Hydrogel Formulations with TEGDMA	Hydrogel Formulations with EGDMA
pHEMA	pHEMA
pHEMA-co-AAm	pHEMA-co-AAm
pHEMA-co-DMA	pHEMA-co-DMA
pHEMA-co-NVP	pHEMA-co-NVP
pHEMA-co-TRIS	pHEMA-co-TRIS

containing at least 50% HEMA (Figure 4-1, Table 4-1). These materials were chosen based on their established use in biomedical applications, such as contact lenses (HEMA and TRIS), their hydrophilicity and ability to enhance hydration of the gel matrix (AAm, DMA, and NVP), and their notable oxygen transport (TRIS, DMA) [148].

4.2.2.1. Gels for Screening

All gel precursors contained 250 µL of monomers (HEMA and necessary comonomers), 2.5 mg of DMPA, 5 µL of crosslinker (TEGDMA or EGDMA), 50 µL of dye solution in DMSO, 90 µL of ethylene glycol, and 107.5 µL of protein solution (GOx or GOx + bovine serum albumin (BSA), see table below). Precursors were injected into glass slide molds with 0.01-in.-thick Teflon spacers. Gels were photopolymerized with UV light (365 nm, 140 watts, three minutes per side). The resulting crosslinked gels were removed from the mold, rinsed with DI water, and placed in 40 mL of PBS. To further immobilize GOx in the gels, 5.6 mg of EDC and 16 mg of sulfo-NHS were dissolved in 250 µL of PBS and added to the tube containing the PBS and polymerized

gel slab. Gels in PBS with EDC/sulfo-NHS were allowed to equilibrate overnight on a nutating mixer (VWR) at room temperature.

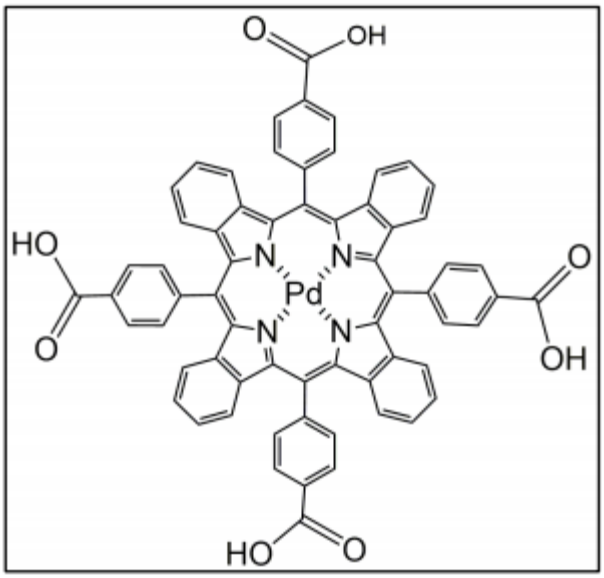

Figure 4-2: Structure of the tetracarboxylate benzoporphyrin (PdBP-acid)

After overnight equilibration in PBS, hydrogel discs (5-mm diameter) were punched with a biopsy punch and placed in tea balls for incubation under physiological conditions (explained in Section 4.2.3). This is one key change in the experimental setup from the thermostability screening experiments conducted in Chapter 3, Sections 3.2.2.1 and 3.3.1. Additionally, the phosphor used in these screening experiments was tetracarboxylated instead of tetramethacrylated (PdBP-acid, Figure 4-2). Only for the purposes of these screening experiments was a tetracarboxylated dye used. The reason

for changing the dye stems from the fact that the tetramethacrylated form of the dye acts as an additional crosslinker to the matrix. The goal of this study was to isolate the matrix properties themselves and evaluate their effect on enzyme stability without any change in water content or substrate transport from the sensing assay itself. In other words, the matrix chemistry itself should be the only factor to influence enzyme stability. Chapter 2 established that PdBP solubility can vary with precursor formulation chemistry, especially the tetramethacrylated version of the dye. If the dye, which could precipitate in some precursor solutions, forms covalent bonds with the polymer matrix but is not completely dissolved, then the amount of total polymerizable crosslinker could vary from formulation-to-formulation, introducing an unnecessary variable into the experiment.

While it is beneficial to have a benzoporphyrin physically present in the hydrogel matrix because the enzyme itself could physically interact with the dye (and to keep the enzyme environment as consistent as possible with the implanted sensors for the sake of consistency in this specific application), the goal of this study was to identify promising gel matrix candidates for promoting enzyme stability in general using this GOx-based sensing platform as a model example of a system requiring optimal enzyme stability. In order to translate findings from this study to other enzymes for other applications, the results should not depend on the use of an additional crosslinker such as PdBP.

4.2.2.1.1. Screening Experiment Set One

For the first set of experiments, GOx (2.3 μM) was added to the gel formulations equivalent to the GOx concentration used in Chapter 3 thermostability screening

experiments (Section 3.2.2.1). The difference between these experiments and the screening experiments in Chapter 3 is that here GOx was incubated in glucose (100 mg/dL) in PBS at 37 °C, as opposed to only PBS at 37 °C (illustrated in Figure 4-3), and was tested for apparent activity over a longer period of time (four weeks versus two weeks in Chapter 3). Keeping the GOx concentration the same as in previous thermostability experiments allowed a direct comparison of incubation with and without glucose for the same GOx concentration.

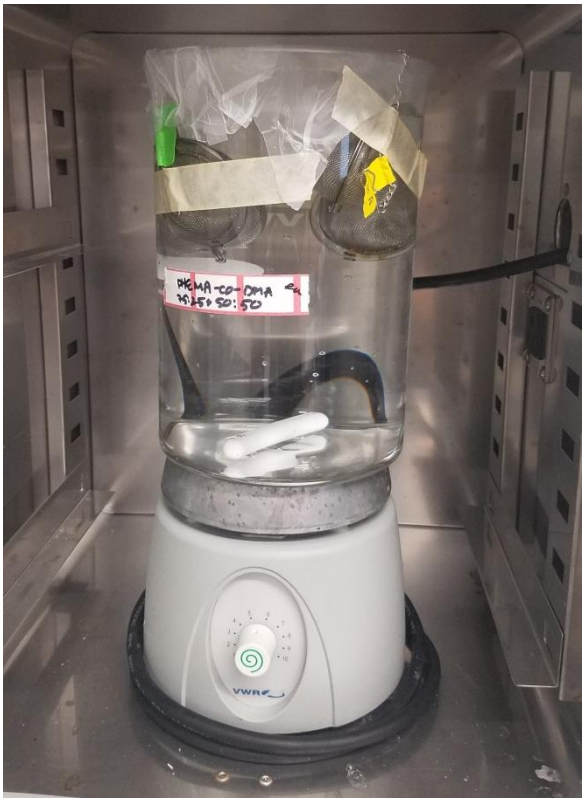

Figure 4-3: Tea wash incubation setup showing gel discs encased in a tea strainer with the chain strapped to the exterior of the beaker. Beaker is filled with PBS, covered with parafilm, and placed on a magnetic stir plate in an incubator at 37 °C.

4.2.2.1.2. Screening Experiment Set Two

For the second set of screening experiments, gels were fabricated as stated in Section 4.2.2.1.1, but the total protein content in the protein solution added to the precursor was kept constant at 40.0 mg/mL, equivalent to the mass of protein in the sensor implant precursor solutions. Various ratios of BSA to GOx in the protein solution were investigated while keeping the total protein content constant at 40.0 mg/mL (Table 4-2). The rationale behind adding BSA to the gels is that enzyme stability is concentration-dependent [43].

BSA has been used as a stabilizing excipient in solution-phase and solid-surface protein immobilization processes, acting as a molecular chaperone or excipient [149-152]. Reducing the overall protein content initially allows a sufficient working range of the assay and a more direct comparison to initial screening studies conducted in Chapter 2. However, enzyme stability is known to be concentration-dependent and could exacerbate enzyme deactivation and negatively impact long-term stability (on the order of weeks) [102, 153].

While the purpose of this study is to investigate the effect of matrix chemistry on enzyme stability in hydrogels by using GOx as a model enzyme, GOx stability results from these screening experiments can also be used as a first-pass test to identify promising hydrogel formulations for implantation. However, one should be mindful of the fact that the GOx concentrations used thus far have been significantly less than the GOx concentrations used in implants, albeit due to different testing conditions during screening tests (static fluid) versus implant strip tests (continuous fluid flow). Because

GOx stability is concentration-dependent, one way to alleviate the effects of accelerated GOx deactivation is to supplement the matrix with a filler protein (i.e., BSA) to ensure that the total protein content is equivalent to that of the implant gels (40.0 mg/mL in the precursor). Additionally, this approach allows for investigating the proportion of GOx relative to the total protein content, a factor that could also affect the overall apparent activity by (1) affecting the overall amount of substrate catalyzed and (2) altering the rate of peroxide generation, a compound known to deactivate GOx. Because of these complex dynamics of enzyme catalysis and stability, the following BSA:GOx ratios were investigated for each candidate gel formulation, outlined in Table 1. Investigating various BSA:GOx ratios could reveal trends of the GOx concentration on GOx stability over time when the total protein content is held constant. By keeping the total protein constant, trends in GOx stability could be extrapolated to predict the stability of GOx at 232.5 µM or 40.0 mg/mL, the concentration traditionally used in the implants.

Table 4-2: Concentrations of BSA and GOx for each respective GOx dilution. Dilution factors are calculated relative to the amount of GOx used in a typical injectable sensor formulation.

GOx Dilution Factor	[GOx] (mg/mL)	[BSA] (mg/mL)
10×	4.0	36.0
20×	2.0	38.0
50×	0.8	39.2
100×	0.4	39.6

4.2.2.2. Gels for Testing Sensor Figures of Merit (i.e., Substrate Transport and Optical Response to Glucose)

Downselected hydrogels (determined by primary screening results) were selected for further investigation. Promising formulations were identified by comparing the apparent activity retained for each gel over the four-week period. Gels exhibiting at least 75% of the change in absorbance per second when compared to the 75:25 HEMA:AAm formulation were selected for further characterization (i.e., substrate transport and optical response to glucose). In addition to screening results, other factors such as the potential for adequate substrate transport balance (i.e., increasing oxygen permeability and reducing glucose permeability relative to 75:25 HEMA:AAm) were considered when designing formulations for implantation.

4.2.3. Hydrogel Incubation

Once the gel slabs were fabricated, they were punched as described in Section 4.2.2 and placed in tea strainers. The tea strainers were used for the purpose of holding the gel discs and allowing the incubation solution to pass through freely during the four-week incubation period. Twenty-four discs of each formulation were placed in individual tea strainers and clamped closed, as well as secured with wire laterally on both sides of the clamp. The eight tea strainers were placed in a 2-L beaker (chains taped to the outside), filled with 2 L of PBS solution with 100 mg/dL glucose added, covered with parafilm, and placed on a stir plate in an incubator overnight. Each day, the solution was exchanged for fresh PBS + glucose solution.

Each week, to prepare the discs for apparent activity testing, six discs from each formulation were placed in a 15-mL centrifuge tube filled with 50-mM NaOAc buffer (pH 5.1) and were allowed to equilibrate overnight at 4 °C. To test for apparent activity, NaOAc-equilibrated gels were placed in a flat-bottom, 96-well plate as described in Section 4.2.4.2.

4.2.4. Testing for Gel Figures of Merit

4.2.4.1. Swelling Ratios

Hydrogels were prepared similar to methods described in Section 3.2.2.2, except the PdBP-acid dye was used in place of the PdBP dye and monomers were altered according to the desired formulation to polymerize. After photocuring and equilibration, five discs from each formulation were punched with a disposable biopsy punch (5 mm diameter, VWR). Each disc was blotted on a Kimwipe to remove excess water and then was weighed on an analytical balance (Mettler Toledo) to obtain the hydrated mass. The gel discs were dried under the house vacuum overnight (>24 hours) and weighed again to obtain the dried weight (W_d). The swelling ratio (equilibrium water content, EWC) was calculated from the percent difference in the two weights according to the following equation:

$$EWC = \frac{W_s - W_d}{W_d} * 100$$

4.2.4.2. Glucose Oxidase Stability—Absorbance-Based Apparent Activity Assays

In order to maximize the number of formulations tested, the apparent activity of the enzyme was tested in the highest-throughput manner possible. In order to accomplish this, 5-mm diameter discs loaded with GOx, BSA, and PdBP-acid were punched from

each hydrogel slab and placed in a 96-well plate for the purposes of quantifying the apparent activity using an o-dianisidine colorimetric absorbance assay. The discs were tested for initial apparent activity, as well as stability over a one-month period by incubating under physiological conditions (PBS, pH 7.4, 37 °C, 100 mg/dL glucose).

Discs were cut from a hydrated gel slab (Figure 4-4, step 1) and prepared for testing by soaking in sodium acetate buffer (NaOAc, 50 mM, pH 5.1, 4 °C) overnight in a 15-mL centrifuge tube on a nutating mixer (Figure 4-4, steps 2 and 3). The following day, the tubes containing gels soaked in sodium acetate were removed from refrigeration and placed in an incubator to warm them near the assay temperature (35 °C) and minimize the temperature gradient between the storage condition (4 °C) and the assay testing condition (35 °C).

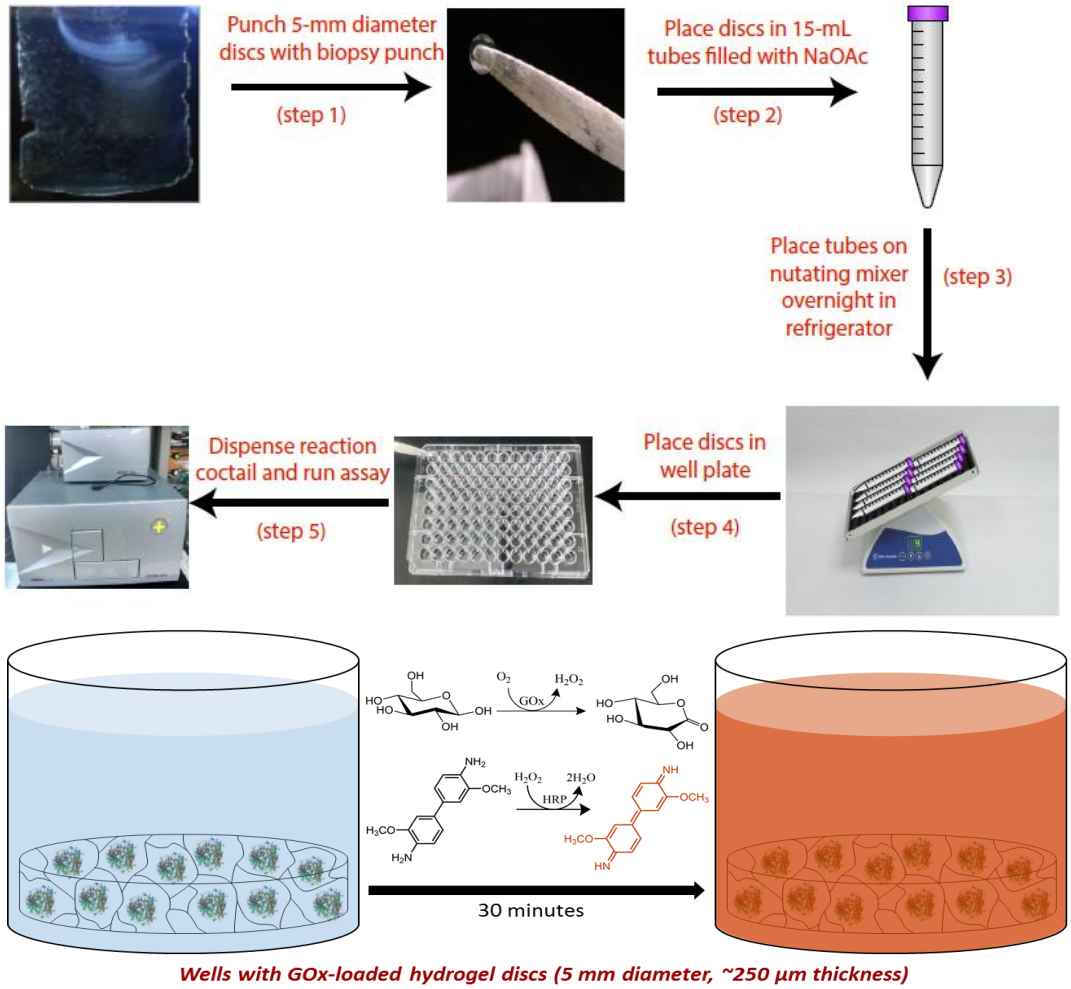

Figure 4-4: (Top) Gel disc preparation and assay setup scheme; (Bottom) Illustration of the colorimetric change which occurs due to the coupled redox reactions in the assay.

To conduct the assay, a reaction cocktail of glucose, o-dianisidine, and HRP in sodium acetate was prepared according to established protocols [129]. Concentrations of each ingredient were made according to a standardized assay method for free GOx enzyme [129]. Gels were tested for GOx apparent activity after initial overnight soaking in PBS (week 0) and weekly thereafter for three additional weeks after exposure to physiological conditions (solution containing PBS at pH 7.4 and 100 mg/dL of glucose

at 37 °C; solution changed daily). All gels were prepared for screening tests by placing the gel discs into 15-mL centrifuge tubes containing sodium acetate buffer at pH 5.1 for 24 hours before running the assay. The next day, the gels were placed in wells of a 96-well plate, and 200 µL of reaction cocktail was dispensed into each well. For each timepoint, a fresh GOx standard solution (9.73-nM enzyme in NaOAc buffer at pH 5.1) was prepared. Briefly, a 2-mg/mL solution of crude protein reagent was made in NaOAc buffer, pH 5.1. This solution was diluted 1000× in the NaOAc buffer to achieve the final GOx concentration. The GOx reagent was determined to be 78% enzyme via UV-Vis. A plate reader (Tecan, Infinite 200 PRO) was used to measure solution absorbance at 495 nm in one-minute kinetic interval cycles for 30 minutes (30 kinetic cycles).

The absorbance versus time for each sample was plotted, and the linear portion of the curve was used to identify where GOx was reacting at its maximum velocity, V_{max}. The slopes of the linear portion of each curve for each sample were used to determine the comparative apparent activity among all samples. This procedure was performed after fabrication and weekly upon storage in 100 mg/dL of glucose in PBS at 37 °C for one month.

4.2.4.3. Substrate Transport

4.2.4.3.1. Oxygen Diffusion—Stern-Volmer Kinetics

Stern-Volmer oxygen diffusion experiments were carried out similar to the methods described in Section 3.2.3.3 and Figure 3-5. Gel strips (0.75 × 0.75 × 5 mm) were tested according to previous methods [28, 65]. Phosphorescence lifetimes were recorded using the previously described custom optical interrogation system with a pulsed LED and

silicon PMT (SensL). Sensors were exposed to various oxygen levels (0, 2, 5, 10, and 21 $\%O_2$) using a custom benchtop system controlled by two mass flow controllers and were confirmed with a picoammeter (Figure 3-5).

4.2.4.3.2. Sucrose Diffusion

Gels for sucrose diffusion were fabricated as described in Section 4.2.2.1 for screening—0.01-in.- (~250-µm-) thick Teflon spacer, glass slide mold—in order to minimize the path length for the saccharide to permeate from the feed chamber (thus

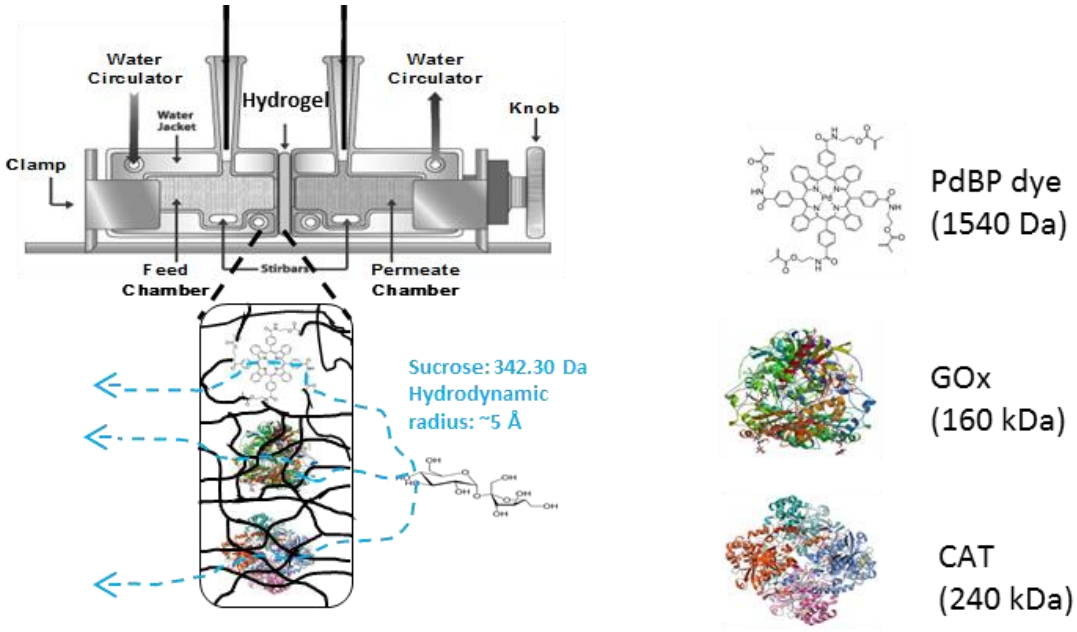

Figure 4-5: Illustration of Side-by-Side diffusion cell setup**.**

expediting results), through the gel, to the permeate chamber. Horizontal side-by-side diffusion cell systems were used as detailed in prior work and illustrated in Figure 4-5 [28, 65]. Square gel cutouts (1 × 1 in.) were immobilized between two reservoir chambers

(one feed chamber with analyte in PBS and one permeate chamber with only PBS). Feed reservoirs contained a 22.2-mM sucrose solution (equivalent to the molar concentration of glucose in blood at the upper end of the physiological hyperglycemic range); choosing a hyperglycemic initial feed chamber concentration created a greater concentration gradient between the feed and permeate chambers, decreasing the time to detect a measurable sucrose concentration on the permeate side and thus decreasing the overall experiment time for each formulation.

Sucrose was used as a surrogate analyte for glucose due to low GOx selectivity for sucrose. Permeate reservoirs contained pure PBS solution. To determine the rate of sucrose diffusion, samples were taken from both chambers three times daily and analyzed using a YSI 2700 Select Biochemistry Analyzer (Yellow Springs, Ohio). A linear fit was applied to the [sucrose] versus time data to calculate the concentration change rate. To calculate a relative diffusion coefficient, Fick's second law of diffusion was used, assuming homogeneous mixing and the following boundary condition: [sucrose] = 0 mM at t(0) in the permeate chamber [10]. Applying these conditions yields the following equation:

$$D = \frac{dC}{dt}\left(\frac{lV}{\Phi A C_0}\right)$$

where D is the diffusion coefficient of sucrose in cm^2/s, $\frac{dC}{dt}$ is the change in permeate reservoir analyte concentration over time, l is the gel thickness, V is the chamber volume, A is the surface area of the orifice between the two chambers, C_0 is the initial

concentration of sucrose in the feed chamber at t=0, and ϕ is the partition coefficient (assumed to be 1, as the apparent diffusivity was of prime interest for these purpose of this study). All formulations were tested in triplicate at 25 °C.

4.2.4.4. Optical Response to Glucose

In this study, sensors were tested at ambient oxygen (21%) using a flow-through system as described in Figure 3-4, Section 3.2.3.2. Glucose levels were modulated from 0 mg/dL (baseline lifetime) to 50, 100, 200, and 400 mg/dL before returning back to baseline levels (0 mg/dL). Glucose concentrations were changed in a step-wise manner and kept constant until sensors reached a steady-state response.

4.2.4.5. Homogeneity Visualization—Confocal Laser Scanning Microscopy

Staining of the gels with Nile Red was adapted from Bailey, *et al*. 2012 [154, 155]. First, a 20-mg/mL solution of Nile Red (Sigma) in methanol was dissolved in a dram vial by vortexing for one minute. A 75-µL aliquot of this dye solution was added to 8 mL of DI water in a 20-mL scintillation vial and was vortexed for one minute. Next, the 8-mL solution was diluted by adding it to 120 mL of PBS in a beaker under constant stirring. Gel discs (5-mm diameter) were punched from the gels with a biopsy punch. Each disc was placed in a separate centrifuge tube filled with 50 mL of the diluted Nile Red solution in PBS and was placed on a nutating mixer at room temperature for 24 hours. After 24 hours, the Nile Red solution in PBS was discarded, and the stained gel discs were placed in fresh centrifuge tubes with 50 mL of fresh PBS, allowing nutation at room temperature for 24 more hours. The washing process was repeated three times, and the discs were stored in PBS until imaging.

Confocal Laser Scanning Microscopy (CLSM) images were taken on an Olympus FV1000 confocal microscope. Excitation of the Nile Red stained gels was accomplished with a helium-neon laser (543 nm); emission was collected from 650 to 700 nm. Images were obtained 100 µm into the sample.

4.3. Results and Discussion

4.3.1. Swelling, Apparent Activity, and Stability—Screening

4.3.1.1. Swelling and Initial Apparent Activity

Gel discs for swelling were weighed and thickness was measured with calipers. Percent changes were calculated as described in Section 4.2.4.1. These data were collected and plotted for comparison to initial apparent activity values, which were gathered as described below. For screening initial apparent activity, gel discs, as well as a GOx standard (2 µg/mL in 50-mM NaOAc buffer, pH 5.1), were loaded into a 96-well flat-bottom polystyrene well plate, as depicted in Figure 4-6. This configuration was maintained for the duration of the study. Assays were run according to methods outlined in Section 4.2.3.2, and results are presented in Figures 4-7 and 4-8.

With the exception of the 50:50 HEMA:AAm and 50:50 HEMA:DMA (TEGDMA crosslinker only), initial apparent activity of the GOx increased with increasing water content, likely due to increased permeability to glucose with increased water content. Considering the two exceptions to this behavior stated previously, the observed behavior can be attributed to (1) lower concentration of enzyme per unit volume of gel after equilibrating in water and (2) more GOx release from the surface of the gel after fabrication versus other formulations. The 50:50 HEMA:AAm formulation

had the highest variability in initial apparent activity of all formulations tested (both TEGDMA and EGDMA crosslinked formulations). Overall, the correlation between apparent activity and thickness (Δt) is not as strong, which can be attributed to manual measurement error with the calipers.

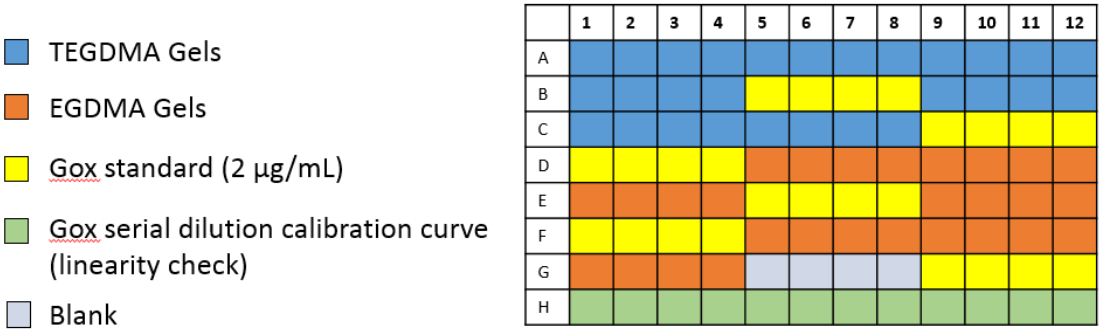

Figure 4-6: Sample diagram of gel layout in well plate for screening assays.

Despite the outliers stated in the previous paragraph, apparent activity increases with increasing swelling ratio. This is expected because increased swelling results in a decreased barrier to glucose, thus increasing glucose diffusion. Because this is a flux-based, diffusion-reaction system, the rate of glucose transport into the system (dC/dt) will increase as the diffusion coefficient value (D) increases according to the following equation.

$$\frac{dC}{dt} = D\frac{d^2C}{dx^2} + r(C)$$

Some formulations did not follow the trend between initial apparent activity and swelling ratio; there are some possible explanations for these outliers. First, the discs tested may have had less GOx encapsulated from the start given prior solubility issues with GOx in these pHEMA-based precursors. GOx precipitation could lead to inhomogeneous dispersion of the enzyme throughout the gel matrix, leading to some gels having less GOx than others. However, this is an unlikely cause due to the fact that these outlying formulations have only 50% HEMA, and previous results in Chapter 3 indicated that gel formulations with higher HEMA contents induce more GOx precipitation; GOx is more likely to be distributed more homogeneously in the outlying formulations containing 50% HEMA content. Another, more probable cause is that GOx could leach out of the matrix after fabrication during PBS equilibration. This is a more likely cause due to the fact that the outlying gel formulations seen here have two of the

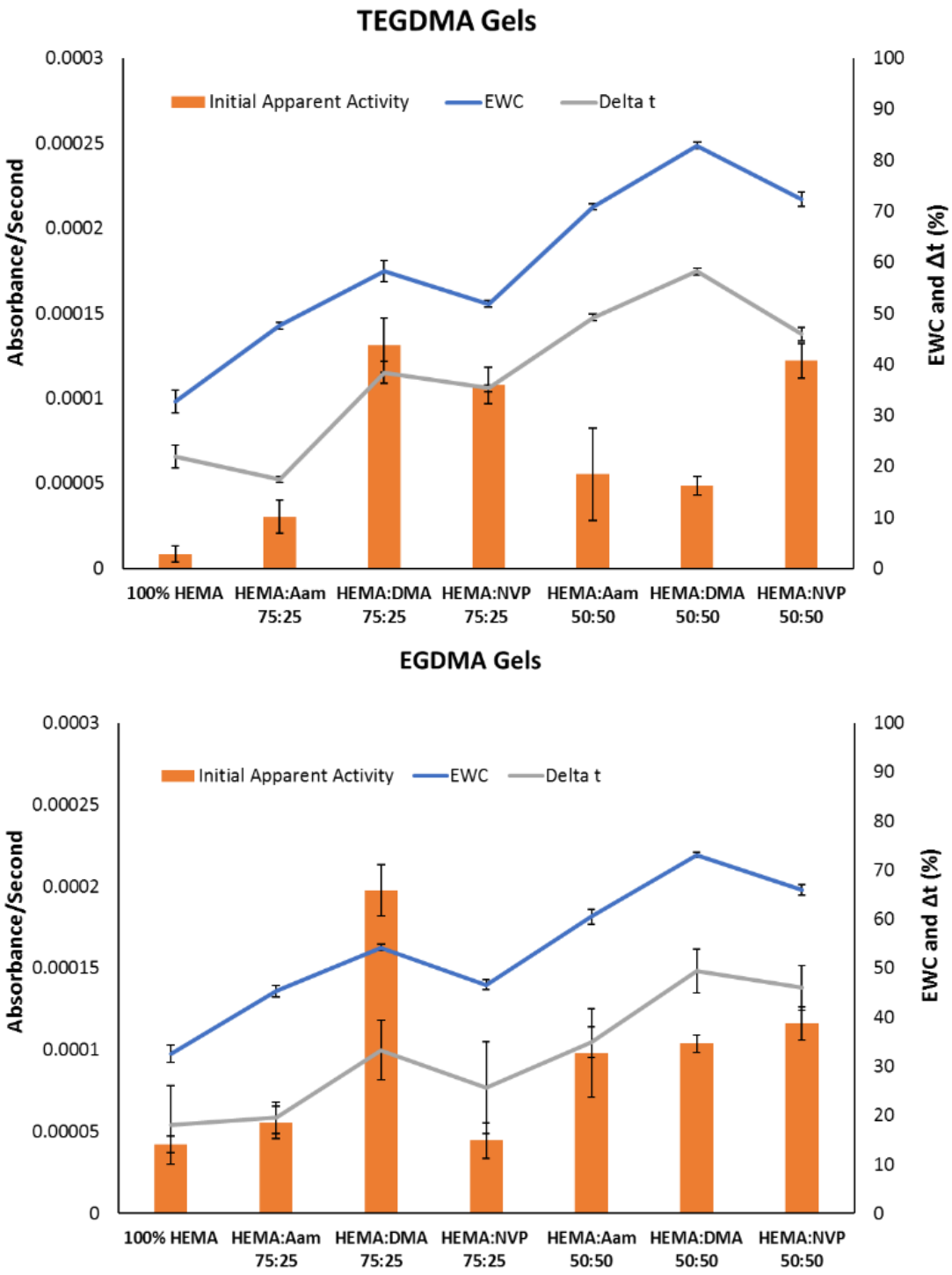

Figure 4-7: Initial apparent activity values (absorbance/second slopes) plotted alongside swelling ratio values (EWC) and gel thickness (percent change from wet to dry) to show the effects of water content on GOx apparent activity. Error bars represent 95% confidence intervals (n = 5).

highest swelling ratios (based on EWC), which could facilitate enzyme diffusion out of the gel matrix. Based on this conjecture, it is recommended that enzyme leaching experiments be conducted after gel fabrication before starting apparent activity screening and stability studies.

4.3.1.2. Screening Experiment #1—Without Bovine Serum Albumin Excipient

According to Figure 4-7, while all gels were active on week 0, with a direct correlation between initial apparent activity and EWC, nearly all gels lost >90% of their apparent activity within the first week of incubation (Figure 4-8). Two formulations showed an exception to this observation: pHEMA and 75:25 HEMA:NVP, both with the EGDMA crosslinker. Although there was no statistically significant difference between week 0 and week 1 values with these formulations, with the pHEMA formulation, the error bars overlap with the x-axis. Therefore, one could say that the pHEMA homopolymer gels were “statistically dead” after one week of incubation. Moreover, there is a negligible difference in the type of crosslinker to preserve enzymatic activity, so TEGDMA was used for all subsequent experiments.

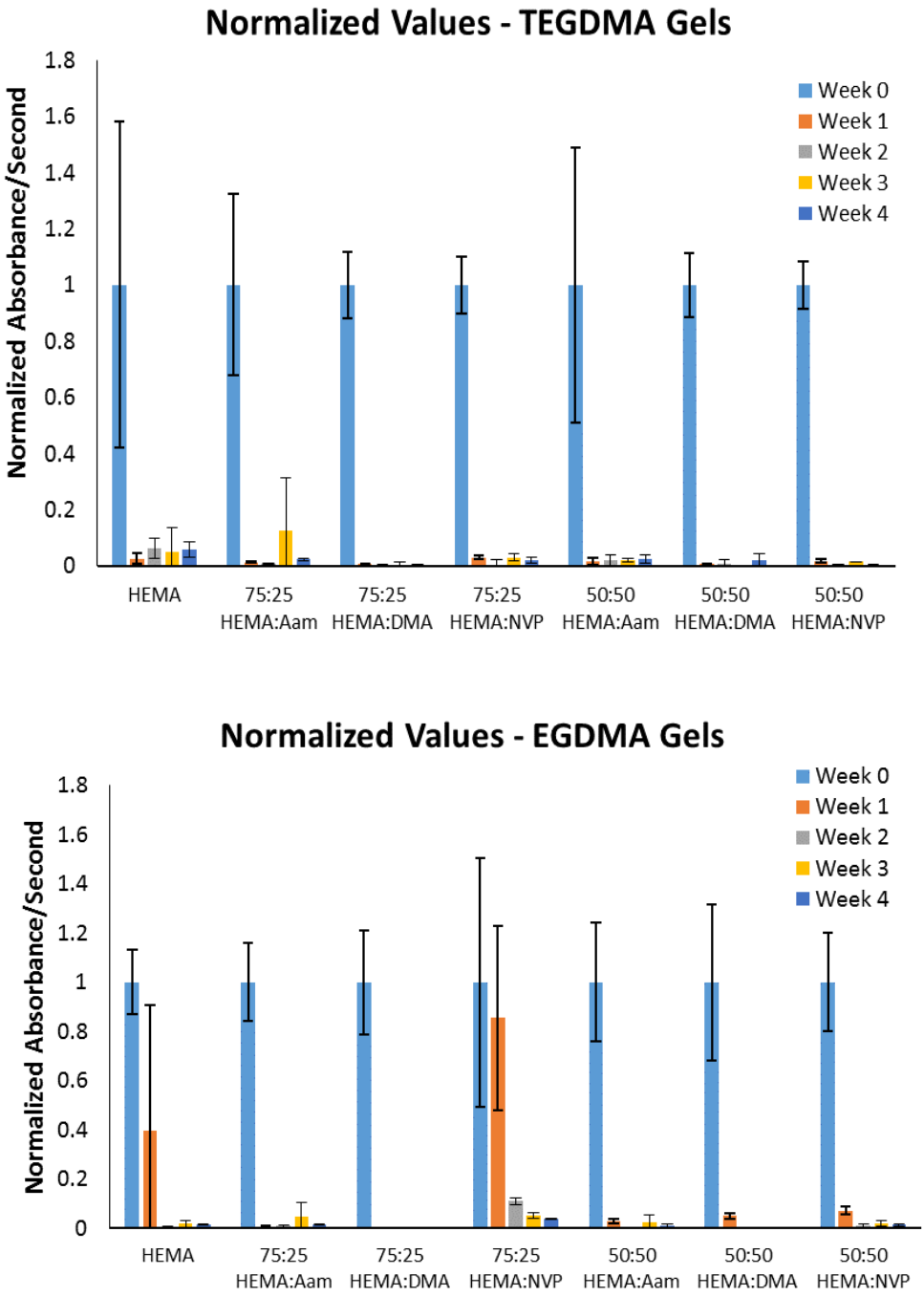

Figure 4-8: Stability over four weeks of gels with 100× dilute GOx (concentration used in Chapter 3). No BSA added.

4.3.1.3. Screening Experiment #2—With Bovine Serum Albumin Excipient

Adding BSA to the gels allowed for a more thorough investigation into the conditions of GOx deactivation during these specified physiologically relevant incubation conditions. In Figure 4-9, initial apparent activity results are presented (raw data). The data show similar apparent activity levels as reported in Figure 4-7 with the exception of the pHEMA gel with 100× dilute GOx. Less immobilized GOx could explain the abnormally low apparent activity seen for this formulation; however, this formulation had very low apparent activity during the entire month-long study. Although apparent activity levels on weeks three and four showed 2.5 and 1.6 times more apparent activity, respectively, than week 0 values for pHEMA with 100× dilute GOx, these levels are still lower than the HEMA gels with higher amounts of GOx. This suggests that these gels had little to no GOx activity throughout the entire experiment.

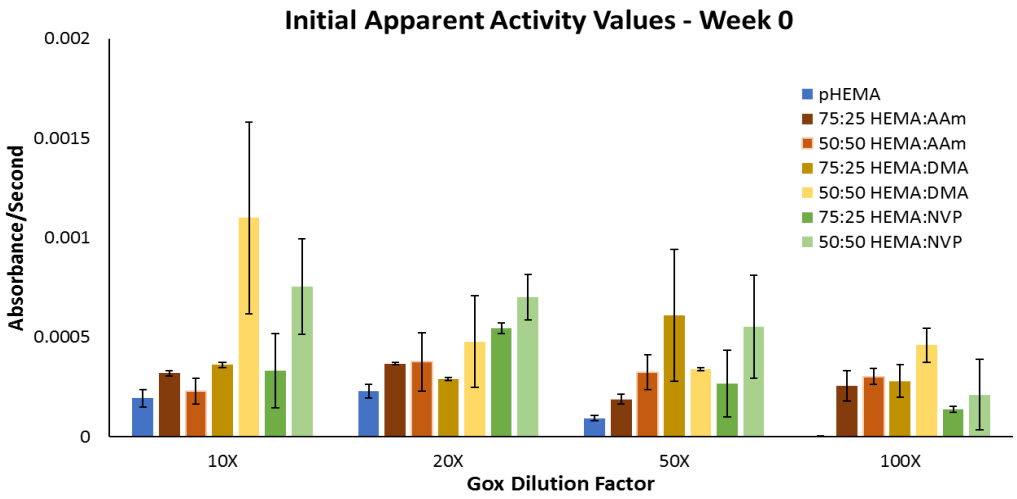

Figure 4-9: Initial apparent activity values of GOx, screening experiment 2, BSA added as an excipient.

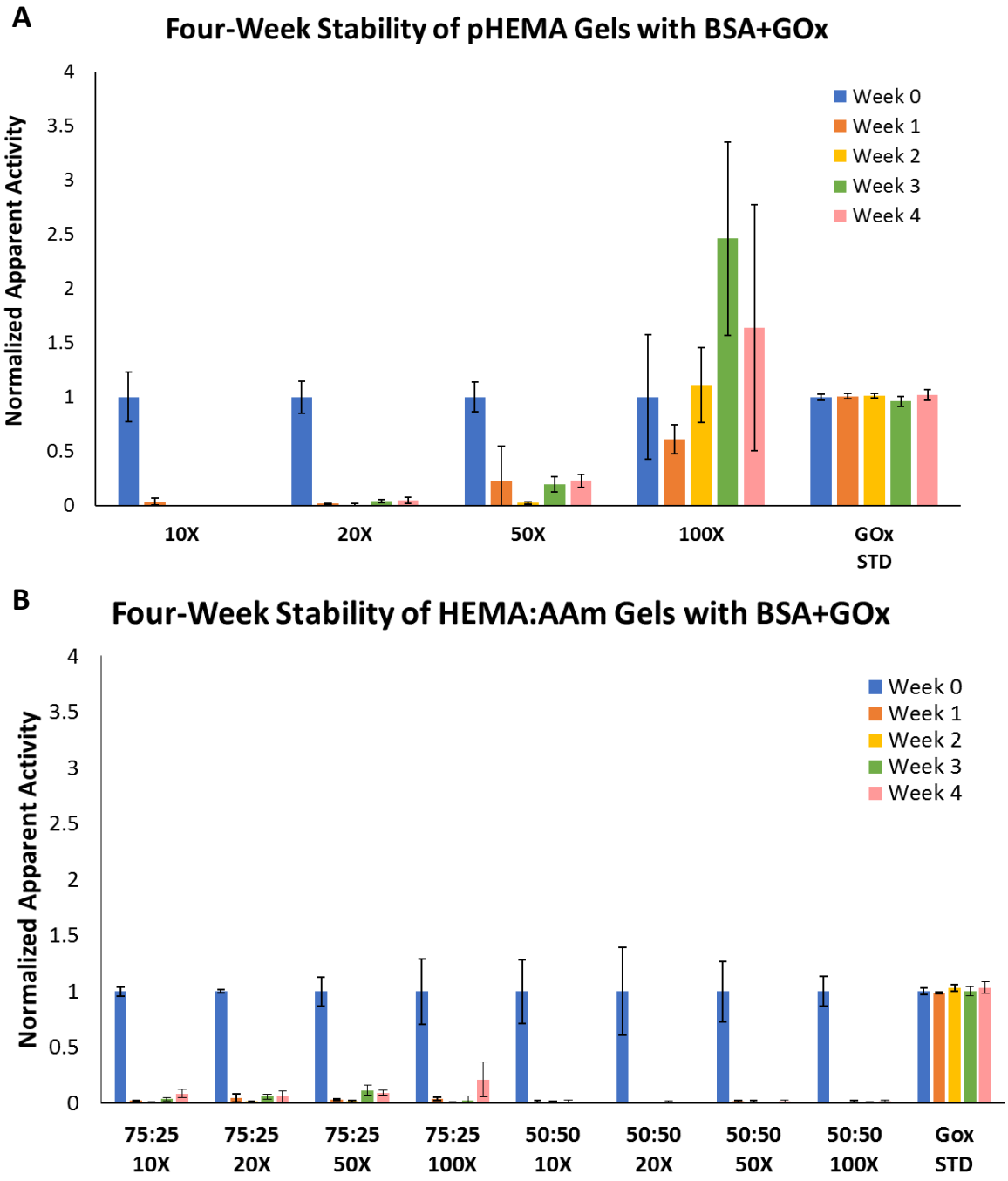

Figure 4-10(A-B): Four-week stability of pHEMA-co-DMA and pHEMA-co-NVP copolymer gels with BSA added.

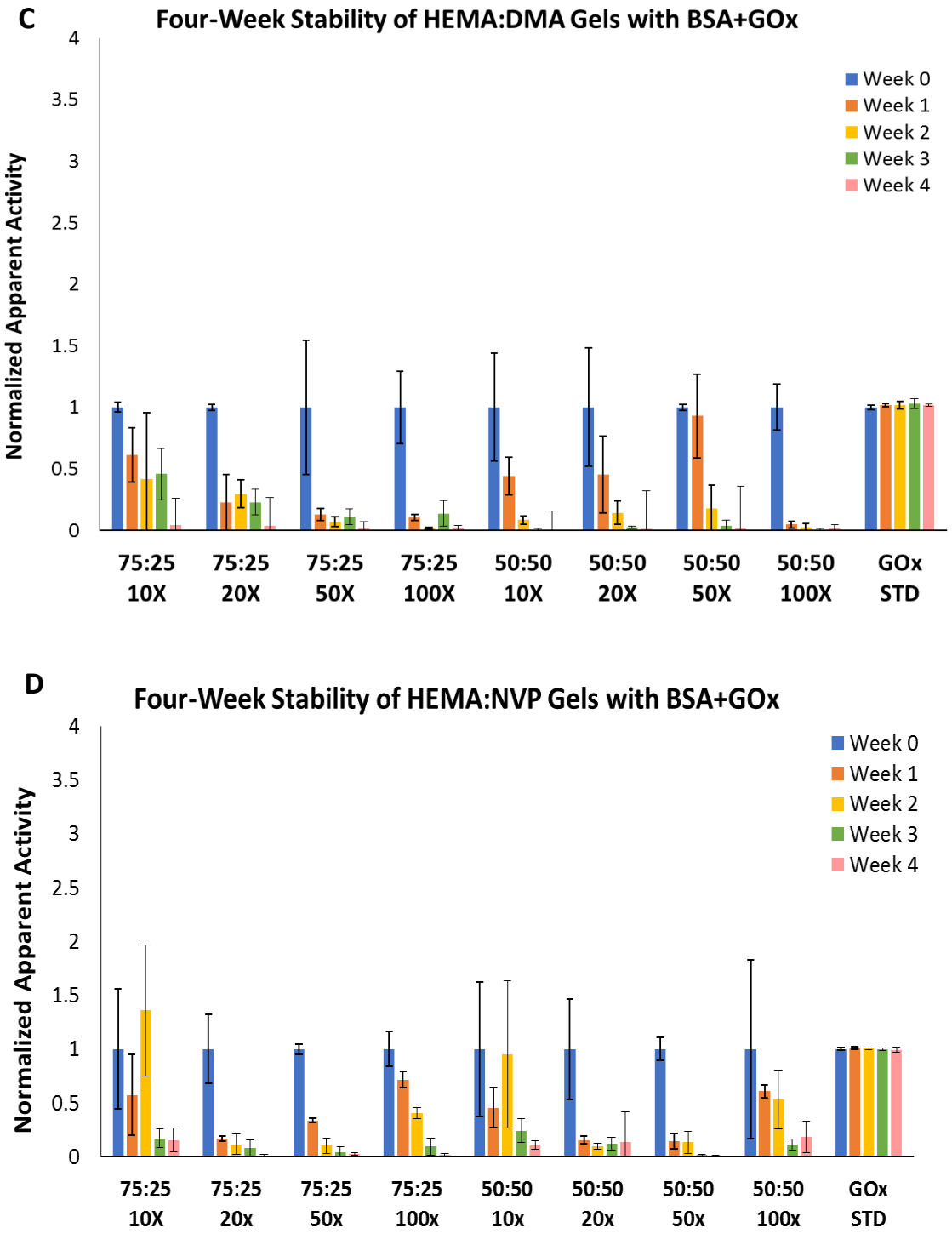

Figure 4-10 (continued, C-D): Four-week stability of pHEMA-co-DMA and pHEMA-co-NVP copolymer gels with BSA added.

No apparent improvement in GOx stability was observed in any of the pHEMA-co-AAm formulations upon adding BSA, but more evidence of GOx stability was observed in both the DMA and NVP copolymer formulations with BSA (Figure 4-10). Considering the pHEMA homopolymer gels specifically (Figure 4-10A), one likely reason for the lack of stability is BSA and GOx precipitation. It was established in Section 3.3.1 that most of the GOx added to a pHEMA hydrogel precursor precipitates out of solution. This could result in GOx "clumping" in the matrix. Not only is clumping undesirable from the perspective of homogeneity and sensor response repeatability, it also potentially causes two other unwanted results: (1) GOx is not able to be protected by the matrix because of the enzyme aggregates throughout the gel and/or (2) GOx is not adequately immobilized in the matrix, but is rather held in the sensor by interacting with the other enzyme molecules in the precipitate, which, upon hydration, could allow GOx to leach out of the matrix and cause the entire gel to lose its apparent activity.

In the case of the AAm copolymers, similar drastic loss in GOx apparent activity was observed (Figure 4-10B). This is contrary to what was expected because AAm polymers and copolymers have been used widely in the literature to immobilize proteins and enzymes, including GOx [141, 144]. Based on this fact and the observations from Section 3.3.1, it was expected that adding AAm would improve GOx stability. However, most previous studies reporting successful GOx immobilization in AAm gels do not report encapsulating another macromolecular species, such as a hydrophobic dye like PdBP. As shown in Section 3.3.1, PdBP precipitates in the aqueous AAm solution. It is hypothesized that the dye aggregates could also affect the stability of GOx. For example,

PdBP contains both bulky aromatic rings that could interact with hydrophobic side chains on amino acid residues like tyrosine and tryptophan, as well as carboxylic acids that could stabilize charged amino acid residues like arginine. PdBP could, when dispersed throughout the matrix, stabilize GOx through secondary bonding interactions just as other hydrophilic/hydrophobic molecular excipients have been shown to do [153]. When precipitated, these added benefits could be nullified. Finally, upon precipitation of the dye in the precursor solution, some monomer (HEMA and/or AAm) or crosslinker (TEGMDA) could coprecipitate in the dye aggregates, preventing them from being accessible to polymerize. This could lead to a less homogeneous matrix overall, which could also impact GOx stability.

Contrary to pHEMA and pHEMA-co-AAm, both DMA and NVP copolymer gels showed an improvement in preserving the apparent activity (Figure 4-10C-D). Although DMA has not been used as extensively as other poly(amides) in the protein immobilization literature (i.e., AAm) [43, 103, 106, 114, 141, 144, 146, 156], DMA is structurally similar to AAm with the only two methyl groups on the pendant nitrogen differentiating the two molecules. This allows greater solubility of both the dye (due to the methyl groups) and the protein (exceptionally high hydrophilicity and EWC, Figure 4-7).

Like DMA, NVP is also hydrophilic and has a hydrocarbon component (an aliphatic hydrocarbon ring pendant group) that could help promote dye solubility and homogeneous distribution throughout the hydrogel matrix, as poly(vinylpyrrolidone) films are commonly used to immobilize benzoporphyrins in the literature [91, 157].

Additionally, the presence of a carbonyl in the side group of NVP (Figure 4-11) imparts the added benefit of being able to hydrogen-bond with other molecules in the matrix, such as GOx; DMA is unable to hydrogen-bond because of the two methyl groups on the pendant nitrogen. Binding to amino acid residues like glutamine or histidine on GOx could impart an additional mechanism for preserving apparent activity over time. This

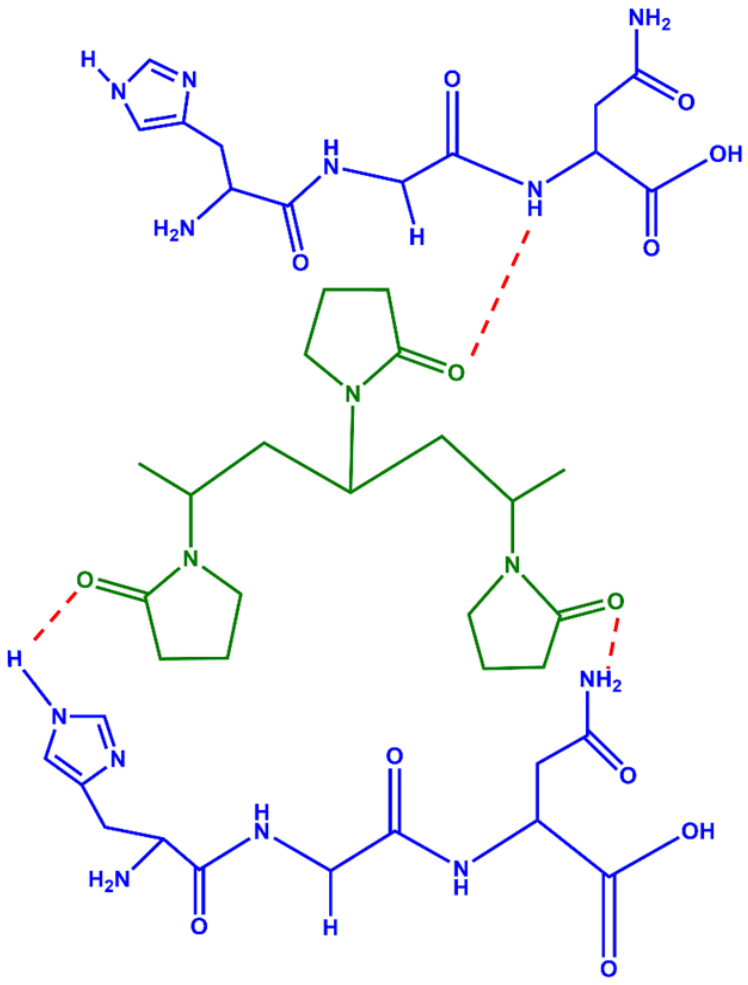

Figure 4-11: Drawing of poly(N-vinyl pyrrolidone) (green) forming hydrogen bonds with a hypothetical amino acid chain (blue). Hydrogen bonds are shown as dashed red lines.

property is exploited in the pharmaceutical industry, as poly(vinylpyrrolidone) is one of the most common excipients for drug formulations [158-160]. While AAm is able to form hydrogen bonds [161], it can also form hydrogen bonds with itself (intra- and interchain bonding) that could compete with hydrogen bonding spots on a protein molecule. Based on these findings and using apparent activity tests as a first-pass criterion to refine the hydrogel formulation design for this biosensing application, NVP and DMA were chosen to investigate further as promising comonomers for developing refined sensor design.

4.3.2. Refined Sensor Fabrication and Characterization

As mentioned in Section 4.1, criteria for an optimized sensor design include maximizing oxygen transport while limiting glucose transport in order to impart a dynamic range that covers the hypoglycemic through hyperglycemic ranges. The goal of this section of work was to design and characterize sensor formulations to meet the following design criteria: (1) promote GOx stability, (2) increase oxygen transport, and (3) limit glucose transport. While HEMA:DMA and HEMA:NVP copolymers proved the best for increasing GOx stability in the previous section (Figure 4-10 C-D), both comonomers increase hydration relative to the pHEMA homopolymer (Figure 4-7). Increasing hydration relative to pHEMA will likely increase glucose transport relative to pHEMA. Therefore, higher amounts of comonomer relative to HEMA will likely decrease the dynamic range of the sensor due to more rapid influx of the analyte, glucose. This is especially important when testing at physiological oxygen conditions *in*

vivo, where the oxygen levels are much lower and substrate transport balance is even more critical than at atmospheric oxygen conditions *in vitro*.

The aim of this section of work was to investigate *in vitro* figures of merit (e.g., glucose response and underlying oxygen response at physiological conditions) of promising material candidates using screening results in Section 4.3.1 as one primary criterion for gel feasibility. Emerging candidates were identified based on their potential to extend dynamic range under physiological conditions by meeting the three aforementioned criteria. Based on the screening data in Section 4.3.1.3 and published literature on all candidate monomers investigated in this chapter (Figure 4-1) [51, 162-166], the following formulations were chosen to investigate comparatively here: 75:25 HEMA:AAm, 75:25 HEMA:DMA, and 60:20:20 HEMA:NVP:TRIS. These specific formulations were chosen based on (1) their use in previous preclinical evaluation with this sensing platform (75:25 HEMA:AAm), (2) their potential to increase oxygen permeability relative to previous standards (75:25 HEMA:DMA and 60:20:20 HEMA:NVP:TRIS), and (3) their potential for extending dynamic range by limiting glucose based on properties stated in literature (60:20:20 HEMA:NVP:TRIS) [72, 167-170].

4.3.2.1. *In Vitro* Characterization of Candidate Formulations

Based on the above designated criteria, results from Section 4.3.1.3, and hydrogel formulations reported in the literature using these materials for contact lens design, HEMA, NVP, and TRIS were chosen as the materials exhibiting the highest potential for designing a hydrogel to meet all three criteria stated above. Although TRIS

was not miscible with pHEMA alone, as investigated in Section 4.3.1, studies have discussed using 20% TRIS with HEMA and other comonomers (including NVP) for improved oxygen permeability and pliability of contact lenses [72, 167-170]. For this reason, a 60:20:20 HEMA:NVP:TRIS formulation was investigated for its ability to respond to glucose at physiological conditions, hypothesizing that TRIS could both increase oxygen permeability (high flexibility of siloxane bonds) and decrease glucose permeability because of its hydrophobicity.

4.3.2.1.1. Oxygen Transport—Stern-Volmer Kinetics

Figure 4-12 and Table 4-3 show the Stern-Volmer oxygen-quenching kinetics and figures of merit for all three candidate formulations. Both 75:25 HEMA:AAm and HEMA:DMA exhibit an extremely linear trend ($R^2 > 0.99$) over the entire range of oxygen concentrations tested, whereas the 60:20:20 HEMA:NVP:TRIS formulation exhibits a distinct plateau in the Stern-Volmer curve from 10 to 21% oxygen, despite having a linear trend from 0 to 10% oxygen. The abnormal trend in Stern-Volmer responses is reflected in the K_{SV} and $k_{q\text{-}eff}$ values ($k_{q\text{-}eff}$ = effective bimolecular quenching constant, accounting for immobilized dye). This plateau at higher oxygens has been reported in other systems where the dye exists in two states: a quenchable state and nonquenchable state. This arises from instability of the dye in solution (i.e., precipitation) or could also be a matrix-dye interaction preventing adequate quenching of the dye [171]. The latter —matrix-dye interactions—is the most plausible scenario here because the natural lifetime, τ_0, of the dye is the highest for the silicone-containing gel. While, in theory, the τ_0 values should be identical (an intrinsic property of the dye)

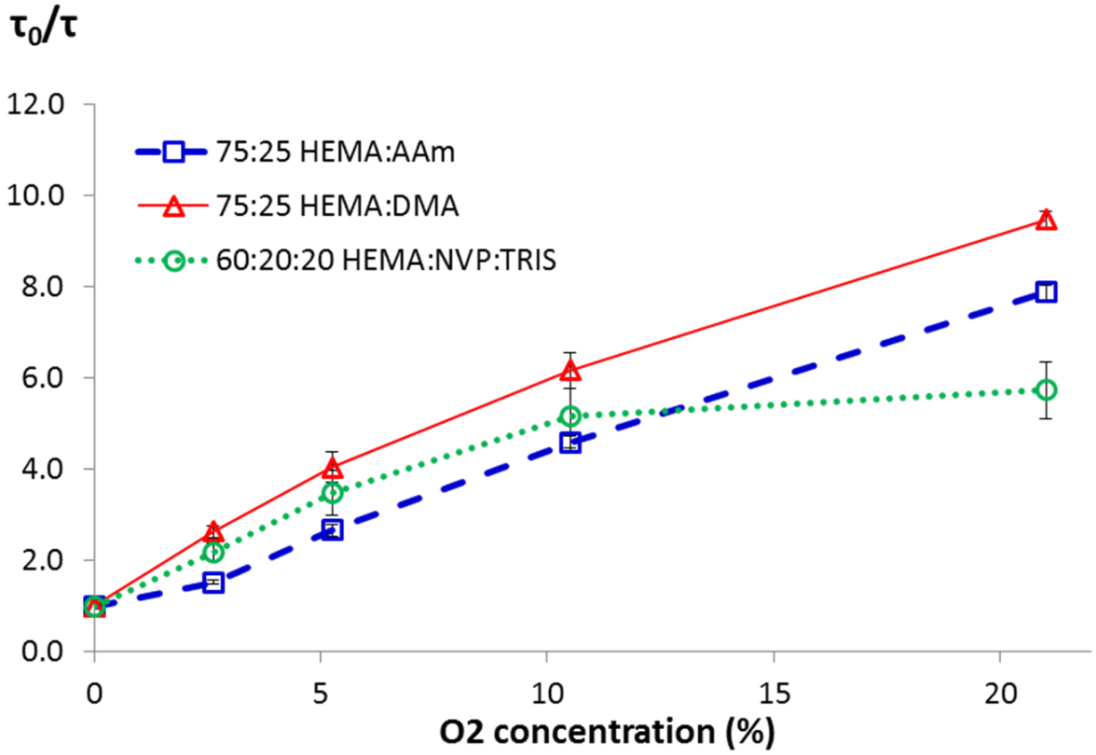

Figure 4-12: Stern-Volmer curves for the four most promising formulations. Reprinted with permission from IEEE. © 2015 by IEEE.

Table 4-3: Figures of merit for all monolith hydrogel formulations for oxygen. Reprinted with permission from IEEE. © 2015 by IEEE.

Hydrogel Formulation	τ_0 (µs)	K_{SV} $[(\%)^{-1}]$	$k_{q\text{-}eff}$ $[10^{-3}\ (\%\text{-}\mu s)^{-1}]$
75:25 HEMA:AAm	264.1 ± 2.7	0.33	1.25
75:25 HEMA:DMA	238.0 ± 1.7	0.43	1.81
60:20:20 HEMA:NVP:TRIS	300.6 ± 5.0	0.27	0.90

regardless of the matrix, interactions of the matrix with the dye may influence its apparent natural lifetime.

As noted above, the Stern-Volmer plot is linear from 0 to 10% oxygen. Therefore, the oxygen response at physiological concentrations (2 to 5% oxygen) should follow standard Stern-Volmer quenching kinetics. However, even though the response is linear at these concentrations of oxygen, the slope of the line is still lower than expected for this siloxane-containing material since the objective behind adding silicone was to substantially increase the oxygen transport.

4.3.2.1.2. Optical Response to Glucose and Saccharide Transport

Baseline lifetimes (τ at 0-mg/dL glucose) were lowest for HEMA:DMA and highest for HEMA:NVP:TRIS (Figure 4-13). Coincidentally, the baseline lifetimes trended inversely with the K_{sv} values, indicating that greater oxygen permeability corresponds to a lower starting lifetime due to more efficient oxygen transport. Additionally, HEMA:NVP:TRIS copolymer exhibited the shortest dynamic range, likely due to matrix inhomogeneities inhibiting oxygen transport, as seen above. Although the HEMA:DMA copolymer performed with the highest measured oxygen transport, the increased oxygen transport had minimal effect on extending dynamic range and altering the overall glucose response profile. This was not expected, considering the 30% increase in oxygen transport based on K_{SV}. In order to increase the dynamic range significantly, glucose must remain the limiting reagent of the GOx reaction over the entire physiological blood glucose range. This could be accomplished by decreasing

glucose diffusion or further increasing the oxygen diffusion, both of which are efforts currently being pursued.

The change in sucrose concentration over time in the permeate chambers was calculated by plotting the change in concentration of sucrose versus time and calculating the slope of the resulting linear trend. Diffusion coefficients were calculated according to the equation in Section 4.2.4.3.2; this was conducted for each formulation. Resulting sucrose diffusion coefficients, $D_{sucrose}$, are presented in Figure 4-13 and Table 4-4. Results indicate the fastest saccharide transport for HEMA:NVP:TRIS. On the contrary, the slowest saccharide diffusion was observed for the HEMA:DMA gels, an unexpected

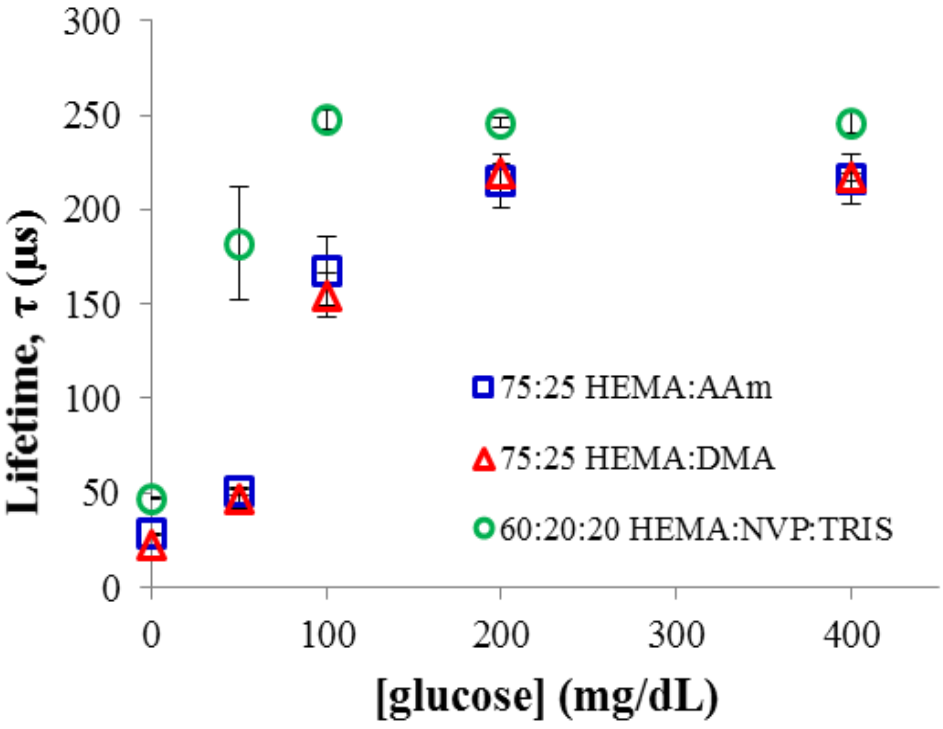

Figure 4-13: Glucose flight plans (ambient oxygen). Reprinted with permission from IEEE. © 2015 by IEEE.

Table 4-4: Figures of merit for all monolith sensor formulations for glucose. Reprinted with permission from IEEE. © 2015 by IEEE.

Hydrogel Formulation	Dynamic Range (mg/dL)	Sensitivity [μs/(mg-dL)]	$D_{sucrose}$ (10^{-6} cm^2/s)
75:25 HEMA:AAm	0.34-188	1.15 ± 0.13	0.89 ± 1.11
75:25 HEMA:DMA	0-194	0.94 ± 0.10	0.11 ± 0.02
60:20:20 HEMA:NVP:TRIS	0-82	0.44 ± 0.15	2.17 ± 4.35

observation based on prior swelling ratio and initial apparent activity calculations in Figure 4-7, which shows 75:25 HEMA:DMA with TEGDMA crosslinker having a much higher swelling ratio and initial apparent activity value compared to 75:25 HEMA:AAm.

Because the PdBP dye can act as a tetrafunctional crosslinker due to the four methacrylate groups, the drastic decrease in average $D_{sucrose}$ is believed to be caused by more efficient polymerization of the dye into the hydrogel matrix in the HEMA:DMA sensor. These results highlight the large extent to which inhomogeneous sensor morphology impacts analyte transport. Large variability in saccharide transport was seen with sensors with pronounced morphological inhomogeneities. This likely affects the overall sensor response repeatability and is investigated further in the following section.

4.3.2.1.3. Investigating Homogeneity

To determine whether the source of discrepancy seen with the silicone gel behavior is due to matrix inhomogeneities as proposed earlier, hydrogels were imaged by both brightfield and confocal microscopy. Results are presented in Figure 4-14. Interestingly, the HEMA:DMA gels were the most uniform in appearance, without any apparent dye precipitation or phase separation, whereas the 75:25 HEMA:AAm gel had granular-like precipitate structures throughout the matrix. The 60:20:20 HEMA:NVP:TRIS gel appeared the least uniform, likely due to phase separation. While it is unclear from the brightfield images which aspects of the gel matrix are phase-separating from the rest of the sensor, a "blank" 60:20:20 HEMA:NVP:TRIS gel (matrix

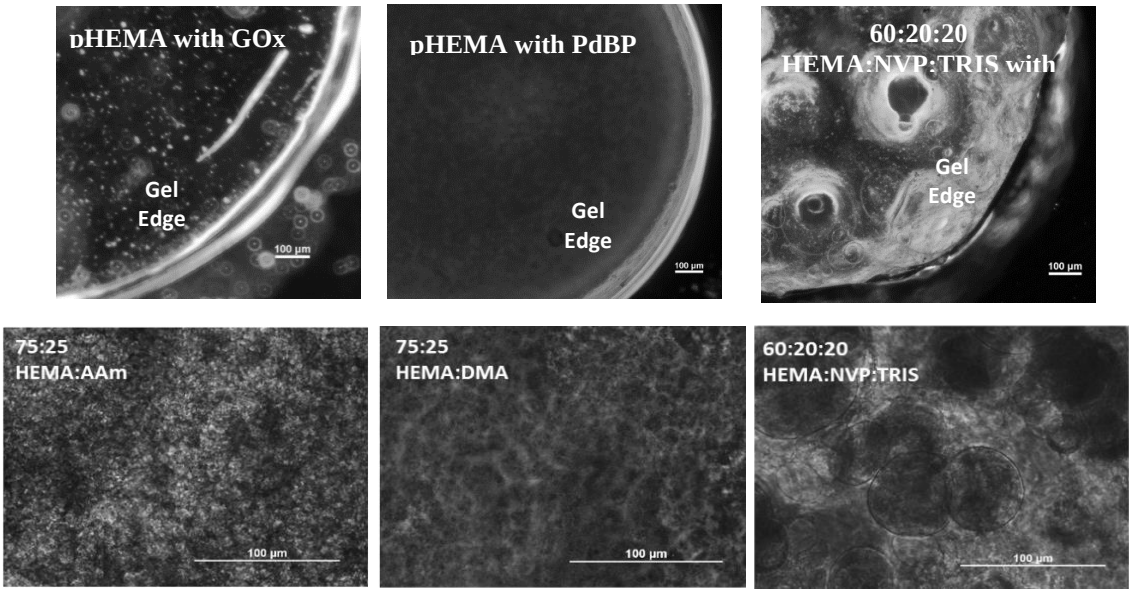

Figure 4-14: Brightfield microscopy images of glucose-sensitive hydrogels with GOx, CAT, and PdBP. Images are at 20× magnification, and scale bars represent 100 µm. Images illustrate granular precipitates throughout the gel in HEMA:AAm, distinct globular regions in HEMA:NVP:TRIS, and the most uniform dispersion throughout HEMA:DMA. Adapted with permission from IEEE. © 2015 by IEEE.

only, no sensing chemistry) was fabricated and stained with Nile Red dye according to methods described in Section 4.2.4.5. A representative CLSM image is displayed in Figure 4-15.

As seen in the image shown in Figure 4-15, inhomogeneities prevail throughout the matrix which is consistent with the findings revealed by brightfield microscopy.

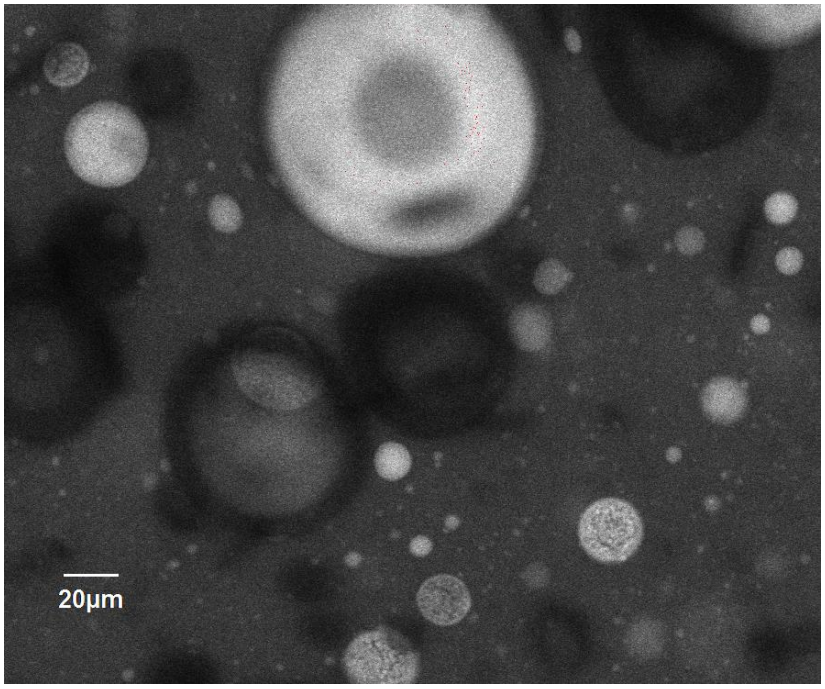

Figure 4-15: CLSM image of a 60:20:20 HEMA:TRIS:DMA gel stained with Nile Red dye revealing spherical domains of silicone (lighter regions) dispersed throughout the surrounding matrix (darker regions).

However, because of the Nile Red dye sequestering to the hydrophobic silicone regions, the images reveal dispersed spheres distinctly brighter than the surrounding matrix, indicative of phase separation containing silicone in the dispersed phase as hypothesized. Although some spherical dispersed regions appear darker than the surrounding matrix (which could indicate a region devoid of dye and, hence, silicone), this is likely an optical effect due to the depth of the dispersed domain in the gel. A montage of slices (images taken at different depths into the gel sample) of the same gel specimen is shown in Figure 4-16. The montage reveals brighter domains closer to the surface of the gel

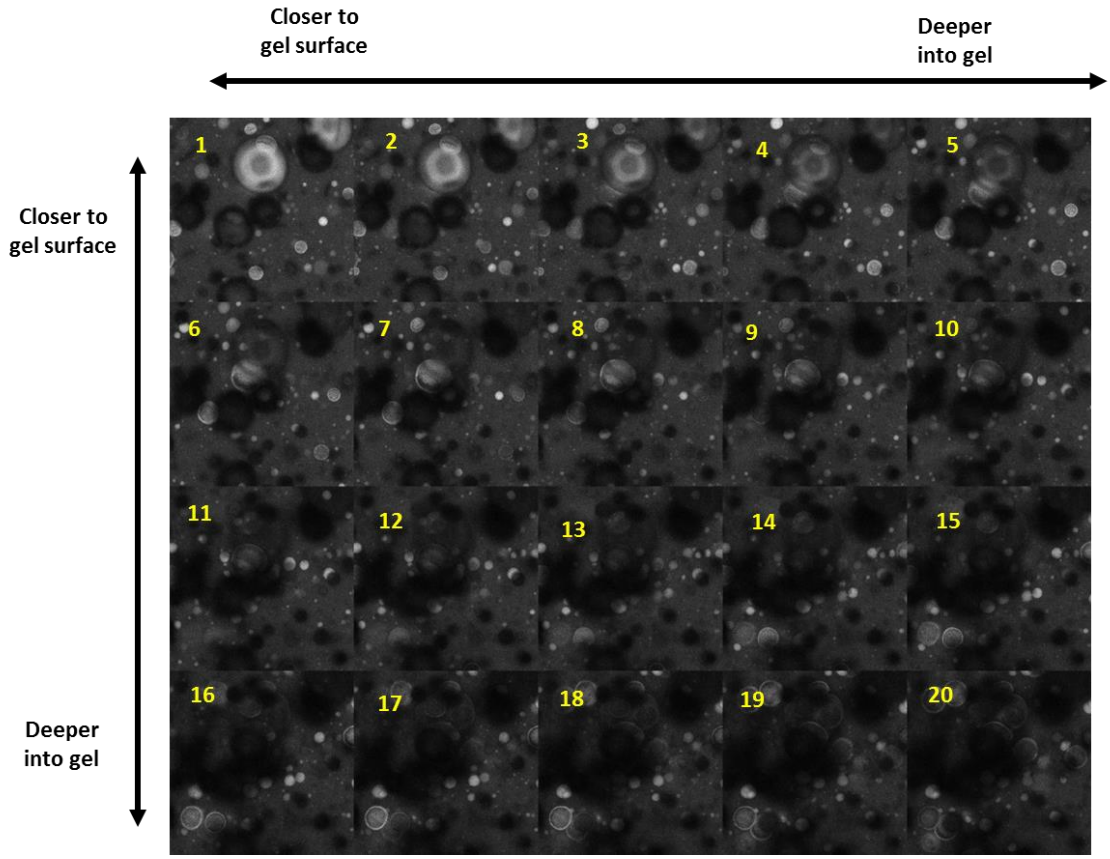

Figure 4-16: Montage of confocal microscopy slices. Slices are numbered according to the depth of the slice in the gel sample. Increasing slice number corresponds to a deeper location within the gel sample. Incremental depth changes between slices is ~5 μm.

becoming increasingly darker as the depth into the sample increases while other lighter domains come into focus. This further supports the fact that darker regions seen in these images are not necessarily devoid of silicone, but rather are at a depth position in the gel that renders its appearance darker; an image of a slice taken closer to the surface of the gel may increase the brightness of these regions and harness the fluorescent properties of the Nile Red dye. These principles should be taken into account in future investigations of gel homogeneity.

4.3.3. Conclusions

This chapter has described several experiments to investigate the impact of various aspects of sensor design on GOx stability and substrate transport to create a more thoughtful sensor design and eventually achieve the vision of preclinical proof of concept long-term (minimum of one month). In order to investigate GOx stability in a more systematic manner than described in Chapter 3, screening experiments were designed with the following improvements in order to expand the knowledge of stability of GOx-hydrogel constructs: 1) expand the library of GOx-loaded materials with this sensing platform beyond the traditional pHEMA homopolymers and pHEMA-co-AAm copolymers, 2) investigate in more detail the amount of GOx used in the matrix in order to optimize the GOx concentration, and 3) identify overarching gel chemical properties that enhance GOx stability. Interestingly, screening results (experiment 2, Section 4.3.1.3) showed that both the pHEMA homopolymer and the HEMA:AAm copolymer gels were the least effective in preserving GOx apparent activity over one month of exposure to physiological conditions, despite the fact that these are the materials that

have been primarily used in the past with this sensing platform because of their prevalence in the literature for decades in other applications involving enzyme immobilization [24, 98, 109]. In fact, pHEMA and HEMA:AAm copolymer gels lost nearly all of their apparent activity within the first week of incubation at physiological conditions. In contrast, gels synthesized with DMA and NVP as comonomers retained between 60 and 93% of the original apparent activity after one week of incubation. Although apparent activity in these gels steadily declined in subsequent weeks regardless of GOx content, the results warranted further investigation of DMA and NVP as comonomers. Furthermore, the ratio of GOx:BSA did not have any significant effect on initial apparent activity of stability the gels, indicating matrix chemistry primarily impacts the stability of these gels.

Subsequent *in vitro* investigation of three promising formulations, based on the screening results, were subjected to tests quantifying substrate transport and overall optical response to glucose. These results of these studies revealed other aspects of matrix chemistry that affect sensor function, namely matrix homogeneity. By performing tests to quantify the underlying oxygen response as well as overall glucose response, these studies further revealed the importance of avoiding precipitation or phase separation within the sensor construct. Because of these findings, it is recommended for subsequent studies that approaches to sensor design be taken with the mindset of ensuring dispersion of all sensor components instead of taking a one-step, “brute force” approach to sensor design. By allocating extra effort on the “front end” (i.e. before preclinical testing) to systematically evaluate matrix homogeneity and ensure

meticulous, precise control over sensor properties independently of one another during the fabrication process, time to preclinical testing should be reduced.

5. HYBRID MATERIALS

5.1. Introduction

In the previous section, approaches were taken to investigate GOx stability in a variety of formulations in order to hone in on the most promising formulations and try to optimize hydrogel design metrics through connecting enzyme stability with other sensor figures of merit (i.e., substrate transport, dynamic range, and sensitivity). However, using DMA and TRIS as comonomers with HEMA only marginally improved GOx stability and had little impact on overall sensor performance. Furthermore, functionalizing these single-network monolith gels with the enzyme-porphyrin assay required a "brute force," one-size-fits-all approach, confounding the effects of various factors and their impact on sensor figures of merit. Without the ability to decouple various physicochemical gel properties (i.e., substrate transport, hydration, mechanical properties, and sensing chemistry solubility) from one another, there is an inability to optimize, or at least fine-tune, the overall sensor response. This chapter expands on the prior monolith work by utilizing IPN hydrogels synthesized using a sequential polymerization process. Ideally, an approach to tune gel properties in an on-demand fashion would pave the way for optimizing glucose sensor longevity *in vivo*. However, because the overall glucose response relies on the underlying oxygen response, optimizing the oxygen transport in the gel matrix independent of matrix chemistry or hydration is a large step forward in optimizing glucose sensor design.

IPN hydrogels are an emerging class of materials that have gained interest because of the ability to use two polymer materials that may have inferior properties (e.g., brittleness, low hydration) as standalone, single-network gels, but, when combined, act in synergy with each other to yield properties superior to those of either polymer network alone [165, 172-174]. IPNs are defined as two networks that have no covalent bonds between them but are intertwined such that neither network can be separated from the other without breaking the covalent bonds of either individual polymer network [175]. Additionally, IPN synthesis involves sequential (polymerization of one network, infiltration of second network precursor) or simultaneous (both networks polymerized at the same time through non-interfering mechanisms) polymerization methods, the latter of which is thought to promote better homogeneity in the bulk gel structure [176]. IPNs of TRIS and DMA have been exploited in recent years as a way to create contact lenses with finer control over oxygen permeability and hydration in the lens material. Nicholson and Wang described the TRIS and DMA construct morphology as isotropic yet heterogeneous, with distinct, intertwining, hydrophobic silicone domains and hydrophilic DMA domains. This allowed transport between the two domains on the molecular scale, resulting in high oxygen transport properties in the overall gel [165, 177]. Coincidentally, the same oxygen diffusion properties are desired for the subcutaneous, fully implantable biosensors described above.

Sphere-templated hydrogels have been used as tissue-integrating constructs for a variety of tissue engineering applications. These templated hydrogels exhibit an inverted colloidal crystal structure that uses the scaffold morphology to promote angiogenesis

throughout the construct and avoid using anti-inflammatory agents or growth factors, which increase material cost, complicate the device fabrication process, and have limited use due to a limited drug payload and limited control over bioactivity and spatiotemporal distribution [178]. Materials used in these studies include pHEMA, poly(NIPAAm) and poly(acrylic acid), among others [24, 69, 70, 73, 179-181]. While these materials have shown cellular infiltration, some studies report zones of cellular necrosis in the scaffolds likely due to nutrient transport limitations (e.g., oxygen and glucose) [180]. Somo *et al*. investigated larger pore sizes (>100 μm) in similar inverted colloidal crystal hydrogels and reported that the interconnection between the pores has a profound effect on the penetration of these blood vessels throughout a sphere-templated gel [182]. In all studies noted above, the scaffolds consisted of the polymer matrix alone and were not functionalized with any optical sensing chemistry. By introducing an oxygen indicator, relationships between tissue ingrowth and oxygen permeability may be determined by fabricating these hydrogels as biosensors.

The aim of this study was to use the two oxygen-permeable materials described in Chapter 4, DMA and TRIS, and use them to fabricate hybrid inorganic-organic silicone-containing IPN hydrogels. In this section of work, these gels were nctionalized with the oxygen-quenched phosphor PdBP. Various chemical properties were evaluated (water content, optical clarity, substrate transport, mechanical properties, and overall device performance) and compared to pHEMA-based biomaterials functionalized with the same sensing chemistry. Capitalizing on the synergistic behavior between the hydrophobic, inorganic TRIS alkylsiloxane and the hydrophilic, organic DMA in an IPN

gel structure, the ability to control gel hydration and mechanical properties independently from substrate (oxygen) transport is investigated. By utilizing an inverted colloidal crystal scaffold, proof of concept of these devices as long-term, tissue-integrating implants is investigated as well.

5.2. Experimental Methods

5.2.1. Reagents and Instrumentation

For photocuring, the UV lamp (Blak Ray-B-100 SP) was purchased from UVP-LLC (Upland, CA). DMA, Nile Red, Irgacure 651, and PBS were purchased from Sigma Aldrich (St. Louis, MO). TRIS was purchased from Silar Laboratories (Wilmington, NC). TEGDMA was purchased from Polysciences (Warrington, PA). PdBP and poly(methyl methacrylate) (PMMA) beadcakes were provided by PROFUSA, Inc. Prior to use, DMA, TRIS, and

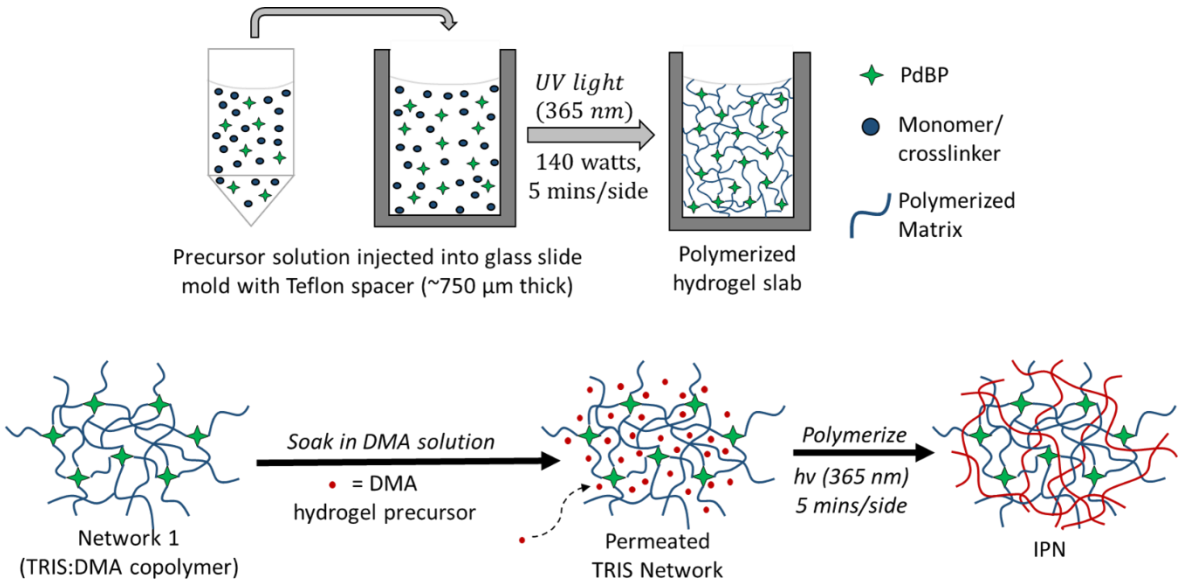

Figure 5-1: Illustration of the hybrid inorganic-organic IPN gel fabrication process

TEGDMA were passed separately through individual inhibitor removal columns (Sigma) to remove the hydroquinone monomethyl ether (MEHQ) inhibitor. All other reagents were used as received unless otherwise stated.

5.2.2. Interpenetrating Network Hydrogel Fabrication

The IPN gels were fabricated using methacrylate-based monomers/crosslinker and a free-radical polymerization, similar to that described in previous sections but with a few changes [24, 65]. This section describes the synthesis of IPN hydrogels using a sequential polymerization process illustrated in Figure 5-1.

In a typical synthesis, appropriate amounts of TRIS and DMA were added to Irgacure 651 (1:99 w/v% initiator:monomer) and vortexed to dissolve the photoinitiator. Next, TEGDMA was added as a crosslinker (2:98 v/v% crosslinker:monomer). All monomer and crosslinker materials were passed through an inhibitor removal column (Sigma) to remove the MEHQ inhibitor. PdBP was dissolved in dichloromethane (DCM) at a concentration of 10 mM; 25 μL of dye solution was added to the precursor solution and vortexed to mix. Finally, appropriate amounts of DCM and isopropanol (IPA) were added; necessary amounts of each solvent were determined based on the ratio of TRIS:DMA used. A too-high IPA content renders the gel tacky and unmanageable, whereas a too-high DCM content renders the gel too brittle and unable to be removed from the glass slide mold. TRIS:DMA ratios and corresponding cosolvent ratios are summarized in Table 5-1. Finally, the precursor solutions were purged with nitrogen gas for three minutes, transferred via pipette to a glass slide mold consisting of a Teflon

Table 5-1: Table of IPN formulations

First Network	Second Network	Morphology	Sensing Chemistry	Co-Solvents	Monomer:Solvent Ratios (v:v)
50:50 TRIS:DMA	pDMA homopolymer	IPN	10 mM PdBP in DCM	75 µL IPA; 50 µL DCM	1:1.04
60:40 TRIS:DMA	pDMA homopolymer	IPN	10 mM PdBP in DCM	62.5 µL IPA; 62.5 µL DCM	1:1.04
70:30 TRIS:DMA	pDMA homopolymer	IPN	10 mM PdBP in DCM	50 µL IPA; 75 µL DCM	1:1.04
80:20 TRIS:DMA	pDMA homopolymer	IPN	10 mM PdBP in DCM	37.5 µL IPA; 87.5 µL DCM	1:1.04
pHEMA homopolymer	N/A	Single network	10 mM PdBP in DMSO	90 µL ethylene glycol; 100 µL DI water	1:1

spacer (760 µm thick) secured with clips, and photopolymerized for 10 minutes (five minutes per side).

Following photocuring, the gel slabs were removed from the mold, placed in a second precursor solution (3-mL total volume; 50:50 v/v% DMA:IPA; 98:2 v/v% DMA:TEGDMA; 1:99 w/v% Irgacure 651:DMA), and allowed to soak on a tabletop shaker overnight. The next day, the soaked gel (Figure 5-1B) permeated with the second DMA precursor was blotted on a Kimwipe to remove excess surface DMA precursor; it

was then photocured between two glass slides to form the second network. The resulting IPN gel was placed in PBS (100 mM, pH 7.4) overnight to hydrate.

5.2.3. In Vitro Physical Characterization

5.2.3.1. Swelling Ratios

Five discs from each monolith, both with dye and without dye (blank), were punched with a disposable biopsy punch (5-mm diameter, VWR). Each disc was blotted on a Kimwipe to remove excess water and was weighed on an analytical balance (Mettler Toledo, Model XS64) to obtain the hydrated mass. The gel discs were dried under the house vacuum overnight (>24 hours) and weighed again to obtain the dried weight (W_d). The EWC was calculated from the percent difference in the two weights according to the equation presented in Section 4.2.4.1

5.2.3.2. Optical Clarity

Five-millimeter blank discs without PdBP dye of each formulation were placed in a 96-well flat-bottom polystyrene well plate, and 200 µL of PBS (Sigma, 10 mM, pH 7.4) was dispensed over each gel. An absorbance scan was conducted in a plate reader (Tecan Model M200) from 400 to 850 nm. Absorbance values (A) were converted to transmittance (%T) values according to the following relationship.

$$\%T = 10^{(2-A)}$$

5.2.3.3. Confocal Laser Scanning Microscopy

Staining of the gels with Nile Red was adapted from Bailey, *et al*. 2012, as described in Section 4.2.4.5, reiterated here for consistency. First, a 20 mg/mL solution

of Nile Red (Sigma) in methanol was dissolved in a dram vial by vortexing for one minute. A 75 µL aliquot of this dye solution was added to 8 mL of DI water in a 20 mL scintillation vial and vortexed for one minute. Next, the 8 mL solution was diluted by adding it to 120 mL PBS in a beaker under constant stirring. Gel discs (5 mm diameter) were punched from the IPN gels with a biopsy punch. Each disc was placed in a separate centrifuge tube filled with 50 mL of the diluted Nile Red solution in PBS and placed on a nutating mixer at room temperature for 24 hours. After 24 hours, the Nile Red solution in PBS was discarded, and the stained gel discs were placed in fresh centrifuge tubes with 50 mL fresh PBS, allowing to nutate at room temperature for 24 more hours. The washing process was repeated three times, and the discs were stored in PBS until imaging.

CLSM images were taken on an Olympus FV1000 confocal microscope. Excitation of the Nile Red stained gels was accomplished with a helium-neon laser (543 nm); emission was collected from 650-700 nm. Images were obtained 100 µm into the sample.

5.2.3.4. Differential Scanning Calorimetry

Differential scanning calorimetry (DSC) (TA Instruments, Q200) was performed on blank hydrogel monolith strips of each formulation. The blank strips were dried in a 2.5-mL microcentrifuge tube under the house vacuum for over 24 hours. Five to 10 mg of each dried gel strip was weighed into an aluminum TZero pan and was then sealed hermetically. Thermal scans were run from 20 to 200 °C at a ramp rate of 10 °C/min. Two heat/cool cycles were run for each sample; the first cycle served to erase any

previous thermal history in the polymer, while the second cycle was used to obtain the glass transition temperature (T_g). T_g values were calculated in the TA Universal Analysis software using the glass transition function. Data reported are the calculated midpoint values for each analysis (n = 3).

5.2.3.5. Rheometry

Dynamic modulus analysis to determine the viscoelastic response was performed on three separate hydrogel discs (10 mm in diameter) of each formulation using a rheometer (Anton Paar, MCR 301). Excess moisture was carefully removed by blotting the sample with a Kimwipe before analysis. A stainless steel, parallel plate geometry 10 mm in diameter was used for frequency tests over the range of 1 to 100 Hz at a constant strain amplitude of 1 Pa. The temperature, 25 and then 37 °C, was controlled by a circulating water bath and built-in Peltier heater.

5.2.3.6. Scanning Electron Microscopy

Gels were freeze-dried in liquid nitrogen then lyophilized (Labconco, Model 7811020) to preserve scaffold morphology. After lyophilizing, the gels were vacuum-dried, mounted on a scanning electron microscope (SEM) stand using carbon tape, and sputtercoated (Tedpella, Model Cressington 108) for one minute to generate a ~2 nm layer of gold. Gels were imaged at 10 kV under low vacuum (JEOL USA, Inc., JCM-5000 Neoscape).

5.2.3.7. Oxygen Transport (Stern-Volmer Kinetics)

Stern-Volmer oxygen diffusion experiments were carried out by immobilizing dye-loaded monolith gel strips in an acrylic sample chamber sealed with an o-ring and

secured with screws. Samples were immobilized in wells with o-rings flush with the side of the well. Oxygen modulation experiments were carried out in an incubator using a recirculating flow system similar to that previously described [183]. Oxygen levels were controlled using a mass flow controller with two gas flow lines: one to nitrogen and the other to house air. Oxygen levels were verified using a picoammeter (Unisense, Denmark). Gas was bubbled into a 2-L Erlenmeyer flask filled with 1 L of PBS and sealed with a rubber stopper with three openings: two for liquid influent and effluent and one for the ceramic gas bubbling tube (VWR).

5.2.4. In Vivo Characterization

5.2.4.1. Implantation and Oxygen Modulation

In vivo oxygen modulation procedures were approved by the Texas A&M IACUC committee. A female Sinclair mini-pig was obtained from Sinclair Bio-Resources (Columbia, MO), anesthetized with an injection of telazol (5 mg/kg) and buprenorphine (0.01 mg/kg), sedated, and intubated. Dorsal hair was shaved, and skin was cleaned and prepared for injections by brushing with dye-free ChloraPrep applicators (CareFusion, San Diego, CA). Anesthesia was maintained with 1.0 to 2.5% isoflurane (v/v in O_2) to effect during sensor injections and oxygen modulation. Sensors were injected subcutaneously into the dorsum of the pig (42.0 kg, one year old) from an 18-gauge cannula with a reverse-action plunger. The sensors were targeted for insertion at ~5 mm deep; average and standard deviation of implant depths were determined to be 5.4 ± 1.9 mm from post-experiment histological evaluation of n = 60 implants (some

implants were used only as controls and for histology for separate studies and are not detailed here).

Optical readers of the same custom-built lifetime detection system used for *in vitro* sensor testing were placed and adhered on the skin over the injected IPN and pHEMA oxygen biosensors and allowed to collect baseline signal. Systemic oxygen challenges were achieved through reduction of the fraction of inspired oxygen. At baseline, the animal was maintained at $fiO_2 = 1.00$. The fiO_2 was then reduced to approximately 0.15 (v/v balance N_2) for up to 15 minutes. After the hypoxic period, the fiO_2 was returned to 1.00.

5.2.4.2. Histology

Following humane euthanasia of the animal, the dorsal pelt was removed via scalpel, and sensors were located using the custom-built lifetime detection system described previously. Once located in the pelt, tissue plugs containing the sensors were isolated with 8-mm biopsy punches. The tissue plugs were immediately placed in formaldehyde and sent to CVPath (Gaithersburg, MD) for histological processing. The histology slides were imaged using a slide scanner with a 20× objective (Mikroscan, Model S2). Images were digitally processed using standard imaging software (Aperio ImageScope, version 11.1.2.760).

5.3. Results and Discussion

5.3.1. In Vitro Physical Characterization

5.3.1.1. Swelling Ratios and Optical Clarity

Hydrogel discs of four IPN formulations, both with and without the tetramethacrylated PdBP dye, were tested for water content. Figure 5-2 shows a general

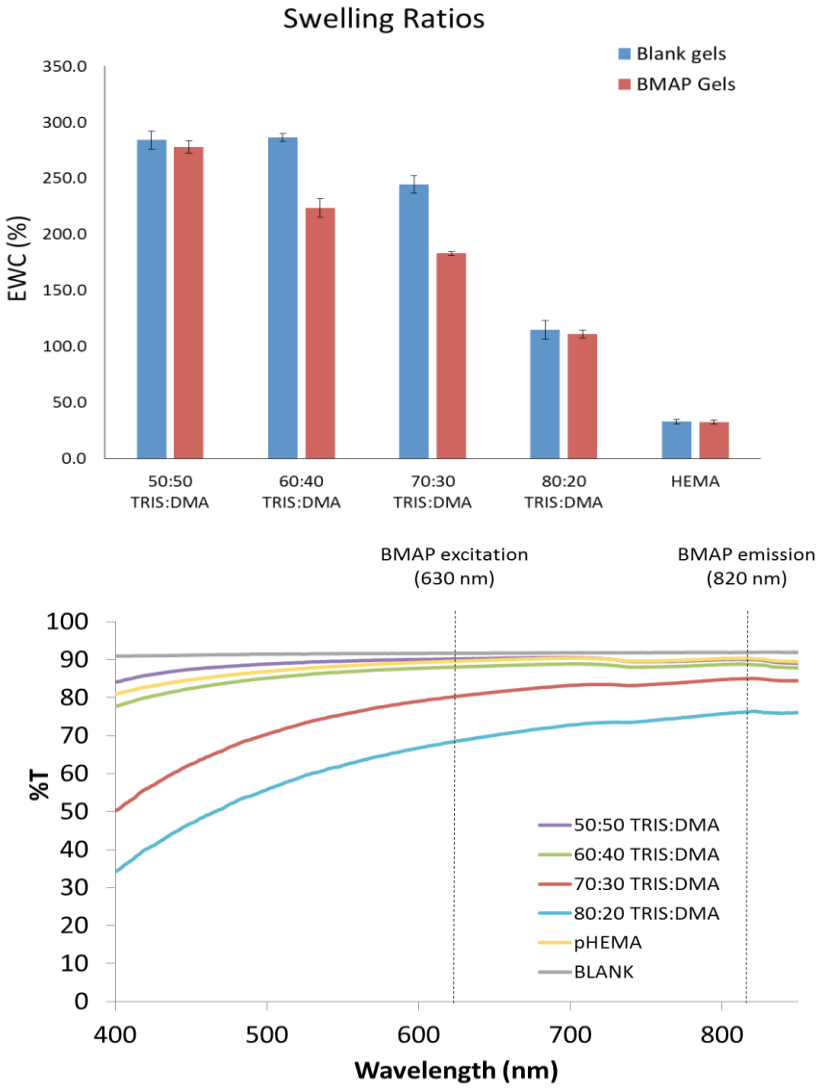

Figure 5-2: Swelling (top) and optical clarity (bottom). Swelling data represent triplicate averages; error bars represent 95% confidence intervals.

decrease in overall water content (EWC) with increasing TRIS content. This trend was expected because of the hydrophobic nature of TRIS; thus, a gel with higher TRIS content should imbibe less water than those with higher DMA content relative to TRIS. With the exception of 60:40 and 70:30 TRIS:DMA, the presence of the PdBP dye does not significantly affect the swelling ratio ($p < 0.05$). Regardless of TRIS:DMA ratio, all IPN gels were significantly more hydrated than pHEMA single-network gels. This was expected because of the highly hydrophilic nature of DMA compared to pHEMA, shown in previous studies using DMA as a wetting agent for contact lenses [72, 148, 167, 169, 176]. Transmission spectra showed that with 70 to 80% TRIS content, the gels began to lose optical clarity over all wavelengths tested. However, 60:40 and 50:50 TRIS:DMA gels both exhibited similar optical transparency behavior to pHEMA (%T values within 2% of pHEMA for both formulations), including in the PdBP excitation/emission window (630 to 820 nm, denoted by dashed black lines, Figure 5-2, bottom).

Additionally, the data suggest that the IPN morphology successfully prevented the phase separation and opacity characteristically reported in the literature for single-network silicone hydrogels [148, 183]. Decreased transparency in gels with higher TRIS content (70 to 80%) was likely caused by incomplete crosslinking of the TRIS chains due to the highly branched structure of the TRIS pendant group causing steric hindrance effects, blocking access of unreacted methacrylate groups to free radicals and slowing the propagation of the free-radical polymerization. Steric hindrance effects have been reported in the literature in similar free-radical-initiated systems using ethylene-glycol-derived crosslinkers [184]. While siloxane materials are notorious for their oxygen

permeability, free-radical polymerizations are inhibited by oxygen, as oxygen is an excellent free-radical scavenger. In the case of TRIS, a siloxane methacrylate, higher amounts of TRIS may have allowed enough oxygen back into the system to stunt the crosslinking with TEGMDA. In fact, oxygen inhibition in similar photocurable siloxanes crosslinked with ethylene-glycol-derived crosslinkers has been reported in research and in the coatings and resins industry [185]. In the current system, the polymer chains containing high amounts of TRIS may not have been fully crosslinked in the first matrix by the TEGDMA crosslinker due to either oxygen inhibition or steric hindrance effects. This could have prevented the second pDMA network from fully reinforcing the first silicone-containing network if polymer chains were not fully tethered to the first matrix, resulting in phase separation in the IPN hydrogels with higher TRIS content.

Despite some variations in transparency with higher silicone content, it is evident that the second network, pDMA, prevents silicone phase separation, at least to some extent, based on the fact that previous work has shown substantial TRIS phase separation in a single network monolith hydrogel with only 20 vol% of TRIS [183]. All formulations here have higher TRIS contents and increased optical clarity, indicating that the IPN network morphology reinforces the silicone and prevents phase separation. This is consistent with previous TRIS-containing IPN hydrogel reports for contact lenses [176, 177].

5.3.1.2. Homogeneity

Confocal microscopy images (Figure 5-3) indicate some phase separation in the 80:20 TRIS:DMA as expected from the loss in optical clarity indicated from the UV-Vis

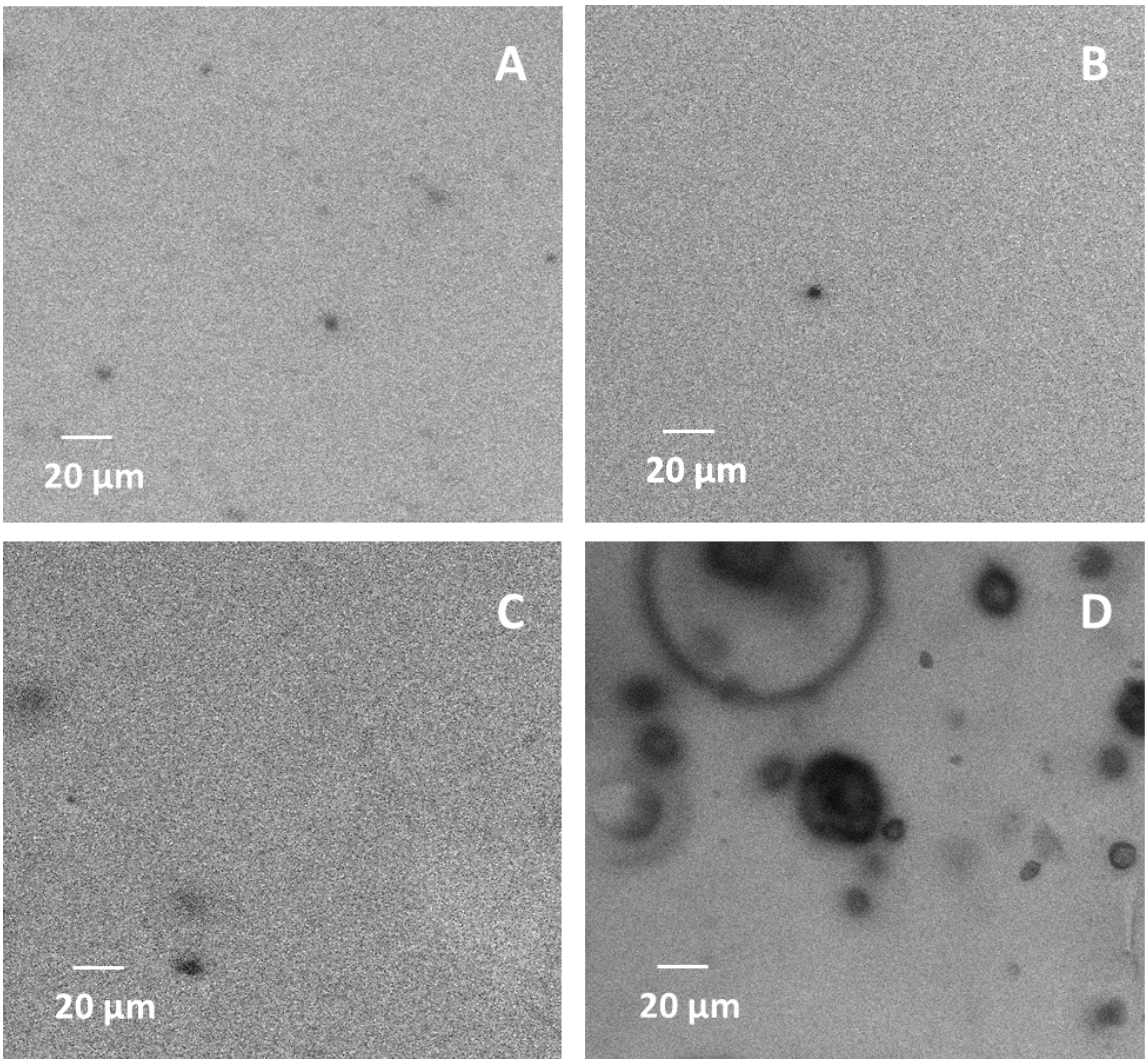

Figure 5-3: CLSM images of IPN hydrogels. Images were taken at 10× magnification. Sections corresponding to the ratio of TRIS:DMA are as follows: A = 50:50, B = 60:40, C = 70:30, D = 80:20.

measurements (Figure 5-2). Lighter regions of the confocal images indicate areas where more dye was sequestered within the gel. The 80:20 TRIS:DMA confocal image (Figure 5-3D) shows darker spherical regions dispersed throughout a lighter bulk gel material.

Confocal images of the other formulations appear much more uniform throughout the gel, despite a few dispersed defects throughout the gels (Figure 5-3 A-C). The phase separation behavior seen in the confocal images is contrary to the hypothesized mode of phase separation based on the phase separation behavior of the 60:20:20 HEMA:NVP:TRIS gel in Section 4.3.2.1.3. With the 60:20:20 HEMA:NVP:TRIS gel, the dye-stained silicone regions were located in the dispersed phase, and these silicone regions were distributed throughout the hydrophilic phase containing HEMA and NVP. Opposite phase separation behavior occurred here likely because four times as much silicone by volume was used to fabricate the 80:20 gels than in Chapter 4. This may allow the DMA to become the dispersed phase, with DMA-rich microdomains dispersed throughout the bulk material. Additionally, these IPN gels were made with a substantial amount of DCM as a precursor co-solvent (35 vol% of the total precursor solution). In previous studies of hybrid inorganic-organic silicone hydrogels, solvent-induced phase separation was desired and accomplished by using DCM as the primary solvent in the precursor solution. This allowed the silicone to remain in the continuous phase; similar behavior is seen here [154, 155]. To facilitate viewing of the three-dimensional distribution of the inhomogeneities throughout the IPN gels, montages of 20 single-slice confocal microscope images are shown in Figure 5-4; distance (depth) between sequential images is 5 μm.

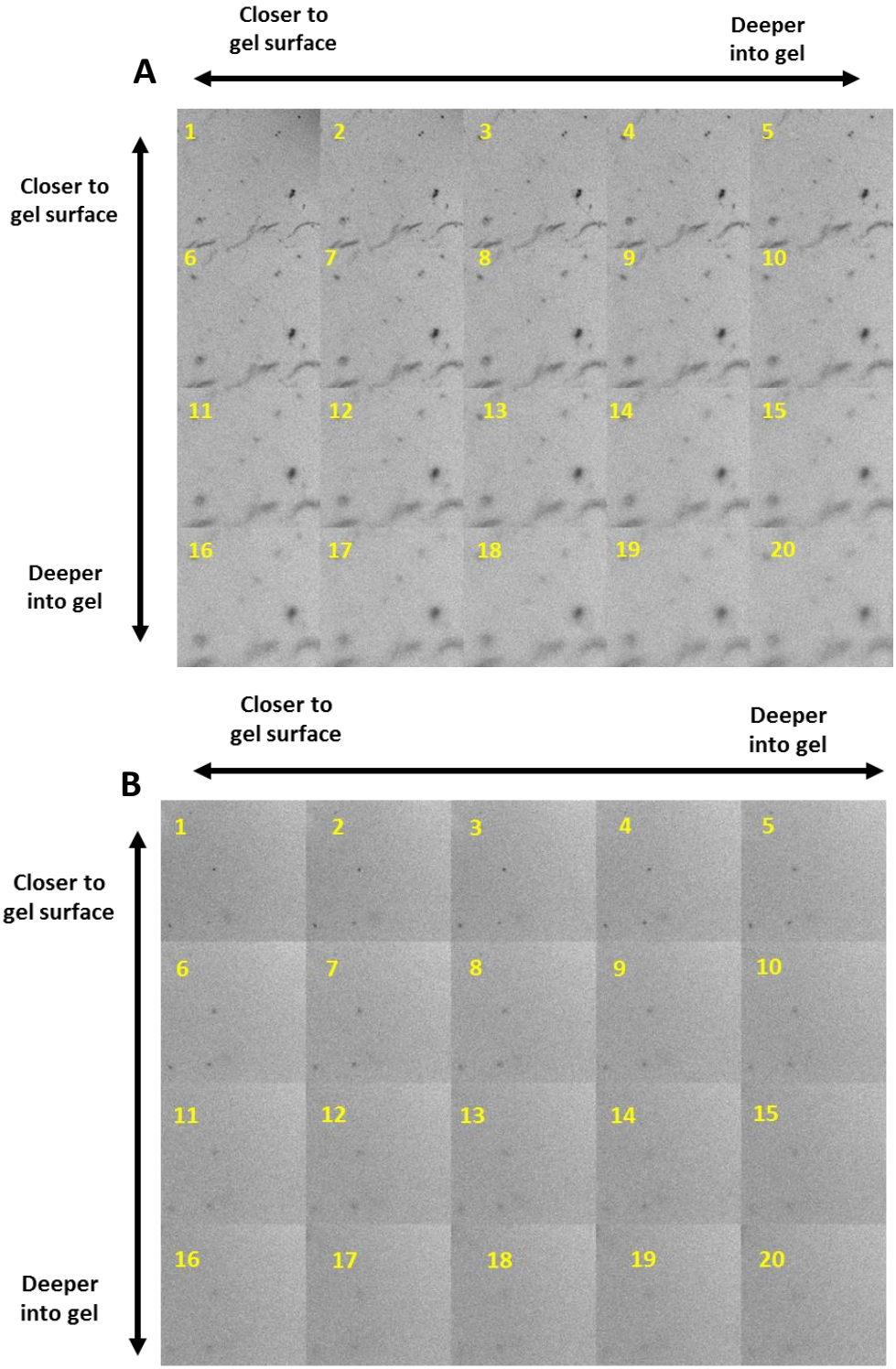

Figure 5-4(A-B): Montages of CLSM images on IPN gels. Sections corresponding to the ratio of TRIS:DMA are as follows: A = 50:50, B = 60:40, C = 70:30, D = 80:20.

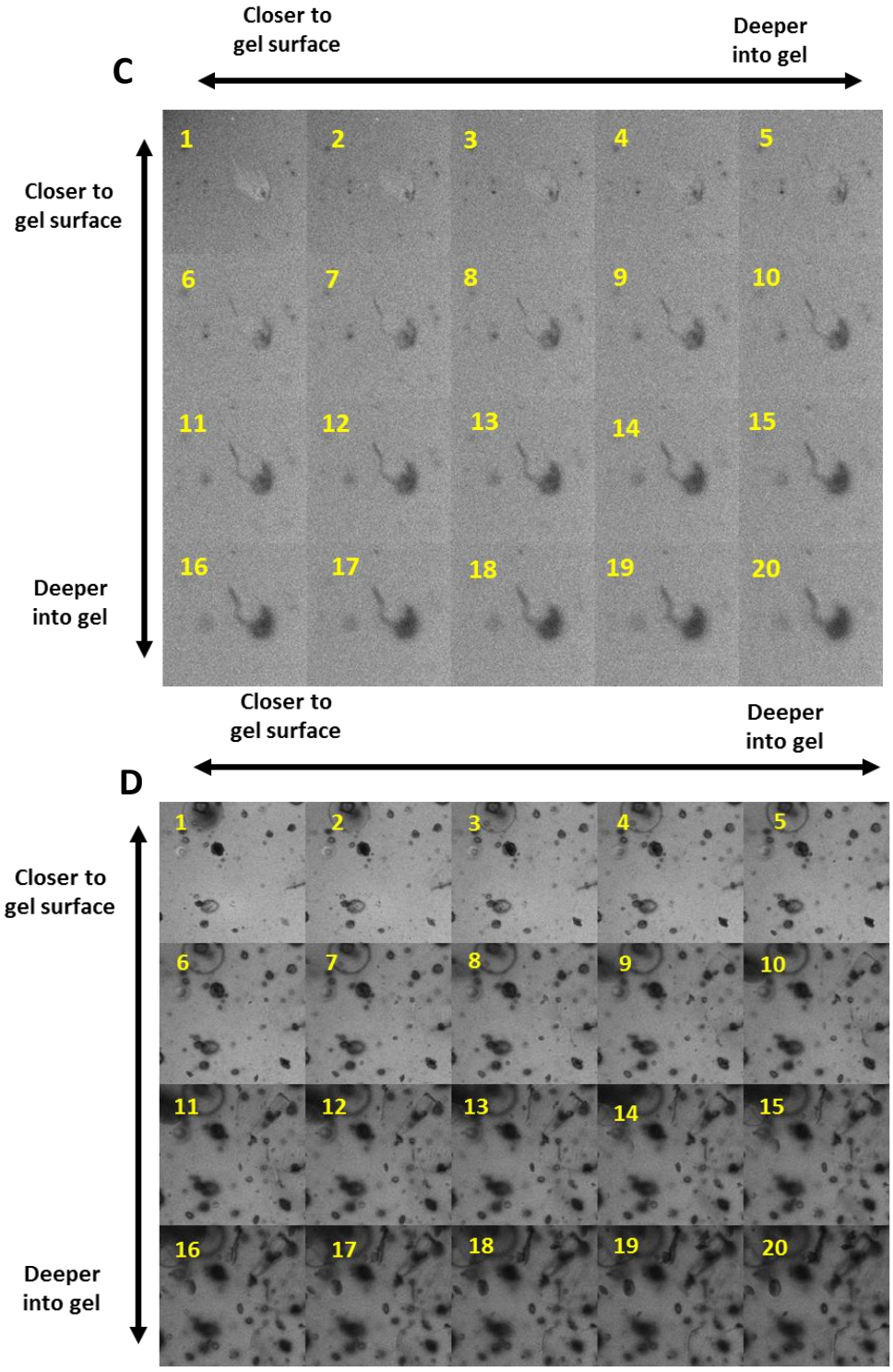

Figure 5-4 (continued, C-D): Montages of CLSM images on IPN gels. Sections corresponding to the ratio of TRIS:DMA are as follows: A = 50:50, B = 60:40, C = 70:30, D = 80:20.

5.3.1.3. Thermomechanical Properties

Figure 5-5 A-B show the real elastic modulus (G') and imaginary viscous modulus (G") results for all formulations tested within their viscoelastic region. As expected, all G' values were found to be higher than their associated G" values, indicating a predominantly elastic response in all IPN formulations [186]. Neither G' nor G" for the 50:50 and 60:40 TRIS: DMA formulation at 25 °C were significantly different (t-test, $\alpha = 0.05$). Increasing temperature resulted in an overall decrease in both G' and G"; elevated temperatures have been shown to transform the hydrogel from its rigid, glassy state to a more flexible, rubbery state, resulting in increased chain mobility and decreased storage and loss modulus [187]. Additionally, there was a slight decrease in modulus with a decrease in TRIS content at the tested frequencies, trending similarly to water content results shown previously (Figure 5-2); a decrease in the hydrophobicity of the IPN (increase in TRIS content) resulted in a decrease in both G' and G". It is important to note the slight increase in G' with increasing frequency for the 80:20 TRIS:DMA IPN, indicating physical, mechanical hindrance of the bulky TRIS sidechains at higher frequencies [188].

The DSC results (Figure 5-5E) showed no statistically significant difference (t-test, $\alpha = 0.05$) between the glass transition temperatures among 50% to 70% TRIS content, all three gels being around 112 °C. However, the gel with 80% TRIS exhibited a significantly depressed T_g, dropping around 50 °C lower than the three other IPN gels. This decreased T_g is attributed to the high siloxane content of the 80:20 formulation, as siloxane bonds are known for their remarkable torsional flexibility, and the branched

TRIS pendant group structure is known for its plasticizing ability [163, 164, 166]. Although a steady decline in T_g with increasing siloxane content was predicted, the behavior seen in Figure 5-5 could be due to the fact that the siloxane linkages were in the polymer pendant groups, not in the backbone. Comparatively, PDMS has one of the

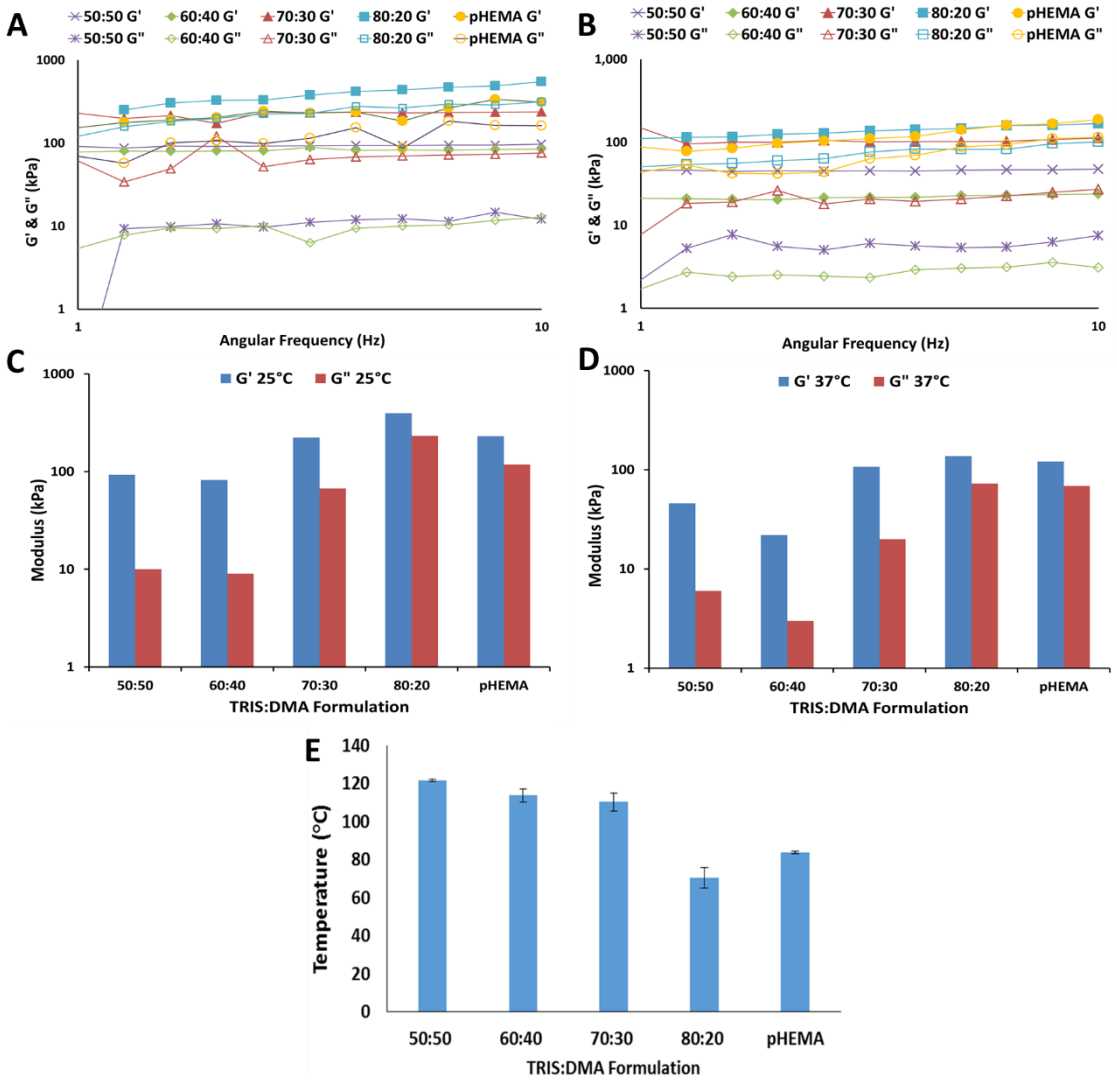

Figure 5-5: Dynamic mechanical testing results composed of storage and loss moduli at 22 °C (A&C) and 37°C (B&D). Glass transition temperatures of dried gels (n=3 ± 95% confidence intervals)

lowest T_g values among polymers; however, those siloxane linkages are in the polymer backbone. With TRIS, the polymer backbone is a vinyl backbone without siloxane bonds, which could justify the fact that depression of the T_g was not seen until the first network contained 80% TRIS. Because T_g is characterized by increased segmented mobility of the polymer backbone, a stronger correlation between T_g and siloxane content may be seen with a polymer containing a siloxane backbone (e.g., PDMS). Furthermore, the entire second network is pDMA; T_g values for 50% to 70% TRIS are similar to T_g values reported for pDMA homopolymers [189]. This suggests that DMA mechanical properties dominate the overall mechanical behavior of the IPNs in this study.

5.3.1.4. Oxygen Transport—Stern-Volmer Kinetics

Figure 5-6 shows a drastic increase in oxygen permeability according to Stern-Volmer diffusion kinetics, as evidenced by the increased linear slopes (K_{SV} values) of all IPN formulations versus the pHEMA standard. Specifically, the IPN monoliths exhibited an average 256% increase in oxygen permeability based on K_{SV} and a 210% increase based on k_q. Although the IPNs overall were significantly more permeable to oxygen than pHEMA (t-test, $\alpha = 0.05$), among IPNs, all formulations were significantly different than pHEMA (t-test, $\alpha = 0.05$). Comparing IPNs among themselves, only the 80:20 formulation was found to be significantly different from 50:50 and 70:30; no other formulations showed statistical difference (t-test, $\alpha = 0.05$). These two anomalies

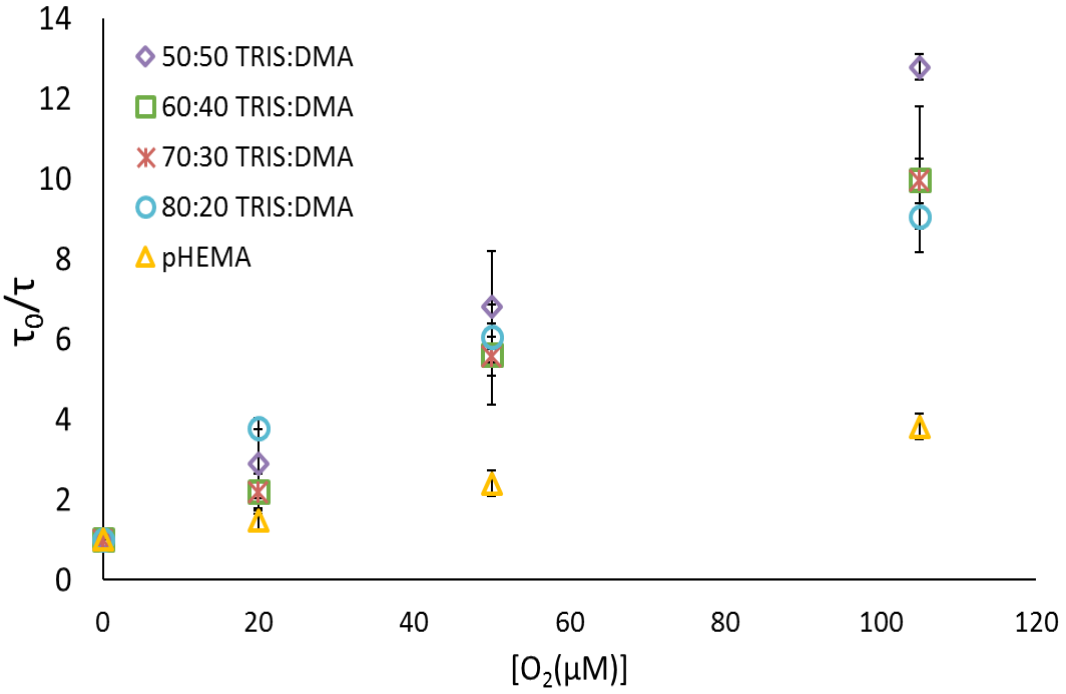

Figure 5-6: Stern-Volmer oxygen diffusion plots and *in vitro* figures of merit on oxygen sensor monoliths. Data represent averages (n=3) ± 95% confidence intervals.

aside, the results indicate that one can maintain a significantly increased oxygen permeability (compared to pHEMA) with these hybrid IPN gels irrespective of the silicone content (Table 5-2).

Table 5-2: Figures of merit for IPN and pHEMA gels

Figure of Merit	50:50 TRIS:DMA	60:40 TRIS:DMA	70:30 TRIS:DMA	80:20 TRIS:DMA	pHEMA
K_{SV} (μM^{-1})	0.112 ± 0.007	0.086 ± 0.019	0.084 ± 0.006	0.083 ± 0.002	0.0256 ± 0.002
τ_0 (µs)	267 ± 4	276 ± 20	307 ± 11	307 ± 5	248 ± 2
k_q ($(\mu s\text{-}\mu M)^{-1}$)	4.18E-04 ± 0.30E-04	3.15E-04 ± 0.82E-04	2.75E-04 ± 0.18E-04	2.70E-04 ± 0.05E-04	1.03E-04 ± 0.08E-04

5.3.2. In Vivo Characterization

5.3.2.1. *In Vivo* Oxygen Modulation—Baseline Analysis

Figure 5-7 shows baseline lifetime averages for all six IPN implants. There is a remarkable difference in baseline averages between the slab and ICC morphologies. For example, while the slab baseline lifetime ranged from 20 to 206 µs on day 34, the baseline lifetime of the ICC implants only varied by 11 µs among all three implants. Similar trends were observed for each subsequent timepoint. There was some variability in baseline lifetimes from day 0 to day 20 for both ICC and slab implants; however, this variability diminished by day 20, whereas slabs did not assume this uniformity.

5.3.2.2. *In Vivo* Oxygen Modulation—Real-time Excursions

Real-time oxygen tracking data in Figure 5-8 show low baseline lifetimes (<50 µs) for both slab and ICC implants after implantation (day 0). Initially, slab sensors exhibited low sensitivity to oxygen with only a 15-µs change in measured phosphorescence lifetime. However, the response sensitivity improved drastically over

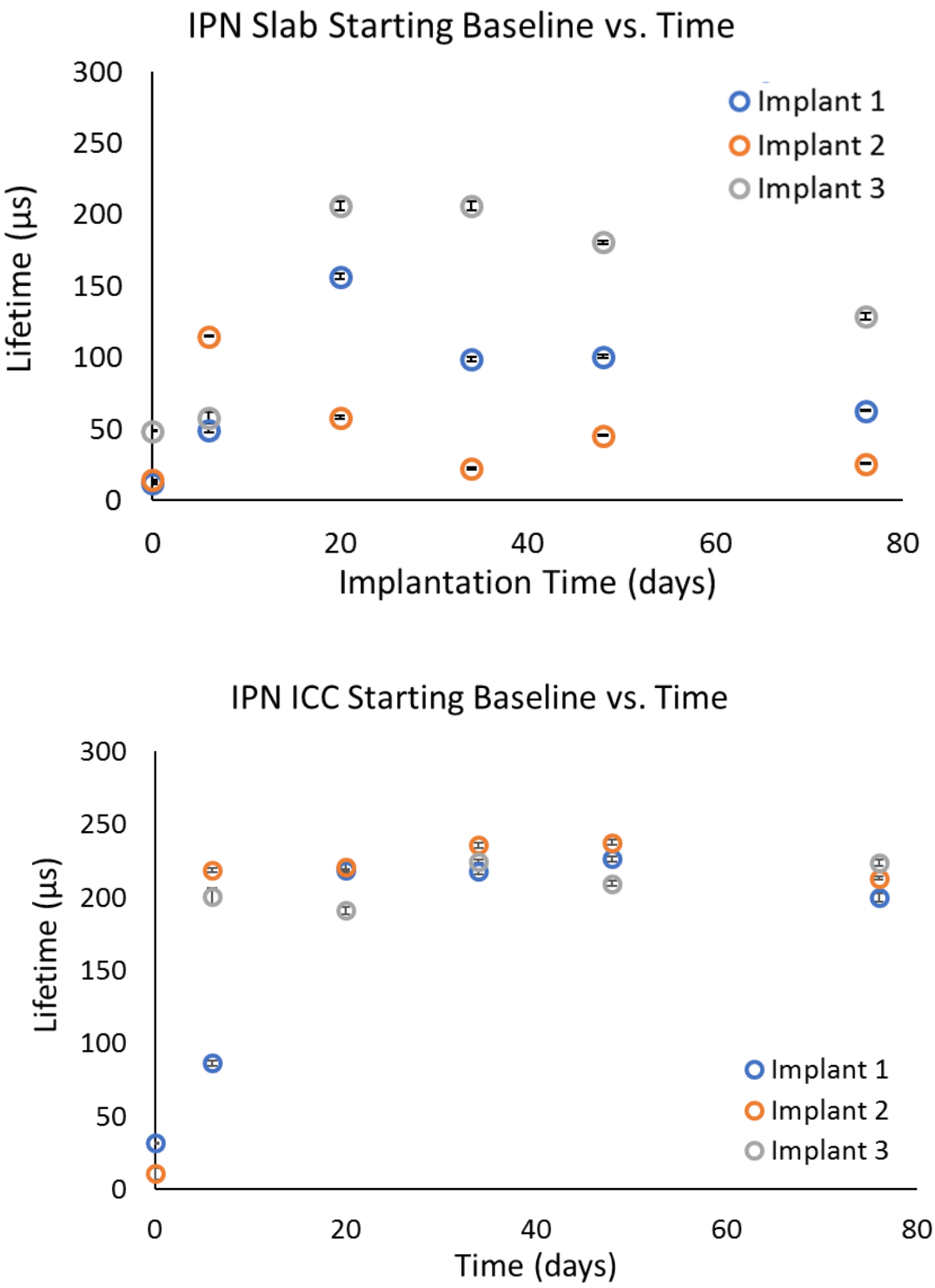

Figure 5-7: Baseline lifetimes of all six IPN implants over 72 days.

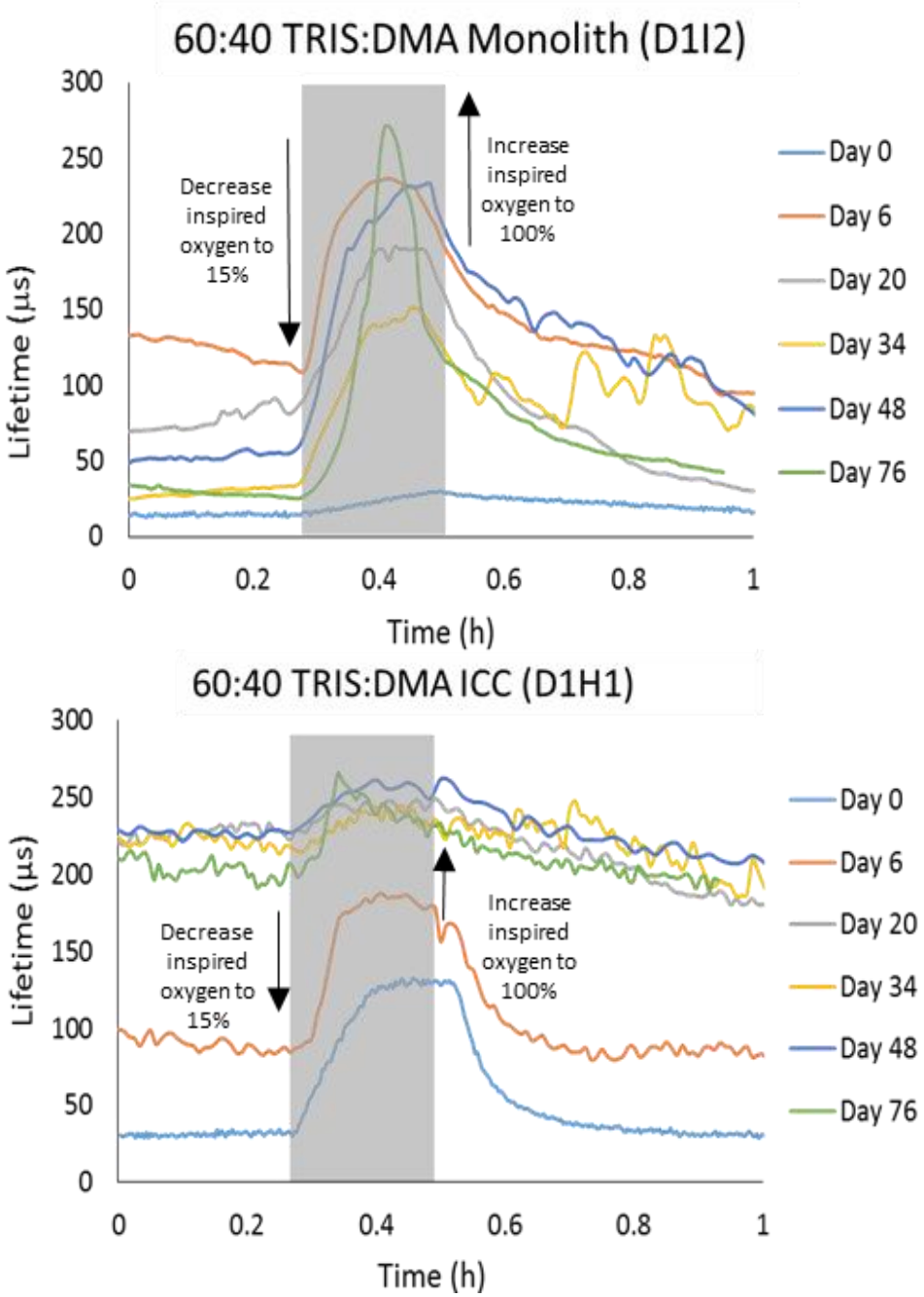

Figure 5-8: Top: Real-time oxygen sensor response profile at 100% inspired oxygen (baseline) and 15% inspired oxygen (modulation) for two representative slab and ICC implants. Modulation time is indicated by shaded regions. Bottom: Luminescence lifetime averages immediately before starting oxygen modulation experiment. Data represent average (n=10 data points) ± 95% confidence intervals.

time for the monolith slab implants, reaching up to a 245-µs change in measured phosphorescence lifetime during modulation (over 1500% improvement from the initial modulation level). These trends rise from the differences in morphology between the slab and ICC implants. The microporated architecture of the ICC tissue-integrating scaffolds afforded those implants a higher surface-area-to-volume-ratio which allowed blood from the fresh wound to penetrate the scaffold more rapidly after implantation, resulting in a quicker response to local changes in oxygen. This is substantiated by the resulting in a quicker response to local changes in oxygen. This is substantiated by the distinct response plateau around 130 µs at day 0 and the subsequent rapid decline to the baseline lifetime value upon resuming 100% inspired oxygen level, a trend that was not observed in the solid monolith implants. However, the sensor sensitivity (% modulation) increased for the solid implants as time progressed, attributed to the wound healing around the implant. As the tissue healed, the local oxygen levels decreased, rendering the dye more sensitive to changes in local oxygen, a known property of oxygen-quenched porphyrins.

Opposite trends were observed for ICC implants. ICC sensors exhibited high sensitivity initially (~100 µs change in lifetime during oxygen modulation). While most of this sensitivity was maintained after six days (within the acute immune response window), ICC sensors began to lose this sensitivity to oxygen as implantation time progressed and the tissue healed, leading to a more steady-state behavior and chronic, end-stage immune response. Although ICC sensor baseline lifetimes were higher and sensor sensitivity decreased, a higher degree of response uniformity was observed

compared to the solid monolith slab sensors. This is due to the tissue-integrating nature of the ICC scaffold. While primarily used to promote angiogenesis throughout the ICC construct, increase in baseline lifetime and lower modulation may be due to some deposition of connective tissue (e.g., collagen) throughout the scaffold. As healing transitioned to the chronic immune response stage, the scaffold baseline lifetime became more consistent, but the sensitivity decreased (down to ~35 µs at day 72). While there was a sacrifice of sensor sensitivity based on change in signal level, the sensor response was relatively consistent from day 20 to day 76 for the tissue-integrating ICC scaffolds.

5.3.2.3. *In Vivo* Oxygen Modulation—Absolute and Percent Signal Changes

Absolute lifetime changes (Figure 5-9) were determined by subtracting the baseline lifetime before modulation (average of 10 data points) from the peak lifetime (highest lifetime observed during the modulation, average of 10 data points). Percent modulation (Figure 5-10) was calculated by determining the percent increase in luminescence lifetime averages from baseline to peak signal during modulation (average of 10 data points for both baseline and peak signals). These calculations were performed for each timepoint measured. Trends are consistent with the real-time modulation data described in Section 5.2.4.1. Overall, the percent modulation was more variable from day to day with the solid slabs and more consistent in the long term with the ICC implants. However, the D1I2 sensor reached up to 1000% change in signal level, the highest change reported *in vivo* for the sensors in this work [65]. Furthermore, it is notable that the slab sensor with the highest percent change during modulation (i.e., the most sensitive, D1I2) was also the sensor with the lowest baseline lifetime throughout

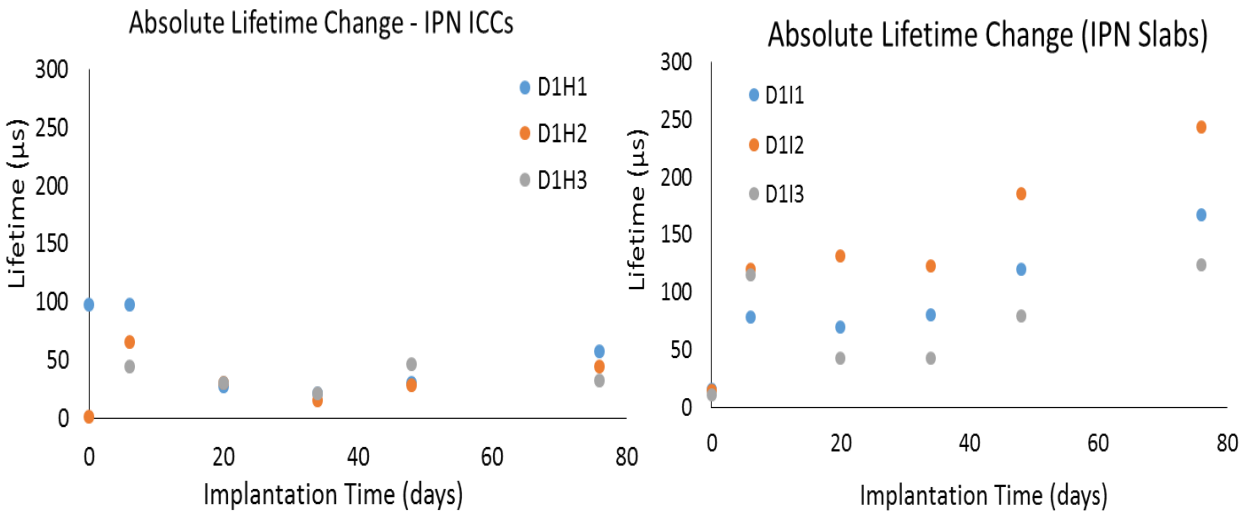

Figure 5-9: Absolute Lifetime change over time for all slab and ICC implants

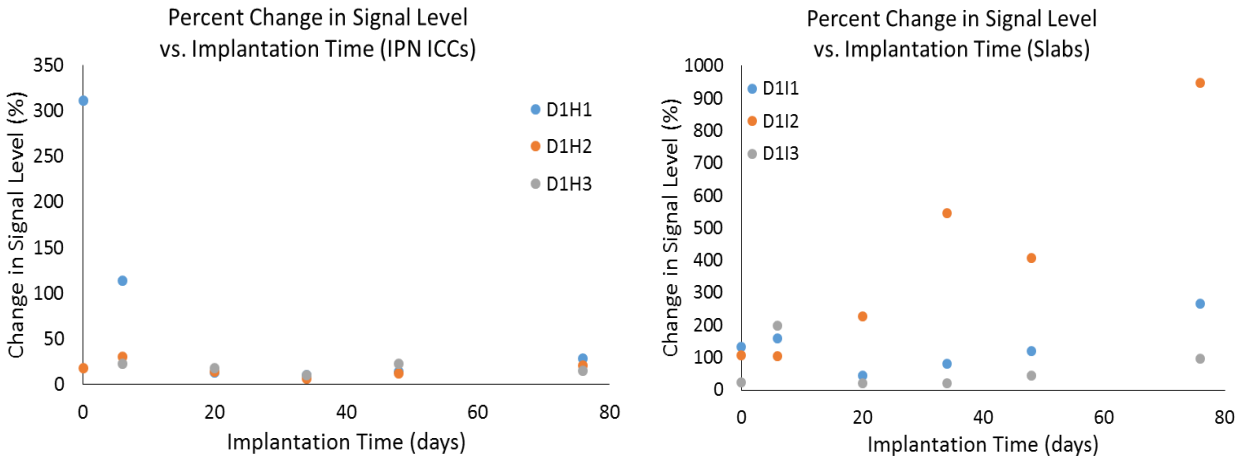

Figure 5-10: Percent modulation versus implantation time for all slab and ICC implants.

the entire study. Conversely, the slab sensor with the highest baseline lifetime in the long term was also the sensor exhibiting the lowest percent change and lowest sensitivity. It is important to keep in mind that these conclusions are drawn based on the percent change values, and the baseline values vary among the slab implants. Similar trends were observed when calculating the absolute lifetime change for all implants. However, all

slab sensors reached a peak lifetime between 230 and 260 μs, regardless of the starting baseline lifetime value. This is reasonable considering that the natural lifetime, τ_0, values were calculated at 275 ± 20 μs for the 60:40 TRIS:DMA formulation and the inspired pig oxygen level during modulation was 15% oxygen.

For the ICC implants, percent modulation significantly decreased (about an order of magnitude), but this was likely due to higher surface area contact of connective tissue ingrowth throughout these tissue-integrating implants. Additionally, the percent modulation and absolute lifetime changes are more consistent for all three sensors among all timepoints. This behavior correlates with the baseline signal consistency observed in Figure 5-7 among the ICC implants.

5.3.2.4. Biocompatability—Relationship between Morphology and Foreign Body Response

Inverted colloidal crystals were fabricated by using a partially-fused microsphere template (called a "beadcake") as a sacrificial template to create porous scaffolds with highly uniform pore spacing. Sintered PMMA beads (80 μm in diameter) were used as the beadcake material to synthesize all IPN ICC hydrogels in this study. A precursor of the first network was dispensed over the beadcake in a Teflon mold. The hydrogel and template were removed from the mold and soaked in a precursor solution of the second network, DMA. After overnight soaking, the beakcake/gel composite was blotted thoroughly on a Kimwipe to remove all of the excess DMA precursor and polymerized as in Section 5.2.2. After the second photocuring process, the hydrogels were placed in a solution of DCM overnight for dissolution of the remaining sintered beads. Figures 5-11

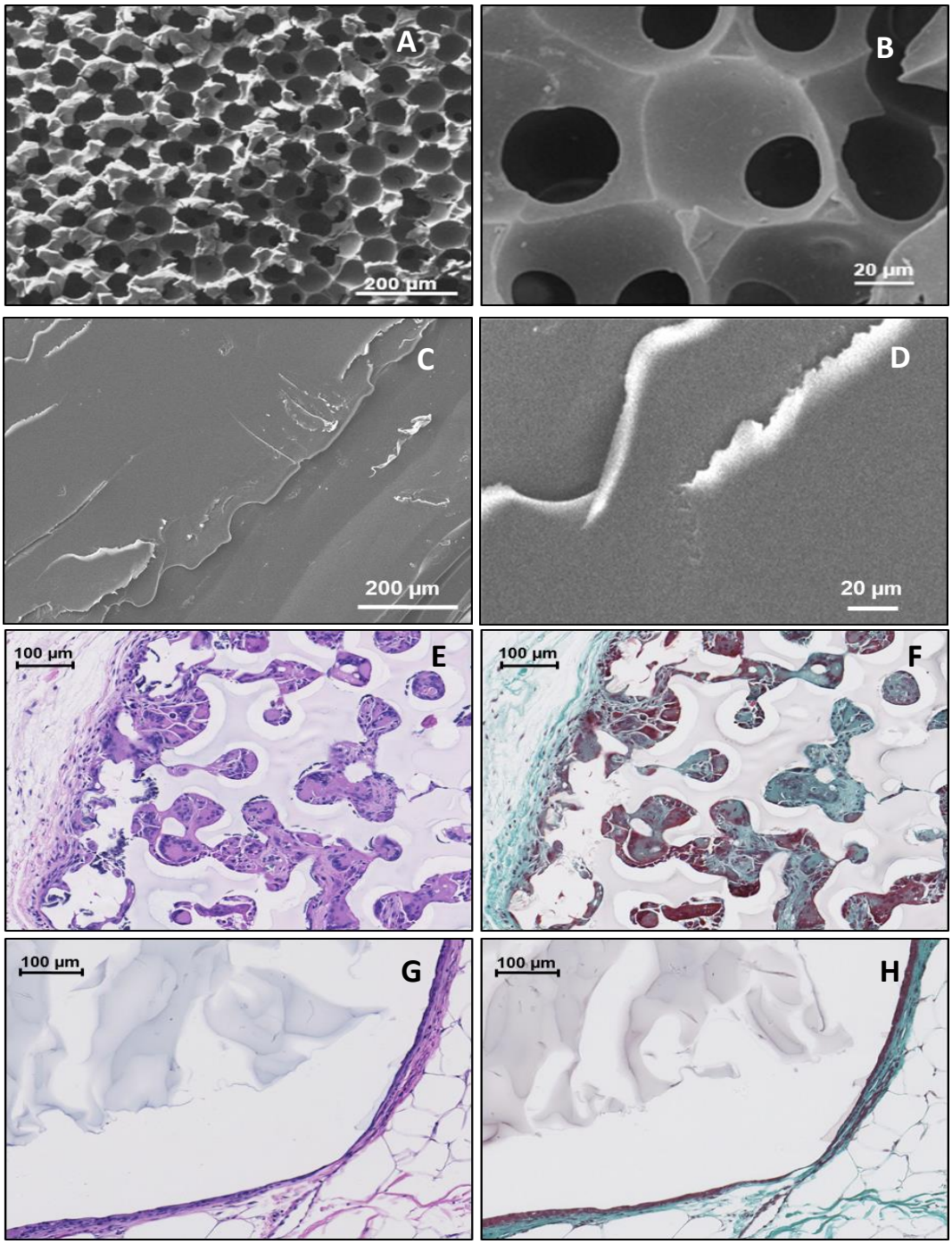

Figure 5-11: SEM images of ICC and slab surface, respectively, at 100× and 540× (A&B) and 20× (C&D) magnification. Histology images of both ICC and slab hydrogels after explantation: Haemotoxylin and Eosin-stained images (E&G) show the presence of tissue ingrowth (pink) and cell nuclei (purple) while Masson's Trichrome stained images (F&H, 20×) further differentiate the presence of loosely-woven collagen (blue) and cellular penetration (red).

A and B consist of SEM images confirming an average pore size of 50 µm after freeze-drying and lyophilization. The slight decrease in pore size was attributed to vacuum-drying of the hydrogels in the lyophilizer. Not only do ICCs generate highly uniform pore structures, but they also have interconnects (Figure 5-11A-B), which are necessary for tissue ingrowth [179]. SEM images of slab hydrogels, shown in Figures 5-11 C and D, were included for comparison and showed a smooth surface, lacking the pores necessary for tissue integration and vascularization.

Tissue integration through the oxygen sensor is thought to extend the sensor lifetime by providing a constant supply of oxygen due to circumventing the fibrous encapsulation caused by the foreign body response. Figure 5-11E shows tissue ingrowth throughout the pores of the ICC implant, as indicated by the red color (H&E stain) interspersed throughout the implant image. Additionally, Figure 5-11F shows loosely-packed collagen indicated by the light teal/blue fibrous structured regions (Mason's Trichrome stain) surrounding the implant. On the contrary, the slab histology H&E stain in Figure 5-11G demonstrates a pink encapsulation layer dotted with dark purple cell nuclei, indicating the presence of an immune response. The trichrome stain of the slab implants in Figure 5-11H reveal densely-packed collagen and cell nuclei around the implant, characteristic of typical fibrosis response to a solid sensor implant [66, 125, 126, 190].

5.4. Conclusions

This chapter demonstrates the ability to fabricate hybrid inorganic-organic IPN silicone hydrogels as optical biosensors. Through *in vitro* characterization, these

hydrogels have been shown to significantly increase the oxygen permeability to the pHEMA standard when functionalized with a long-lifetime, oxygen-quenched phosphor. This work further demonstrated the ability to maintain increased oxygen permeability while altering gel hydration, glass transition temperature, and mechanical properties, key novelties from previous single-network gels (Chapter 4) where water content and substrate transport directly influenced each other, and inhomogeneities within the gel matrix curtailed the oxygen transport and dynamic range of the sensors.

Furthermore, fabrication of these hybrid IPN gels with an inverted colloidal crystal microarchitecture had not been demonstrated with a sequential polymerization process prior to this work. These inverted colloidal crystal oxygen-sensing scaffolds were shown to promote tissue ingrowth and vascularization throughout the scaffold, showing much more loosely-packed collagen surrounding the implants versus the densely-packed fibrous capsule typically found around solid implants which includes the IPN monolith sensor implants in this study. Both solid monolith and porous ICC implants responded to real-time oxygen modulations *in vivo.* Despite the unexpected sacrifice in sensor sensitivity (based on percent signal change during oxygen modulation) *in vivo,* the response among ICC implants became more repeatable and uniform due to the tissue integration. Loss in ICC sensitivity could be mitigated by using a beadcake consisting of PMMA microspheres of a different diameter (i.e., 40 μm). Smaller pores (i.e., 40 μm) have been used in other ICC implant studies, albeit not for biosensing applications and not in porcine models [70, 73, 179-181]. It is recommended for future preclinical trials that alternative pore sizes be investigated alongside 80-μm

diameter pores when fabricating IPN ICC sensors. Delving further into utilizing different pore sizes with these IPN ICC sensors will allow researchers to correlate the sensor sensitivity to local oxygen changes in real time as well as to the extent of fibrosis around and throughout the implants. This is useful not only from an exploratory standpoint, but also for the purpose of optimizing the repeatability and sensitivity of these oxygen sensors to ultimately transduce signals representative of other analytes besides oxygen (i.e., glucose and lactate).

6. CONCLUSIONS AND FUTURE WORK

Proper substrate transport, retention of enzymatic apparent activity, and achieving proper balance between both diffusion and reaction are major barriers to achieving long-term sensor function *in vivo.* This dissertation presents the evaluation of three approaches toward achieving long-term *in vivo* function of a fully implantable CGM. Various sensor formulations and morphologies were tested by characterizing the underlying oxygen response and overall glucose response on the benchtop and in porcine models. Each aim of this work describes a different approach to evaluating feasibility on the benchtop and preclinical performance.

6.1. pHEMA-co-AAm Single-Network Monolith Hydrogels

In the first approach (Chapter 3), pHEMA-co-AAm gels were functionalized with a red-excitable assay consisting of GOx, CAT, and PdBP. Gels were subjected to a peroxide-based absorbance assay to assess apparent GOx activity and thermostability over a two-week period. A 75:25 HEMA:AAm formulation was chosen for further investigation. Stern-Volmer testing revealed a linear quenching trend (R^2>0.99) at physiological oxygen levels, and *in vitro* glucose challenges revealed a distinct stair-step response in the hypo- and euglycemic ranges with high sensitivity and a quick response time (less than 10 minutes). Upon implantation in a porcine model, these sensors responded in real time to infusion of glucose via IV 2.5 hours after implantation, with the first report tracking rising and falling blood glucose levels in real time using a phosphorescence lifetime-based sensing platform. However, baseline lifetimes rose

significantly (more than 200 μs) after two weeks, and these sensors did not respond to glucose long term, which can be attributed to drastic decreases in the tissue oxygen levels surrounding the implant. After six weeks, these sensors were explanted and responded to glucose at physiological conditions, indicating that substrate transport balance, not total enzyme activity loss, was the cause for the lack of long-term response *in vivo.* Because this study was designed to show proof of concept *in vitro* and *in vivo* with the red-excitable glucose sensing assay, materials were selected based on previous studies with a similar assay (green-excitable), using a 75:25 HEMA:AAm copolymer as a "common middle ground" for both the enzyme and dye components of the sensor. Although it was shown that the GOx retained some activity after six weeks *in vivo* (evidenced by *ex vivo* testing), exactly how much GOx apparent activity was preserved was not apparent from the study's design. The concentration of GOx and CAT used in this study was based on prior work [24] that did not describe a method to optimize enzyme concentration. Although sensor function *ex vivo* was maintained after six weeks *in vivo*, an excess of GOx in the sensor could mask the apparent activity loss and the fundamental enzyme stabilization efficiency of the gel. In fact, if an excess of GOx is used in the sensor, then loss in enzyme activity could be masked. While compensating for enzyme activity loss may appear valuable at first glance, from a production standpoint, this could lead to unused, wasted reagent in the sensor fabrication pipeline and could also affect the aforementioned reaction/diffusion balance. Therefore, a more fundamental study was designed to further understand the fundamentals of enzyme activity loss as a function of the ratio of GOx to the total protein in the sensor and as a

result of prolonged exposure to physiological conditions (glucose, pH, and temperature) with the rationale that probing deeper into the fundamentals behind GOx apparent activity retention over time will pave the way for a more thoughtful sensor design and accelerate the time to achieve long-term preclinical proof of concept.

6.2. Alternative Single-Network Monolith Hydrogels

The above questions directed the approach for Aim 2 (Chapter 4), which involved investigating a library of materials for feasibility in this long-term glucose-sensing application by exposing the candidate materials to glucose (100 mg/dL) at physiological pH and temperature (where previous experiments only tested thermostability at physiological pH) to further replicate the *in vivo* environment and further investigate the efficacy of materials to better optimize GOx apparent activity long term. This second approach to refining sensor design started with identifying a library of promising material candidates, fabricating gels out of these candidates by incorporating various amounts of GOx into the precursor, and testing them weekly in a high-throughput o-dianisidine assay, incubating in physiological conditions between each assay timepoint. This study showed, surprisingly, that pHEMA and pHEMA-co-AAm gels were the least effective in preserving GOx apparent activity, regardless of the concentration of GOx loaded in the gel. However, pHEMA-co-DMA and pHEMA-co-NVP gels were more effective in preserving GOx activity, preserving 60 to 92% of the apparent activity after one week of incubation versus HEMA:AAm and HEMA homopolymer gels, which lost nearly all of their activity within the first week. Although this high-throughput assay method proved to be less sensitive to changes in GOx

concentration than originally anticipated, it served as a first-pass evaluation of a broad set of materials, revealing general trends between hydrogel formulation and GOx stability. Using this first-pass test to hone in on the most promising material candidates guided the development of more oxygen-permeable gel formulations, specifically ones with silicone (TRIS) and DMA.

In conjunction with identifying gel formulations that simultaneously enhance GOx stability and oxygen permeability, other factors influencing sensor performance were revealed. Specifically, it was shown that matrix inhomogeneities can adversely affect sensor performance, reducing dynamic range and the oxygen permeability. This was apparent in the silicone-containing gels (60:20:20 HEMA:TRIS:NVP), where phase separation was observed and silicone domains acted to sequester oxygen. These silicone domains competed with the surrounding matrix for oxygen; instead of allowing the expected enhanced oxygen permeability, these inhomogeneities decreased the oxygen transport properties of the gel. These findings led to the investigation of ways to showcase the oxygen permeability properties of the siloxane monomer, explored in Chapter 5.

6.3. Hybrid Materials—Summary and Future Improvements

The third approach discussed in this dissertation to refine sensor design toward achieving long-term *in vivo* function involved creating hybrid inorganic-organic materials as IPNs to 1) prevent or reduce silicone phase separation throughout the gels and 2) introduce an added degree of control over the gel physicochemical properties, altering them independently of one another instead of the previously used one-step,

"brute force" sensor fabrication method. This study showed the ability to increase oxygen permeability throughout the gels by over 250% based on K_{sv} compared to pHEMA; this increase in permeability was maintained regardless of the amount of TRIS in the gel. Coincidentally, the water content and optical clarity decreased with increasing TRIS content, but still three times as much TRIS could be incorporated into the first network (60%) without a significant change in optical clarity properties compared to pHEMA in the relevant *in vivo* optical window. In comparison, the 60:20:20 HEMA:NVP:TRIS gel investigated in Aim 2 showed phase separation even at only 20% TRIS.

Decreased transparency in gels with higher TRIS content (70 to 80%) is likely caused by incomplete crosslinking of the TRIS chains due to the highly branched structure of the TRIS pendant group causing steric hindrance effects, blocking access of unreacted methacrylate groups to free radicals and slowing the propagation of the free radical polymerization. Steric hindrance effects have been reported in the literature in similar free-radical-initiated systems using ethylene-glycol-derived crosslinkers [184]. While siloxane materials are notorious for their oxygen permeability, free-radical polymerizations are inhibited by oxygen, as oxygen is an excellent free-radical scavenger. In the case of TRIS, a siloxane methacrylate, higher amounts of TRIS may have allowed enough oxygen back into the system to stunt the crosslinking with TEGMDA. In fact, oxygen inhibition in similar photocurable siloxanes crosslinked with ethylene-glycol-derived crosslinkers has been reported in research and the coatings and resins industry [185].

While gelation time was shown to be affected by certain things like TRIS content and solvent ratios, one other factor to consider when considering the polymerization kinetics of this system is that free-radical polymerization is oxygen-inhibited. While all gel precursor solutions in this work were purged with nitrogen gas, the high oxygen permeability of the TRIS could decrease the efficacy of the nitrogen purge. Some air is introduced into the system when mixing the precursor with a pipette aspiration and dispensing the precursor into the mold. While this likely happens to some extent with all precursor formulations, the effect could be much more pronounced with the TRIS-containing gels due to the high oxygen permeability. Two possible ways to overcome this are 1) polymerize the gel in a vacuum oven purged with nitrogen or 2) employ a polymerization mechanism that is not inhibited by oxygen.

6.3.1. Alternative Polymerization Mechanism—Thiol-Ene Click Chemistry

Click chemistry is a genre of synthesis reactions that capitalize on nature's preference for carbon-heteroatom bonds over carbon-carbon bonds to give rise to materials with unique properties [191]. While carbonyl-based reactions, such as methacrylate polymerization, have traditionally been the focus of many synthesis applications, Click Chemistry has emerged as a focus to revolutionize molecular synthesis and expedite material fabrication processes [191-193]. Some applications of Click Chemistry include olefin synthesis, renewable or "green" polymer synthesis, bio-orthogonal functionalization and telechelic biopolymer fabrication, and dental restoratives [194-196].

Thiol-ene Click Chemistry has been used in the industrial coatings and resins, rubber manufacturing, and dental implant industries for many years, sometimes even being used in conjunction with epoxy-, vinyl-, or acrylate-based materials [197, 198]. One striking property of thiol-ene click reactions is that they are not inhibited by oxygen [192, 193, 197, 199]. Utilizing this property for creating the hybrid gels described herein could increase homogeneity and decrease gelation time since siloxanes are highly oxygen-permeable, and completely eliminating oxygen from the system during polymerization is difficult. While other click reactions, such as an alkyne-azide click reaction, could be useful for fabricating these gels, thiol-ene synthesis has been established with siloxane materials in the coatings and resins, photolithography manufacturing, and dental restoratives industries [198-200]. There are a wide variety of inexpensive vinyl and thiolated siloxane macromers commercially available that could be used for this application, which makes thiol-ene step-growth synthesis the most logical alternative to a random methacrylate-based addition synthesis, or at least to improve the efficacy of fabricating these hybrid materials with high silicone content.

6.3.2. Simultaneous Polymerization

Because the hybrid IPN gels described in this dissertation are made solely with methacrylate-based materials polymerized by the same mechanism, two separate curing steps were necessary to create two separate networks. This required soaking the gels in a second precursor solution to infiltrate the second network precursor components throughout the first as described in Chapter 5. This significantly delayed fabrication time, adding up to 24 hours to the fabrication process. One way to eliminate the need for

an overnight soaking time is to use two noninterfering polymerization mechanisms such that both networks can be polymerized simultaneously but independently, interweaving throughout each other without forming covalent bonds between the two networks. Various simultaneous polymerization mechanisms have been investigated for IPN polymers such as combining cationic and radical polymerization with acrylate, epoxy, and vinyl ether blends [201], with natural and synthetic materials using thiol click reactions [202], and even silicone-based materials such as PDMS and TRIS [203, 204]. Not only could using a simultaneous fabrication method increase fabrication time, eliminating the soaking step, but it could also allow for a more uniform matrix (without relying on external diffusion of a second precursor solution). Finally, eliminating a soaking stage in the fabrication process provides a more facile way to incorporate sensitive biomolecules, such as GOx, into the matrix; with the current sequential polymerization process, the organic solvent used in the IPN fabrication causes GOx to precipitate and denature [107, 205].

6.3.3. Introducing Glucose Responsive Functionality—Preliminary Studies

One other avenue to be pursued with these IPN gels is to functionalize them with alternate sensing chemistries to detect analytes such as glucose. With the enzymatic assays discussed in this dissertation, adding enzymes to these IPN gels is no trivial task. A solution of GOx is typically made in aqueous buffer before adding to a gel precursor solution. However, these IPN gels cannot be fabricated with water because TRIS is immiscible with water. Therefore, one must dissolve the GOx in either DCM or IPA to incorporate it into the precursor solution, both solvents that cause GOx to precipitate out

of solution. In fact, IPA is used to precipitate enzymes for purification purposes [205]. In order to avoid GOx precipitation throughout the gel, the enzyme can be introduced to a system already immobilized in a vessel, such as a microsphere. The McShane lab has experience working with various types of microspheres for enzymatic immobilization. Immobilizing the GOx in a microsphere platform and then immobilizing the enzyme-loaded sphere into the gel precursor can yield a gel with distinct, enzyme-containing microdomains within which GOx is evenly dispersed due to previously being immobilized before being introduced into the precursor. Preliminary results from incorporating these microdomains into IPN gels are presented below.

6.3.3.1. Nanofilm-Coated Capsules—Coprecipitation with Vaterite

Some preliminary work has been done on immobilizing GOx in these IPN gels by introducing higher-order architectures as described above. Ideally, if GOx were to be introduced into the matrix using a microsphere, the sphere should be made of a material which can protect the GOx from the harmful organic solvents (DCM and IPA). For the preliminary work in this area, calcium carbonate microspheres were used to immobilize GOx and introduce the GOx into the IPN. Previously, the McShane lab has used calcium carbonate (vaterite) microspheres to as a mild, facile way to encapsulate sensing chemistry components, specifically GOx [206, 207]. When coated in a polymer film, such as a layer-by-layer (LbL) polyelectrolyte nanofilm, the calcium carbonate has been shown to be successfully dissolved as a sacrificial template, leaving behind a hollow, nanofilm-coated domain containing the desired cargo which was previously coprecipitated into the calcium carbonate sphere [25, 206-208]. It was hypothesized that

here, the crystalline structure of the calcium carbonate microspheres could be used to shield GOx from organic solvents, ultimately preserving GOx activity and leaving behind discrete, glucose-sensitive domains when the calcium carbonate core is dissolved.

6.3.3.1.1. Microcomposite Interpenetrating Network Hydrogel Fabrication

GOx-containing vaterite microparticles were fabricated according to previous protocols [208], except poly (allylamine hydrochloride) (PAH) was labeled with rhodamine isothiocyanate (RITC) was used during the LbL self-assembly process for the purpose of visualizing the distribution of the microparticles in the gel. LbL nanofilm-coated vaterite microspheres, as well as the PdBP dye, were incorporated into the first

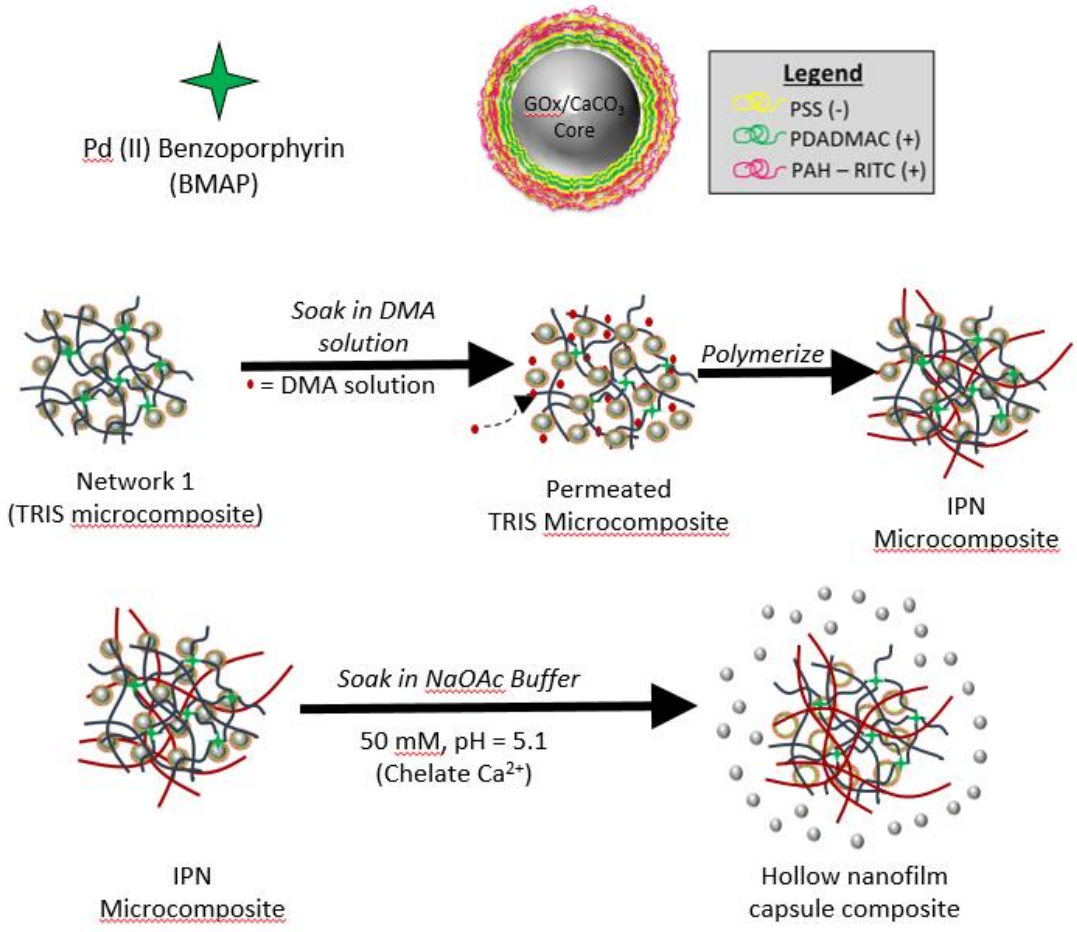

Figure 6-1: Cartoon drawing of IPN microcomposite hydrogel and sacrificial template concept.

network of the IPN matrix due to their size microscale size; introducing them to the system in the second network is impractical because they would not be able to permeate the network (Figure 6-1). After immobilizing the sensing chemistry in the silicone-containing first network, the composite gel was soaked in a DMA precursor as described in Chapter 5. In this preliminary study, three formulations of IPNs were investigated, altering the chemistry of the first network: 100:0 TRIS:DMA, 75:25 TRIS:DMA, and 50:50 TRIS:DMA. Gel formulations are shown in Table 6-1 below:

Table 6-1: IPN microcomposite precursor formulation components

TRIS:DMA Ratio	Vol. TRIS (μL)	Vol. DMA (μL)	Vol. TEGMDA (μL)	Vol. PdBP (μL)	Vol. $CaCO_3$ suspension (μL)
50:50	125	125	5	50	100
75:25	187.5	62.5	5	50	100
100:0	250	0	5	50	100

The PdBP dye was dissolved in DCM at a concentration of 10 mM; the GOx $CaCO_3$ suspension was fabricated in sodium bicarbonate buffer, but was washed in triplicate with IPA to remove the water and ensure miscibility of the capsule suspension with the other precursor components. The microparticle suspension itself was determined to contain 133 mg/mL of particles by weighing 30 μL aliquots in a microcentrifuge tube under house vacuum overnight. Higher TRIS contents were

focused on in this study because of the desire to limit glucose permeability as much as possible. Using a silicone material like TRIS not only enhances oxygen permeability but should also decrease glucose permeability because of its hydrophobicity, a logical postulation based on observations of swelling behavior with the IPN monolith oxygen sensors in Section 5.3.1.1.

Because of the higher IPA content with these gels due to the capsule suspension, these gels were polymerized in the glass slide molds described previously, but the entire glass slide mold (clips and spacer removed) was placed in a 50-mL centrifuge tube and allowed to soak in the second network DMA precursor overnight on a nutating mixer. This was to preserve the morphology of the gel despite the "tackiness" imparted by the high IPA content. Gels were photopolymerized after soaking overnight, and the resulting IPN gel was removed from the mold after the second photocuring process. To dissolve the calcium carbonate core, the gels were hydrated in sodium acetate buffer at pH 5.1 overnight.

6.3.3.1.2. Morphological Characterization

To observe capsule distribution throughout the matrix, confocal microscopy and SEM images were taken of the gels. The confocal image reveals closely packed, relatively monodisperse particles throughout the gel matrix, ca. 5 μm in diameter. Images were assigned red for contrast. Additionally, SEM images reveal hollow capsule morphology manifested as pores throughout the gel (Figure 6-2).

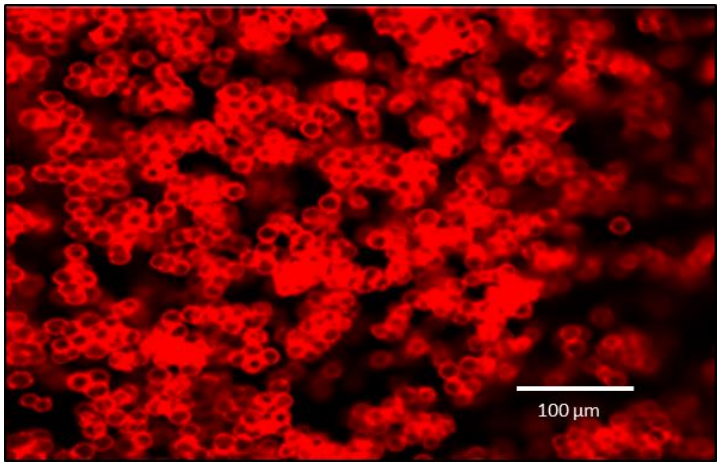

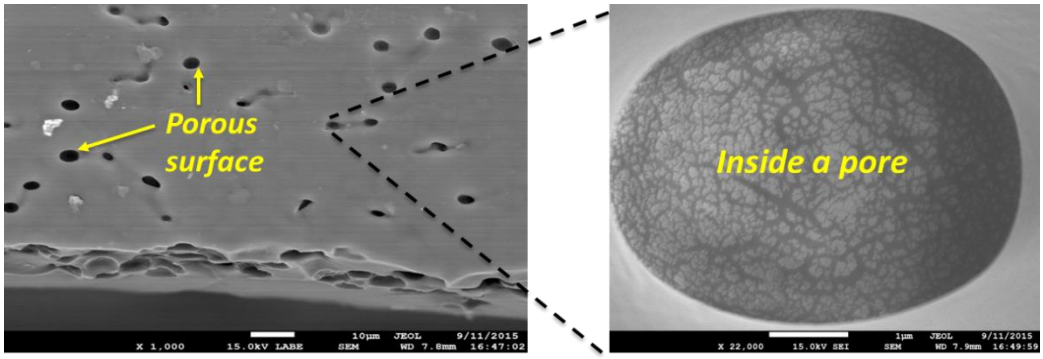

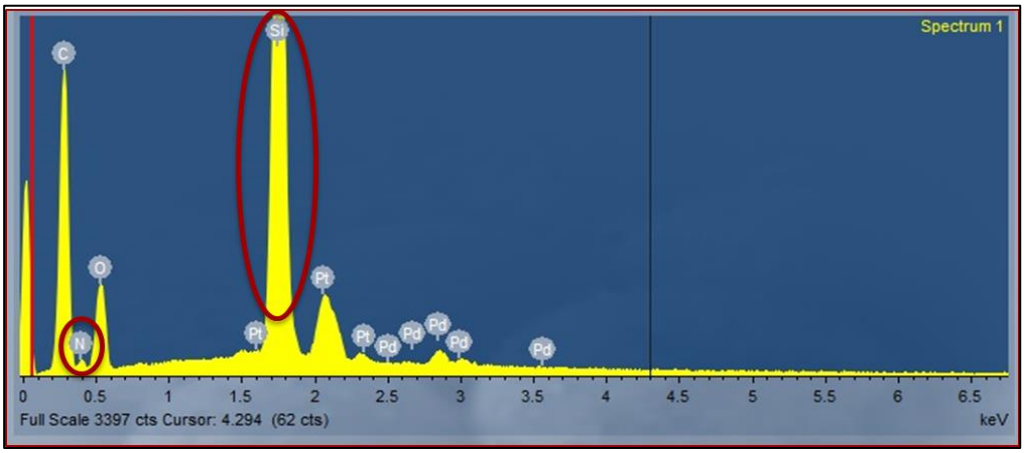

Figure 6-2: CLSM (top) and SEM (middle) images reveal distributed, hollow capsules (50:50 TRIS:DMA); Energy-dispersive spectroscopy (EDS) spectrum reveals presence of key elements (Si, O, N, C) and does not indicate presence of calcium.

While hollow pores were observed via SEM, determining the efficacy of calcium carbonate core dissolution is necessary. EDS results presented in Figure 6-2 indicate the presence of silicon, carbon, oxygen, and nitrogen, but no calcium peak was generated. The peaks present on the EDS spectrum expected based on the matrix chemistry. Absence of calcium supports the efficacy of sodium acetate dissolution of the $CaCO_3$ core and is consistent with the porous morphology seen in Figure 6-2.

6.3.3.1.3. Apparent Glucose Oxidase Activity

Five discs from each formulation were subjected to screening for apparent GOx activity as described in Chapters 3 and 4. One advantage of using sodium acetate buffer to dissolve the sacrificial core is that this is the same buffer necessary to test for apparent

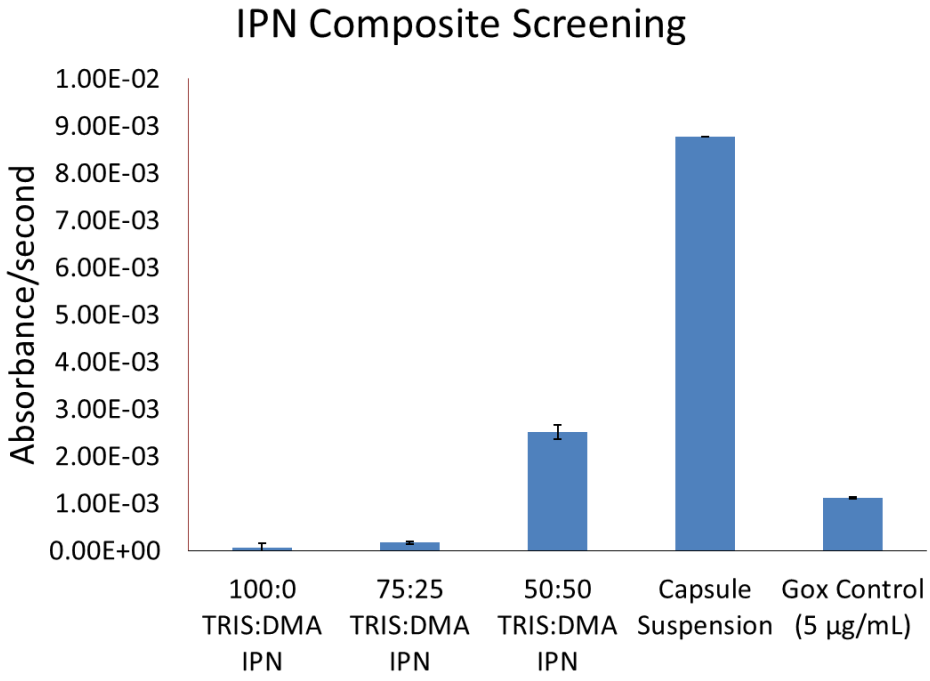

Figure 6-3: Apparent activity measurements of capsule suspension and IPN composite gels.

activity using the o-dianisidine assay [129], and the gels are already equilibrated for testing using the assay. Shown in Figure 6-3, the 50:50 gels were found to be six times more active than the 75:25 gels, and the 100:0 gels showed effectively no apparent activity. Additionally, the 50:50 TRIS:DMA gels showed a three-fold decrease in apparent activity compared to the capsule suspension with an equivalent volume of particles used in the precursor solution (100 μL). The observed decrease in apparent activity in the gels is attributed to both the presence of the network restricting glucose influx throughout the particles and the possibility of some deactivation of GOx that may be immobilized on the surface of the particle during coprecipitation.

6.3.3.1.4. Substrate Transport

Stern-Volmer plots in Figure 6-4 indicate an increase with the 50:50 TRIS:DMA gel as expected from Chapter 5. However, consulting Table 6-2, the K_{sv} and k_q values are nearly half that of those seen in Chapter 5. This is most likely because of the in-mold soaking used due to the high IPA content in the precursor to avoid disturbing the gel morphology. This soaking method may reduce the amount of water intake after polymerizing the second network. In the future, more batches of gels need to be made to determine if, in fact, the decrease in oxygen transport is correlated to hydration. In fact, Table 6-3 reveals that the 50:50 IPN composite gel is 45.8% less permeable to sucrose compared to pHEMA and 89.6% less permeable to sucrose compared to a 75:25 HEMA:AAm gel. Because these were preliminary studies to investigate proof of concept with these microspheres in the IPN, evaluating trends between hydration and substrate was not a focus of this study but should be investigated in the future.

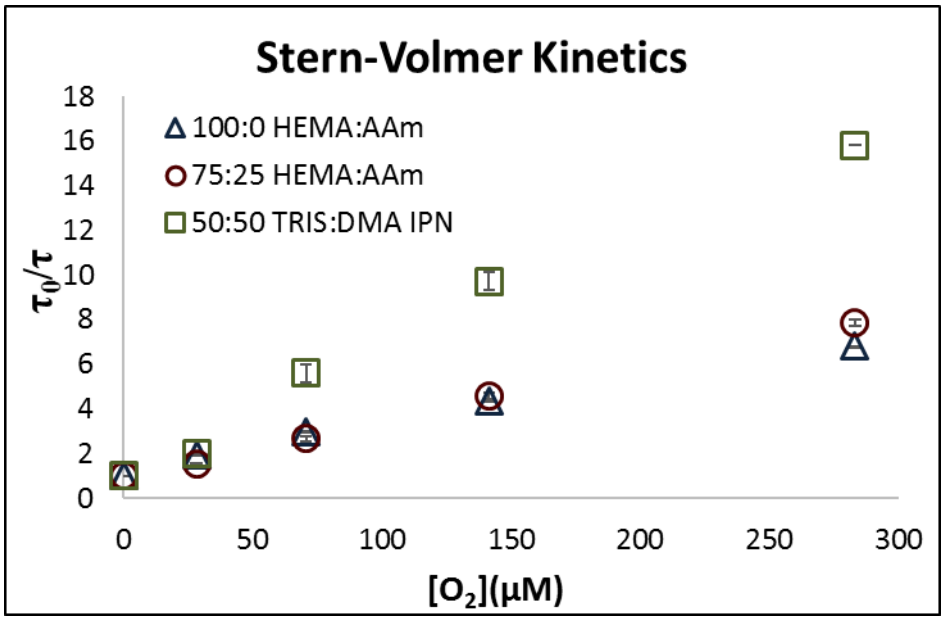

Figure 6-4: Stern-Volmer plots of IPN microcomposite

Table 6-2: IPN composite gel figures of merit compared to pHEMA and 75:25 HEMA:AAm gels

Formulation ID	K_{sv} *10^{-2} $(\mu M)^{-1}$	k_q*10^{-5} $(\mu M - \mu s)^{-1}$	τ_0 (μs)
100:0 HEMA:Aam	1.99	7.32	272.0
75:25 HEMA:Aam	2.47	9.35	264.1
50:50 TRIS:DMA IPN	5.34	21.0	254.1

Table 6-3: Sucrose transport diffusion coefficients

pHEMA	75:25 HEMA:Aam	50:50 TRIS:DMA IPN
6.60 E–7 cm^2/s	3.45 E–6 cm^2/s	3.58 E–7 cm^2/s

6.3.3.1.5. Optical Response to Glucose

To test sensors at physiological oxygen conditions, an in-line membrane degasser and vacuum pump were used, as illustrated in Figure 6-5. The membrane degasser was implemented to remove the dissolved air from the pump influent in order to decrease the oxygen levels closer to physiological oxygen. This was done in order to simulate the

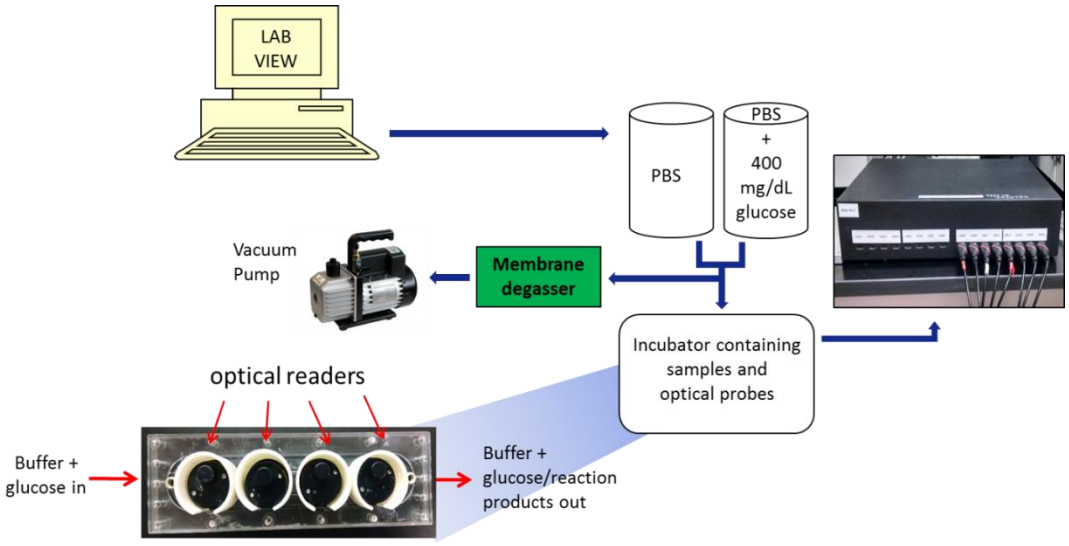

Figure 6-5: Scheme of low oxygen testing system used to determine overall glucose response at physiological oxygen levels.

environment the sensors will experience in the subcutaneous tissue *in vivo*. Because the goal of this chapter is to describe ways to accelerate sensor feasibility testing and validation before implantation, mimicking the *in vivo* environment as closely as possible

is key to predicting how the sensors will perform *in vivo* over an extended period of time (i.e., weeks to months).

To execute a low oxygen glucose challenge *in vitro,* buffer was flowed over the sensors for several hours while the pump, which was connected to the membrane degasser, removed dissolved gas from the buffer. In all low oxygen experiments, the sensor well closest to the effluent line was a pHEMA oxygen reference (pHEMA matrix functionalized with only PdBP, no enzyme); the other three wells were assigned glucose sensors (PdBP + enzyme microcapsules). The system was determined to be at "low oxygen" when the pHEMA oxygen reference reached at least 100 μs, the lifetime of pHEMA sensors at 5% oxygen, determined by Stern-Volmer experiments. It is worth noting that in order to remove enough dissolved gas from the system to reach physiological oxygen concentrations, the pump flow rate was decreased from 4 mL/min (at ambient oxygen) to 1.5 mL/min (low oxygen). This extended the runtime of each experiment from 3 hours to over 20 hours (at least 8 hours of baseline equilibration at low oxygen plus 2 hours of runtime at each glucose concentration). While this is not ideal from a throughput standpoint, more refined degassing systems can be implemented and are recommended for future studies. The data presented in this chapter were used to gain preliminary knowledge of sensor profiles at low oxygen.

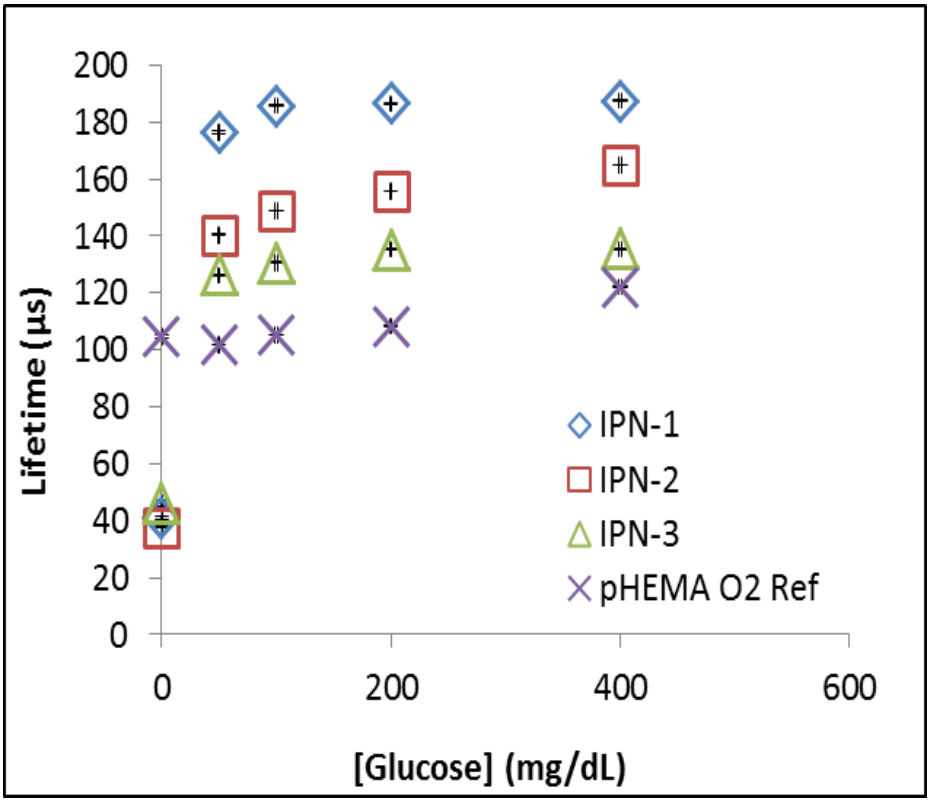

Figure 6-6: Optical response of the 50:50 TRIS:DMA sensors at physiological oxygen (5%) based on Stern-Volmer measurements.

It is noteworthy that the baseline lifetime (0 mg/dL glucose) hovers around 40 µs, similar to the baseline lifetime of pHEMA sensors at ambient oxygen concentrations (Figure 6-6). In other words, while the baseline lifetime of pHEMA rises above 100 µs at 5% oxygen, the IPNs exhibit phosphorescence lifetime behavior similar to that of pHEMA at ambient conditions. However, upon exposing the IPNs to 50-mg/dL glucose, the lifetime signal drastically increases and plateaus, failing to respond at higher glucose concentrations. However, in all three sensor strips, the glucose response plateaus below the natural lifetime of PdBP (measured to be 254.1 µs by Stern-Volmer). This indicates that the system is reaction-limited rather than substrate-limited (Figure 1-1). Adding

more GOx capsules in the gel and tuning the permeability of the nanofilms and the matrix itself could allow further extension of the dynamic range of these sensors.

6.4. Future Work and Recommendations on Design Principles

Based on the results described in this dissertation, it is recommended that pursuing higher-order architectures such as IPNs and microcomposite gels is the best prospective method for achieving long-term function of a fully implantable enzymatic biosensor at physiological conditions using an enzyme/porphyrin sensing platform. Because of the complex nature of the sensing platform, higher-order systems impart the necessary control to optimize conditions for each sensing chemistry component individually. The hydrophilicity of enzymes and their ability to denature in harsh conditions juxtaposed with the hydrophobicity of the benzoporphyrin dye is an excellent paradigm for a composite system wherein discrete compartments can be implemented to efficiently immobilize the disparate molecules individually, yet incorporate both components into the same end structure (ideally without compromising the function of either encapsulated species). Furthermore, using a hybrid material, such as an IPN hydrogel matrix, adds degrees of control over sensor performance by allowing the alteration of matrix physicochemical properties independently of one another by altering the chemistry of one matrix or both matrices.

Considering these points, it is recommended that future work be focused on refining this hybrid microcomposite design paradigm rather than a one-step, “brute-force” synthesis. Fabrication of these hybrid composite sensors can be refined in several ways including the following: simultaneous polymerization, optimizing GOx

microparticle concentration and immobilization platform, and restricting glucose transport further by altering the bulk matrix chemistry and the permeability of the nanofilm coatings around GOx domains.

REFERENCES

[1] C. E. Koop *et al.*, "Future delivery of health care: Cybercare," *IEEE Engineering in Medicine and Biology Magazine,* vol. 27, no. 6, pp. 29-38, 2008.

[2] J. F. Coughlin, J. E. Pope, and B. R. Leedle, "Old Age, New Technology, and Future Innovations in Disease Management and Home Health Care," *Home Health Care Management & Practice,* vol. 18, no. 3, pp. 196-207, 2006.

[3] M. J. Coye, A. Haselkorn, and S. DeMello, "Remote patient management: technology-enabled innovation and evolving business models for chronic disease care," *Health Affairs,* vol. 28, no. 1, pp. 126-135, 2009.

[4] M. A. Hamburg and F. S. Collins "The Path to Personalized Medicine," *New England Journal of Medicine,* vol. 363, no. 4, pp. 301-304, 2010.

[5] M. U. Ahmed, I. Saaem, P. C. Wu, and A. S. Brown, "Personalized diagnostics and biosensors: a review of the biology and technology needed for personalized medicine," *Critical Reviews in Biotechnology*, vol. 34, no. 2, pp. 180-196, 2014.

[6] S. Hamine, E. Gerth-Guyette, D. Faulx, B. B. Green, and S. A. Ginsburg, "Impact of mHealth Chronic Disease Management on Treatment Adherence and Patient Outcomes: A Systematic Review," *J Med Internet Res,* vol. 17, no. 2, p. 52, 2015.

[7] O. Tokel, F. Inci, and U. Demirci, "Advances in Plasmonic Technologies for Point of Care Applications," *Chemical Reviews,* vol. 114, no. 11, pp. 5728-5752, 2014.

[8] P. K. Drain *et al.*, "Evaluating Diagnostic Point-of-Care Tests in Resource-Limited Settings," *The Lancet infectious diseases,* vol. 14, no. 3, pp. 239-249, 2014.

[9] H. Inan *et al.*, "Photonic crystals: emerging biosensors and their promise for point-of-care applications," *Chemical Society Reviews,* vol. 46, no. 2, pp. 366-388, 2017.

[10] M. Zarei, "Portable biosensing devices for point-of-care diagnostics: Recent developments and applications," *TrAC Trends in Analytical Chemistry,* vol. 91, pp. 26-41, 2017.

[11] A. D. Association, "Economic costs of diabetes in the US in 2012," *Diabetes care,* vol. 36, no. 4, pp. 1033-1046, 2013.

[12] J. P. Boyle *et al.*, "Projection of diabetes burden through 2050," *Diabetes care,* vol. 24, no. 11, pp. 1936-1940, 2001.

[13] C. f. D. Control and Prevention, "National diabetes statistics report: estimates of diabetes and its burden in the United States, 2014," *Atlanta, GA: US Department of Health and Human Services,* 2014. Available: https://www.cdc.gov/diabetes/pdfs/data/2014-report-acknowledgments.pdf.

[14] L. S. Phillips, R. E. Ratner, J. B. Buse, and S. E. Kahn, "We Can Change the Natural History of Type 2 Diabetes," *Diabetes Care,* vol. 37, no. 10, pp. 2668-2676, 2014.

[15] A. Szypowska, A. Ramotowska, K. Dżygało, and D. Golicki, "Management of endocrine disease: beneficial effect of real-time continuous glucose monitoring

system on glycemic control in type 1 diabetic patients: systematic review and meta-analysis of randomized trials," *European Journal of Endocrinology,* vol. 166, no. 4, pp. 567-574, 2012.

[16] L. Hoeks, W. Greven, and H. De Valk, "Real-time continuous glucose monitoring system for treatment of diabetes: a systematic review," *Diabetic Medicine,* vol. 28, no. 4, pp. 386-394, 2011.

[17] K. L. Helton, B. D. Ratner, and N. A. Wisniewski, "Biomechanics of the Sensor-Tissue Interface—Effects of Motion, Pressure, and Design on Sensor Performance and the Foreign Body Response—Part I: Theoretical Framework," *Journal of Diabetes Science and Technology,* vol. 5, no. 3, pp. 632-646, 2011.

[18] K. L. Helton, B. D. Ratner, and N. A. Wisniewski, "Biomechanics of the Sensor–Tissue Interface—Effects of Motion, Pressure, and Design on Sensor Performance and Foreign Body Response—Part II: Examples and Application," *Journal of Diabetes Science and Technology,* vol. 5, no. 3, pp. 647-656, 2011.

[19] J. Hermanides, M. Phillip, and J. H. DeVries, "Current Application of Continuous Glucose Monitoring in the Treatment of Diabetes," *Pros and cons,* vol. 34, no. Supplement 2, pp. S197-S201, 2011.

[20] A. Reynolds, H. Tekinkaya, and B. Venn, "The effect on day-long glycemia of consuming lower and higher glycemic index diets in people with type 2 diabetes: a randomized crossover study," *J Diabetes Metab,* vol. 5, no. 436, p. 2, 2014.

[21] Z. Mahmoudi, M. D. Johansen, J. S. Christiansen, and O. Hejlesen, "Comparison Between One-Point Calibration and Two-Point Calibration Approaches in a

Continuous Glucose Monitoring Algorithm," *Journal of Diabetes Science and Technology,* vol. 8, no. 4, pp. 709-719, 2014.

[22] J. Q. Brown, R. Srivastava, and M. J. McShane, "Encapsulation of glucose oxidase and an oxygen-quenched fluorophore in polyelectrolyte-coated calcium alginate microspheres as optical glucose sensor systems," *Biosensors and Bioelectronics,* vol. 21, no. 1, pp. 212-216, 2005.

[23] J. Q. Brown, R. Srivastava, H. Zhu, and M. J. McShane, "Enzymatic fluorescent microsphere glucose sensors: evaluation of response under dynamic conditions," *Diabetes technology & therapeutics,* vol. 8, no. 3, pp. 288-295, 2006.

[24] J. R. Roberts, J. Park, K. Helton, N. Wisniewski, and M. J. McShane, "Biofouling of Polymer Hydrogel Materials and its Effect on Diffusion and Enzyme-Based Luminescent Glucose Sensor Functional Characteristics," *Journal of Diabetes Science and Technology,* vol. 6, no. 6, pp. 1267-1275, 2012.

[25] J. R. Roberts, D. W. Ritter, and M. J. McShane, "A design full of holes: functional nanofilm-coated microdomains in alginate hydrogels," *Journal of Materials Chemistry B,* vol. 1, no. 25, pp. 3195-3201, 2013.

[26] E. W. Stein, P. S. Grant, H. Zhu, and M. J. McShane, "Microscale enzymatic optical biosensors using mass transport limiting nanofilms. 1. Fabrication and characterization using glucose as a model analyte," *Analytical chemistry,* vol. 79, no. 4, pp. 1339-1348, 2007.

[27] E. W. Stein, S. Singh, and M. J. McShane, "Microscale enzymatic optical biosensors using mass transport limiting nanofilms. 2. Response modulation by

varying analyte transport properties," *Analytical chemistry,* vol. 80, no. 5, pp. 1408-1417, 2008.

[28] L. Andrus, R. Unruh, N. Wisniewski, and M. McShane, "Characterization of Lactate Sensors Based on Lactate Oxidase and Palladium Benzoporphyrin Immobilized in Hydrogels," *Biosensors,* vol. 5, no. 3, pp. 398-416, 2015.

[29] A. D. Association, "Standards of medical care in diabetes—2014," *Diabetes care,* vol. 37, no. Supplement 1, pp. S14-S80, 2014.

[30] J. M. Evans, R. W. Newton, D. A. Ruta, T. M. MacDonald, R. J. Stevenson, and A. D. Morris, "Frequency of blood glucose monitoring in relation to glycaemic control: observational study with diabetes database," *BMJ,* vol. 319, no. 7202, pp. 83-86, 1999.

[31] J. Gerich, "Diabetic control and the late complications of diabetes," *American family physician,* vol. 16, no. 2, p. 85, 1977.

[32] M. I. Harris, "Frequency of Blood Glucose Monitoring in Relation to Glycemic Control in Patients With Type 2 Diabetes," *Diabetes Care,* vol. 24, no. 6, pp. 979-982, 2001.

[33] L. S. Kumosa, T. L. Routh, J. T. Lin, J. Y. Lucisano, and D. A. Gough, "Permeability of subcutaneous tissues surrounding long-term implants to oxygen," *Biomaterials,* vol. 35, no. 29, pp. 8287-8296, 2014.

[34] S. Singh and M. McShane, "Role of porosity in tuning the response range of microsphere-based glucose sensors," *Biosensors and Bioelectronics,* vol. 26, no. 5, pp. 2478-2483, 2011.

[35] R. C. Rodrigues, C. Ortiz, A. Berenguer-Murcia, R. Torres, and R. Fernandez-Lafuente, "Modifying enzyme activity and selectivity by immobilization," *Chemical Society Reviews,* vol. 42, no. 15, pp. 6290-6307, 2013.

[36] A. S. Bommarius and M. F. Paye, "Stabilizing biocatalysts," *Chemical Society Reviews,* vol. 42, no. 15, pp. 6534-6565, 2013.

[37] C. Garcia-Galan, Á. Berenguer-Murcia, R. Fernandez-Lafuente, and R. C. Rodrigues, "Potential of Different Enzyme Immobilization Strategies to Improve Enzyme Performance," *Advanced Synthesis & Catalysis,* vol. 353, no. 16, pp. 2885-2904, 2011.

[38] J. M. Harris, C. Reyes, and G. P. Lopez, "Common Causes of Glucose Oxidase Instability in *In Vivo* Biosensing: A Brief Review," *Journal of Diabetes Science and Technology,* vol. 7, no. 4, pp. 1030-1038, 2013.

[39] T. Jesionowski, J. Zdarta, and B. Krajewska, "Enzyme immobilization by adsorption: a review," *Adsorption,* journal article vol. 20, no. 5, pp. 801-821, 2014.

[40] F. Jia, B. Narasimhan, and S. Mallapragada, "Materials-based strategies for multi-enzyme immobilization and co-localization: A review," *Biotechnology and Bioengineering,* vol. 111, no. 2, pp. 209-222, 2014.

[41] A. M. Klibanov, "Enzyme stabilization by immobilization," *Analytical Biochemistry,* vol. 93, pp. 1-25, 1979.

[42] Y. Wang, J. Zhang, and J. Yin, "Progress of enzyme immobilization and its potential application," *Desalination and Water Treatment,* vol. 1, no. 1-3, pp. 157-171, 2009.

[43] P. H. Tse and D. A. Gough, "Time-dependent inactivation of immobilized glucose oxidase and catalase," *Biotechnology and bioengineering,* vol. 29, no. 6, pp. 705-713, 1987.

[44] H. J. Bright and M. Appleby, "The pH dependence of the individual steps in the glucose oxidase reaction," *Journal of Biological Chemistry,* vol. 244, no. 13, pp. 3625-3634, 1969.

[45] R. Wilson and A. Turner, "Glucose oxidase: an ideal enzyme," *Biosensors and Bioelectronics,* vol. 7, no. 3, pp. 165-185, 1992.

[46] Y. Onuki, U. Bhardwaj, F. Papadimitrakopoulos, and D. J. Burgess, "A review of the biocompatibility of implantable devices: current challenges to overcome foreign body response," *Journal of diabetes science and technology,* vol. 2, no. 6, pp. 1003-1015, 2008.

[47] D. Rickert, A. Lendlein, I. Peters, M. A. Moses, and R.-P. Franke, "Biocompatibility testing of novel multifunctional polymeric biomaterials for tissue engineering applications in head and neck surgery: an overview," *European Archives of Oto-Rhino-Laryngology and Head & Neck,* journal article vol. 263, no. 3, pp. 215-222, 2006.

[48] S. P. Nichols, A. Koh, W. L. Storm, J. H. Shin, and M. H. Schoenfisch, "Biocompatible Materials for Continuous Glucose Monitoring Devices," *Chemical Reviews,* vol. 113, no. 4, pp. 2528-2549, 2013.

[49] N. Sachedina and J. Pickup, "Performance assessment of the Medtronic-MiniMed continuous glucose monitoring system and its use for measurement of glycaemic control in type 1 diabetic subjects," *Diabetic medicine,* vol. 20, no. 12, pp. 1012-1015, 2003.

[50] R. L. Weinstein, T. A. Peyser, G. V. McGarraugh, J. R. Bugler, S. L. Schwartz, and R. L. Brazg, "Accuracy of the 5-Day FreeStyle Navigator Continuous Glucose Monitoring System: Comparison with frequent laboratory reference measurements [electronic resource]," *Diabetes care,* vol. 30, no. 5, pp. 1125-1130, 2007.

[51] G. McGarraugh, "The chemistry of commercial continuous glucose monitors," *Diabetes technology & therapeutics,* vol. 11, no. S1, pp. S-17-S-24, 2009.

[52] T. Nunnold, S. R. Colberg, M. T. Herriott, and C. T. Somma, "Use of the noninvasive Glucowatch® Biographer® during exercise of varying intensity," *Diabetes technology & therapeutics,* vol. 6, no. 4, pp. 454-462, 2004.

[53] L. De Groot *et al.*, "Monitoring Technologies–Continuous Glucose Monitoring, Mobile Technology, Biomarkers of Glycemic Control--Endotext," 2000.

[54] F. Moussy, D. J. Harrison, and R. V. Rajotte, "A miniaturized Nafion-based glucose sensor: *in vitro* and *in vivo* evaluation in dogs," (in eng), *The International journal of artificial organs,* vol. 17, no. 2, pp. 88-94, 1994.

[55] E. A. Blubaugh and A. R. Brunsman, "Glucose sensor," USA Patent US5964993A, 1999. Available: https://www.google.com/patents/US5964993.

[56] J. D. Andrade, *Hydrogels for medical and related applications*. ACS Publications, Washington, D.C., 1976.

[57] K. Deligkaris, T. S. Tadele, W. Olthuis, and A. van den Berg, "Hydrogel-based devices for biomedical applications," *Sensors and Actuators B: Chemical,* vol. 147, no. 2, pp. 765-774, 2010.

[58] I. Gibas and H. Janik, "Review: synthetic polymer hydrogels for biomedical applications," *Chemistry & Chemical Technology,* vol. 4, no. 4, pp. 297-304, 2010.

[59] A. S. Hoffman, "Hydrogels for biomedical applications," *Advanced drug delivery reviews,* vol. 64, pp. 18-23, 2012.

[60] N. A. Peppas, J. Z. Hilt, A. Khademhosseini, and R. Langer, "Hydrogels in Biology and Medicine: From Molecular Principles to Bionanotechnology," *Advanced Materials,* vol. 18, no. 11, pp. 1345-1360, 2006.

[61] B. D. Ratner and A. S. Hoffman, "Synthetic hydrogels for biomedical applications," *ACS Symposium Series,* vol. 31, pp. 1-36, 1976.

[62] A. K. Gaharwar, N. A. Peppas, and A. Khademhosseini, "Nanocomposite hydrogels for biomedical applications," *Biotechnology and bioengineering,* vol. 111, no. 3, pp. 441-453, 2014.

[63] A. Chaudhary, M. J. McShane, and R. Srivastava, "Glucose response of dissolved-core alginate microspheres: towards a continuous glucose biosensor," *Analyst*, vol. 135, no. 10, pp. 2620-2628, 2010.

[64] A. Chaudhary, M. Raina, H. Harma, P. Hanninen, M. J. McShane, and R. Srivastava, "Evaluation of glucose sensitive affinity binding assay entrapped in fluorescent dissolved-core alginate microspheres," *Biotechnology and Bioengineering*, vol. 104, no. 6, pp. 1075-1085, 2009.

[65] R. M. Unruh, J. R. Roberts, S. P. Nichols, S. Gamsey, N. A. Wisniewski, and M. J. McShane, "Preclinical Evaluation of Poly(HEMA-co-acrylamide) Hydrogels Encapsulating Glucose Oxidase and Palladium Benzoporphyrin as Fully Implantable Glucose Sensors," *Journal of Diabetes Science and Technology*, vol. 9, no. 5, pp. 985-992, 2015.

[66] H. E. Koschwanez, F. Y. Yap, B. Klitzman, and W. M. Reichert, "*In vitro* and *in vivo* characterization of porous poly-L-lactic acid coatings for subcutaneously implanted glucose sensors," *Journal of Biomedical Materials Research Part A*, vol. 87A, no. 3, pp. 792-807, 2008.

[67] O. Wichterle and D. Lim, "Hydrophilic gels for biological use," *Nature*, vol. 185, no. 4706, pp. 117-118, 1960.

[68] B. D. Ratner, A. S. Hoffman, F. J. Schoen, and J. E. Lemons, *Biomaterials science: an introduction to materials in medicine*. Elsevier Academic Press, San Diego, CA, 2004.

[69] W. Teng, T. J. Long, Q. Zhang, K. Yao, T. T. Shen, and B. D. Ratner, "A tough, precision-porous hydrogel scaffold: Ophthalmologic applications," *Biomaterials,* vol. 35, no. 32, pp. 8916-8926, 2014.

[70] B. D. Ratner, "A pore way to heal and regenerate: 21st century thinking on biocompatibility," *Regenerative Biomaterials,* vol. 3, no. 2, pp. 107-110, 2016.

[71] M. Van Beek, L. Jones, and H. Sheardown, "Hyaluronic acid containing hydrogels for the reduction of protein adsorption," *Biomaterials,* vol. 29, no. 7, pp. 780-789, 2008.

[72] G. Guidi, M. Korogiannaki, and H. Sheardown, "Modification of Timolol Release From Silicone Hydrogel Model Contact Lens Materials Using Hyaluronic Acid," *Eye & Contact Lens,* vol. 40, no. 5, pp. 269-276, 2014.

[73] A. J. Marshall and B. D. Ratner, "Quantitative characterization of sphere-templated porous biomaterials," *AIChE Journal,* vol. 51, no. 4, pp. 1221-1232, 2005.

[74] R. Ballerstadt and J. S. Schultz, "A Fluorescence Affinity Hollow Fiber Sensor for Continuous Transdermal Glucose Monitoring," *Analytical Chemistry,* vol. 72, no. 17, pp. 4185-4192, 2000.

[75] A. Chaudhary, H. Harma, P. Hanninen, M. J. McShane, and R. Srivastava, "Glucose response of near-infrared alginate-based microsphere sensors under dynamic reversible conditions," *Diabetes technology & therapeutics,* vol. 13, no. 8, pp. 827-835, 2011.

[76] S. Chinnayelka, H. Zhu, and M. McShane, "Near-infrared resonance energy transfer glucose biosensors in hybrid microcapsule carriers," *Journal of Sensors*, vol. 2008, pp. 1-11, 2008.

[77] Y. J. Heo, H. Shibata, T. Okitsu, T. Kawanishi, and S. Takeuchi, "Long-term *in vivo* glucose monitoring using fluorescent hydrogel fibers," *Proceedings of the National Academy of Sciences,* vol. 108, no. 33, pp. 13399-13403, 2011.

[78] J. C. Pickup, F. Hussain, N. D. Evans, O. J. Rolinski, and D. J. S. Birch, "Fluorescence-based glucose sensors," *Biosensors and Bioelectronics,* vol. 20, no. 12, pp. 2555-2565, 2005.

[79] R. Ballerstadt and J. S. Schultz, "Competitive-binding assay method based on fluorescence quenching of ligands held in close proximity by a multivalent receptor," *Analytica Chimica Acta,* vol. 345, no. 1, pp. 203-212, 1997.

[80] S. Chinnayelka and M. J. McShane, "Glucose-Sensitive Nanoassemblies Comprising Affinity-Binding Complexes Trapped in Fuzzy Microshells," *Journal of fluorescence,* vol. 14, no. 5, pp. 585-595, 2004.

[81] S. Chinnayelka and M. J. McShane, "Resonance Energy Transfer Nanobiosensors Based on Affinity Binding between Apo-Enzyme and Its Substrate," *Biomacromolecules,* vol. 5, no. 5, pp. 1657-1661, 2004.

[82] S. Chinnayelka and M. J. McShane, "Microcapsule Biosensors Using Competitive Binding Resonance Energy Transfer Assays Based on Apoenzymes," *Analytical Chemistry,* vol. 77, no. 17, pp. 5501-5511, 2005.

[83] M. J. McShane, R. J. Russell, M. V. Pishko, and G. L. Cote, "Glucose monitoring using implanted fluorescent microspheres," *IEEE Engineering in Medicine and Biology Magazine,* vol. 19, no. 6, pp. 36-45, 2000.

[84] R. J. Russell, M. V. Pishko, C. C. Gefrides, M. J. McShane, and G. L. Coté, "A Fluorescence-Based Glucose Biosensor Using Concanavalin A and Dextran Encapsulated in a Poly(ethylene glycol) Hydrogel," *Analytical Chemistry,* vol. 71, no. 15, pp. 3126-3132, 1999.

[85] B. M. Cummins, M. Li, A. K. Locke, D. J. S. Birch, G. Vigh, and G. L. Coté, "Overcoming the aggregation problem: A new type of fluorescent ligand for ConA-based glucose sensing," *Biosensors and Bioelectronics,* vol. 63, pp. 53-60, 2015.

[86] A. K. Locke, B. M. Cummins, A. A. Abraham, and G. L. Coté, "PEGylation of Concanavalin A to Improve Its Stability for an *In Vivo* Glucose Sensing Assay," *Analytical Chemistry,* vol. 86, no. 18, pp. 9091-9097, 2014.

[87] D. W. Piston and G.-J. Kremers, "Fluorescent protein FRET: the good, the bad and the ugly," *Trends in biochemical sciences,* vol. 32, no. 9, pp. 407-414, 2007.

[88] J. O. Escobedo, O. Rusin, S. Lim, and R. M. Strongin, "NIR dyes for bioimaging applications," *Current opinion in chemical biology,* vol. 14, no. 1, pp. 64-70, 2010.

[89] S. A. Vinogradov, L. W. Lo, W. T. Jenkins, S. M. Evans, C. Koch, and D. F. Wilson, "Noninvasive imaging of the distribution in oxygen in tissue *in vivo*

using near-infrared phosphors," *Biophysical Journal,* vol. 70, no. 4, pp. 1609-1617, 1996.

[90] S. A. Vinogradov and D. F. Wilson, "Metallotetrabenzoporphyrins. New phosphorescent probes for oxygen measurements," *Journal of the Chemical Society, Perkin Transactions 2,* vol. 0, no. 1, pp. 103-111, 1995.

[91] S. M. Borisov, G. Nuss, and I. Klimant, "Red Light-Excitable Oxygen Sensing Materials Based on Platinum(II) and Palladium(II) Benzoporphyrins," *Analytical Chemistry,* vol. 80, no. 24, pp. 9435-9442, 2008.

[92] B. B. Collier and M. J. McShane, "Time-resolved measurements of luminescence," *Journal of Luminescence,* vol. 144, pp. 180-190, 2013.

[93] Y. Kostov, P. Harms, L. Randers-Eichhorn, and G. Rao, "Low-cost microbioreactor for high-throughput bioprocessing," *Biotechnology and Bioengineering,* vol. 72, no. 3, pp. 346-352, 2001.

[94] M. E. Lippitsch, S. Draxler, and D. Kieslinger, "Luminescence lifetime-based sensing: new materials, new devices," *Sensors and Actuators B: Chemical,* vol. 38, no. 1, pp. 96-102, 1997.

[95] Y. Arica and V. N. Hasirci, "Immobilization of glucose oxidase in poly(2-hydroxyethyl methacrylate) membranes," *Biomaterials,* vol. 8, no. 6, pp. 489-495, 1987.

[96] D. Ritter, J. Newton, and M. McShane, "Modification of PEGylated enzyme with glutaraldehyde can enhance stability while avoiding intermolecular crosslinking," *RSC Advances,* vol. 4, no. 53, pp. 28036-28040, 2014.

[97] S. A. Ansari and Q. Husain, "Potential applications of enzymes immobilized on/in nano materials: A review," *Biotechnology Advances,* vol. 30, no. 3, pp. 512-523, 2012.

[98] T. Danisman, S. Tan, Y. Kacar, and A. Ergene, "Covalent immobilization of invertase on microporous pHEMA–GMA membrane," *Food Chemistry,* vol. 85, no. 3, pp. 461-466, 2004.

[99] P. Pandey *et al.*, "Application of Thiolated Gold Nanoparticles for the Enhancement of Glucose Oxidase Activity," *Langmuir,* vol. 23, no. 6, pp. 3333-3337, 2007.

[100] N. Pekel, B. Salih, and O. Güven, "Enhancement of stability of glucose oxidase by immobilization onto metal ion-chelated poly(N-vinyl imidazole) hydrogels," *Journal of Biomaterials Science, Polymer Edition,* vol. 16, no. 2, pp. 253-266, 2005.

[101] J. Raba and H. A. Mottola, "Glucose Oxidase as an Analytical Reagent," *Critical Reviews in Analytical Chemistry*, vol. 25, no. 1, pp. 1-42, 1995.

[102] D. W. Ritter, J. R. Roberts, and M. J. McShane, "Glycosylation site-targeted PEGylation of glucose oxidase retains native enzymatic activity," *Enzyme and Microbial Technology,* vol. 52, no. 4–5, pp. 279-285, 2013.

[103] J. M. Rodriguez-Nogales, "Kinetic behaviour and stability of glucose oxidase entrapped in liposomes," *Journal of Chemical Technology & Biotechnology,* vol. 79, no. 1, pp. 72-78, 2004.

[104] R. A. Sheldon, "Enzyme Immobilization: The Quest for Optimum Performance," *Advanced Synthesis & Catalysis,* vol. 349, no. 8-9, pp. 1289-1307, 2007.

[105] A. Vikartovská, M. Bučko, D. Mislovičová, V. Pätoprstý, I. Lacík, and P. Gemeiner, "Improvement of the stability of glucose oxidase via encapsulation in sodium alginate–cellulose sulfate–poly(methylene-co-guanidine) capsules," *Enzyme and Microbial Technology,* vol. 41, no. 6–7, pp. 748-755, 2007.

[106] H. Zhu, R. Srivastava, J. Q. Brown, and M. J. McShane, "Combined Physical and Chemical Immobilization of Glucose Oxidase in Alginate Microspheres Improves Stability of Encapsulation and Activity," *Bioconjugate chemistry,* vol. 16, no. 6, pp. 1451-1458, 2005.

[107] S. B. Bankar, M. V. Bule, R. S. Singhal, and L. Ananthanarayan, "Glucose oxidase — An overview," *Biotechnology Advances,* vol. 27, no. 4, pp. 489-501, 2009.

[108] M. Y. Arıca and G. Bayramoğlu, "Polyethyleneimine-grafted poly(hydroxyethyl methacrylate-co-glycidyl methacrylate) membranes for reversible glucose oxidase immobilization," *Biochemical Engineering Journal,* vol. 20, no. 1, pp. 73-77, 2004.

[109] S. Brahim, D. Narinesingh, and A. Guiseppi-Elie, "Kinetics of glucose oxidase immobilized in p(HEMA)-hydrogel microspheres in a packed-bed bioreactor," *Journal of Molecular Catalysis B: Enzymatic,* vol. 18, no. 1–3, pp. 69-80, 2002.

[110] A. Guiseppi-Elie, S.-H. Choi, K. E. Geckeler, B. Sivaraman, and R. A. Latour, "Ultrasonic Processing of Single-Walled Carbon Nanotube–Glucose Oxidase

Conjugates: Interrelation of Bioactivity and Structure," *NanoBiotechnology,* vol. 4, no. 1, pp. 9-17, 2008.

[111] G. P. Hicks and S. J. Updike, "The preparation and characterization of lyophilized polyacrylamide enzyme gels for chemical analysis," (in eng), *Analytical chemistry,* vol. 38, no. 6, pp. 726-730, 1966.

[112] H. Ichijo, J. i. Nagasawa, and A. Yamauchi, "Immobilization of biocatalysts with poly(vinyl alcohol) supports," *Journal of Biotechnology,* vol. 14, no. 2, pp. 169-178, 1990.

[113] A. Joshi, S. Solanki, R. Chaudhari, D. Bahadur, M. Aslam, and R. Srivastava, "Multifunctional alginate microspheres for biosensing, drug delivery and magnetic resonance imaging," *Acta Biomaterialia,* vol. 7, no. 11, pp. 3955-3963, 2011.

[114] S. I. Kang and Y. H. Bae, "A sulfonamide based glucose-responsive hydrogel with covalently immobilized glucose oxidase and catalase," *Journal of Controlled Release,* vol. 86, no. 1, pp. 115-121, 2003.

[115] K. Podual, F. J. Doyle Iii, and N. A. Peppas, "Preparation and dynamic response of cationic copolymer hydrogels containing glucose oxidase," *Polymer,* vol. 41, no. 11, pp. 3975-3983, 2000.

[116] J. N. Anker, W. P. Hall, O. Lyandres, N. C. Shah, J. Zhao, and R. P. Van Duyne, "Biosensing with plasmonic nanosensors," *Nature Materials,* vol. 7, no. 6, pp. 442-453, 2008.

[117] T. Vo-Dinh, H.-N. Wang, and J. Scaffidi, "Plasmonic nanoprobes for SERS biosensing and bioimaging," *Journal of biophotonics,* vol. 3, no. 0, pp. 89-102, 2010.

[118] R. A. Tripp, R. A. Dluhy, and Y. Zhao, "Novel nanostructures for SERS biosensing," *Nano Today,* vol. 3, no. 3, pp. 31-37, 2008.

[119] M. F. Cardinal *et al.*, "Expanding applications of SERS through versatile nanomaterials engineering," *Chemical Society Reviews,* vol. 46, no. 13, pp. 3886-3903, 2017.

[120] O. Lyandres, J. M. Yuen, N. C. Shah, R. P. VanDuyne, J. T. Walsh, and M. R. Glucksberg, "Progress Toward an *In Vivo* Surface-Enhanced Raman Spectroscopy Glucose Sensor," *Diabetes Technology & Therapeutics,* vol. 10, no. 4, pp. 257-265, 2008.

[121] K. Ma, J. M. Yuen, N. C. Shah, J. T. Walsh, M. R. Glucksberg, and R. P. Van Duyne, "*In Vivo*, Transcutaneous Glucose Sensing Using Surface-Enhanced Spatially Offset Raman Spectroscopy: Multiple Rats, Improved Hypoglycemic Accuracy, Low Incident Power, and Continuous Monitoring for Greater Than 17 Days," *Analytical chemistry,* vol. 83, no. 23, pp. 9146-9152, 2011.

[122] A. Heller and B. Feldman, "Electrochemical glucose sensors and their applications in diabetes management," *Chemical reviews,* vol. 108, no. 7, pp. 2482-2505, 2008.

[123] T. U. Luu, S. C. Gott, B. W. K. Woo, M. P. Rao, and W. F. Liu, "Micro- and Nanopatterned Topographical Cues for Regulating Macrophage Cell Shape and

Phenotype," *ACS Applied Materials & Interfaces,* vol. 7, no. 51, pp. 28665-28672, 2015.

[124] A.-K. Östberg, U. Dahlgren, Y.-T. Sul, and C. B. Johansson, "Inflammatory cytokine release is affected by surface morphology and chemistry of titanium implants," *Journal of Materials Science: Materials in Medicine,* vol. 26, no. 4, p. 155, 2015.

[125] N. Wisniewski, B. Klitzman, B. Miller, and W. Reichert, "Decreased analyte transport through implanted membranes: differentiation of biofouling from tissue effects," *Journal of biomedical materials research,* vol. 57, no. 4, pp. 513-521, 2001.

[126] N. Wisniewski, F. Moussy, and W. M. Reichert, "Characterization of implantable biosensor membrane biofouling," *Fresenius' Journal of Analytical Chemistry,* vol. 366, no. 6, pp. 611-621, 2000.

[127] Y. H. You, A. Nagaraja, A. Biswas, H. Marks, G. L. Coté, and M. J. McShane, "SERS-based hydrogel sensors for pH and enzymatic substrates," in *2015 IEEE SENSORS*, Busan, South Korea, 2015, pp. 1-4: IEEE Xplore, 2015.

[128] J. W. Parker and M. E. Cox, "Mass transfer of oxygen in poly(2-hydroxyethyl methacrylate)," *Journal of Polymer Science Part A: Polymer Chemistry,* vol. 26, no. 4, pp. 1179-1188, 1988.

[129] S. Aldrich. (2017, 04/25/2017). *Enzymatic Assay of Glucose Oxidase* [Website]. Available: http://www.sigmaaldrich.com/technical-documents/protocols/biology/enzymatic-assay-of-glucose-oxidase.html.

[130] S. W. Kim, Y. H. Bae, and T. Okano, "Hydrogels: Swelling, Drug Loading, and Release," *Pharmaceutical Research,* vol. 9, no. 3, pp. 283-290, 1992.

[131] C. Özeroglu and A. Birdal, "Swelling properties of acrylamide-N, N′-methylene bis (acrylamide) hydrogels synthesized by using meso-2, 3-dimercaptosuccinic acid-cerium (IV) redox couple," *Express Polym Lett,* vol. 3, pp. 168-176, 2009.

[132] L. Brannon-Peppas and N. A. Peppas, "Dynamic and equilibrium swelling behaviour of pH-sensitive hydrogels containing 2-hydroxyethyl methacrylate," *Biomaterials,* vol. 11, no. 9, pp. 635-644, 1990.

[133] L. W. Lo, L.-W. Lo, C. Koch, and D. Wilson, "Calibration of Oxygen-Dependent Quenching of the Phosphorescence of Pd-meso-tetra (4-Carboxyphenyl) Porphine: A Phosphor with General Application for Measuring Oxygen Concentration in Biological Systems," *Analytical biochemistry,* vol. 236, no. 1, pp. 153-160, 1996.

[134] M. Sinaasappel and C. Ince, "Calibration of Pd-porphyrin phosphorescence for oxygen concentration measurements *in vivo*," *Journal of Applied Physiology,* vol. 81, no. 5, pp. 2297-2303, 1996.

[135] M. T. Novak, F. Yuan, and W. M. Reichert, "Macrophage embedded fibrin gels: An in vitro platform for assessing inflammation effects on implantable glucose sensors," *Biomaterials,* vol. 35, no. 36, pp. 9563-9572, 2014.

[136] J. Bolincier, U. Ungerstedt, and P. Arner, "Microdialysis measurement of the absolute glucose concentration in subcutaneous adipose tissue allowing glucose

monitoring in diabetic patients," *Diabetologia,* vol. 35, no. 12, pp. 1177-1180, 1992.

[137] U. Fischer *et al.*, "Assessment of subcutaneous glucose concentration: validation of the wick technique as a reference for implanted electrochemical sensors in normal and diabetic dogs," *Diabetologia,* vol. 30, no. 12, pp. 940-945, 1987.

[138] J. Kost, T. A. Horbett, B. D. Ratner, and M. Singh, "Glucose-sensitive membranes containing glucose oxidase: Activity, swelling, and permeability studies," *Journal of Biomedical Materials Research,* vol. 19, no. 9, pp. 1117-1133, 1985.

[139] Q. Liu, A. M. Rauth, and X. Y. Wu, "Immobilization and bioactivity of glucose oxidase in hydrogel microspheres formulated by an emulsification–internal gelation–adsorption–polyelectrolyte coating method," *International Journal of Pharmaceutics,* vol. 339, no. 1–2, pp. 148-156, 2007.

[140] M. Burow and N. Minoura, "Molecular Imprinting: Synthesis of Polymer Particles with Antibody-like Binding Characteristics for Glucose Oxidase," *Biochemical and Biophysical Research Communications,* vol. 227, no. 2, pp. 419-422, 1996.

[141] E. Fernández, D. López, E. López-Cabarcos, and C. Mijangos, "Viscoelastic and swelling properties of glucose oxidase loaded polyacrylamide hydrogels and the evaluation of their properties as glucose sensors," *Polymer,* vol. 46, no. 7, pp. 2211-2217, 2005.

[142] M. A. Lange and J. Q. Chambers, "Amperometric determination of glucose with a ferrocene-mediated glucose oxidase/polyacrylamide gel electrode," *Analytica Chimica Acta*, vol. 175, pp. 89-97, 1985.

[143] J. P. Montheard, M. Chatzopoulos, and D. Chappard, "2-Hydroxyethyl Methacrylate (HEMA): Chemical Properties and Applications in Biomedical Fields," *Journal of Macromolecular Science, Part C*, vol. 32, no. 1, pp. 1-34, 1992.

[144] J. R. Retama, B. Lopez-Ruiz, and E. Lopez-Cabarcos, "Microstructural modifications induced by the entrapped glucose oxidase in cross-linked polyacrylamide microgels used as glucose sensors," *Biomaterials*, vol. 24, no. 17, pp. 2965-2973, 2003.

[145] S. Sershen and J. West, "Implantable, polymeric systems for modulated drug delivery," *Advanced Drug Delivery Reviews*, vol. 54, no. 9, pp. 1225-1235, 2002.

[146] P. D. Weston and S. Avrameas, "Proteins coupled to polyacrylamide beads using glutaraldehyde," *Biochemical and Biophysical Research Communications*, vol. 45, no. 6, pp. 1574-1580, 1971.

[147] L. B. Wingard, C. C. Liu, and N. L. Nagda, "Electrochemical measurements with glucose oxidase immobilized in polyacrylamide gel: Constant current voltametry," *Biotechnology and Bioengineering*, vol. 13, no. 5, pp. 629-639, 1971.

[148] Z. Zhao, H. Xie, S. An, and Y. Jiang, "The Relationship between Oxygen Permeability and Phase Separation Morphology of the Multicomponent Silicone

Hydrogels," *The Journal of Physical Chemistry B,* vol. 118, no. 50, pp. 14640-14647, 2014.

[149] D. W. Ritter, J. M. Newton, J. R. Roberts, and M. J. McShane, "Albuminated Glycoenzymes: Enzyme Stabilization through Orthogonal Attachment of a Single-Layered Protein Shell around a Central Glycoenzyme Core," *Bioconjugate Chemistry,* vol. 27, no. 5, pp. 1285-1292, 2016.

[150] T. E. Finn, A. C. Nunez, M. Sunde, and S. B. Easterbrook-Smith, "Serum albumin prevents protein aggregation and amyloid formation and retains chaperone-like activity in the presence of physiological ligands," *Journal of Biological Chemistry,* vol. 287, no. 25, pp. 21530-21540, 2012.

[151] I. Marini, R. Moschini, A. D. Corso, and U. Mura, "Chaperone-like features of bovine serum albumin: a comparison with α-crystallin," *Cellular and Molecular Life Sciences CMLS,* vol. 62, no. 24, pp. 3092-3099, 2005.

[152] R. Wetzel *et al.*, "Temperature Behaviour of Human Serum Albumin," *European Journal of Biochemistry,* vol. 104, no. 2, pp. 469-478, 1980.

[153] W. N. Ye, D. Combes, and P. Monsan, "Influence of additives on the thermostability of glucose oxidase," *Enzyme and Microbial Technology,* vol. 10, no. 8, pp. 498-502, 1988.

[154] B. M. Bailey, R. Fei, D. Munoz-Pinto, M. S. Hahn, and M. A. Grunlan, "PDMSstar–PEG hydrogels prepared via solvent-induced phase separation (SIPS) and their potential utility as tissue engineering scaffolds," *Acta Biomaterialia,* vol. 8, no. 12, pp. 4324-4333, 2012.

[155] B. M. Bailey, L. N. Nail, and M. A. Grunlan, "Continuous gradient scaffolds for rapid screening of cell–material interactions and interfacial tissue regeneration," *Acta Biomaterialia,* vol. 9, no. 9, pp. 8254-8261, 2013.

[156] P. H. Tse, J. K. Leypoldt, and D. A. Gough, "Determination of the intrinsic kinetic constants of immobilized glucose oxidase and catalase," *Biotechnology and bioengineering,* vol. 29, no. 6, pp. 696-704, 1987.

[157] S. M. Borisov, G. Nuss, W. Haas, R. Saf, M. Schmuck, and I. Klimant, "New NIR-emitting complexes of platinum(II) and palladium(II) with fluorinated benzoporphyrins," *Journal of Photochemistry and Photobiology A: Chemistry,* vol. 201, no. 2, pp. 128-135, 2009.

[158] V. Bühler, *Polyvinylpyrrolidone excipients for pharmaceuticals: povidone, crospovidone and copovidone*. Springer Science & Business Media, 2005.

[159] T. W. Randolph, "Phase separation of excipients during lyophilization: Effects on protein stability," *Journal of Pharmaceutical Sciences,* vol. 86, no. 11, pp. 1198-1203, 1997.

[160] V. I. Teberekidis and M. P. Sigalas, "Theoretical study of hydrogen bond interactions of felodipine with polyvinylpyrrolidone and polyethyleneglycol," *Journal of Molecular Structure: THEOCHEM,* vol. 803, no. 1, pp. 29-38, 2007.

[161] Z. W. Low, P. L. Chee, D. Kai, and X. J. Loh, "The role of hydrogen bonding in alginate/poly(acrylamide-co-dimethylacrylamide) and alginate/poly(ethylene glycol) methyl ether methacrylate-based tough hybrid hydrogels," *RSC Advances,* vol. 5, no. 71, pp. 57678-57685, 2015.

[162] F. Abbasi, H. Mirzadeh, and A.-A. Katbab, "Modification of polysiloxane polymers for biomedical applications: a review," *Polymer International,* vol. 50, no. 12, pp. 1279-1287, 2001.

[163] Y. C. Lai, "Role of bulky polysiloxanylalkyi methacrylates in oxygen-permeable hydrogel materials," *Journal of Applied Polymer Science,* vol. 56, no. 3, pp. 317-324, 1995.

[164] T. M. Madkour, S. K. Mohamed, and A. M. Barakat, "Interplay of the polymer stiffness and the permeability behavior of silane and siloxane polymers," *Polymer,* vol. 43, no. 2, pp. 533-539, 2002.

[165] P. C. Nicolson and J. Vogt, "Soft contact lens polymers: an evolution," *Biomaterials,* vol. 22, no. 24, pp. 3273-3283, 2001.

[166] M. F. Refojo, "Polymers, Dk, and Contact Lenses: Now and in the Future," *Eye & Contact Lens,* vol. 22, no. 1, pp. 38-40, 1996.

[167] F. Lasowski, G. Conant, and H. Sheardown, "Exploring Silicone Hydrogel Material Properties to Deliver Various Ocular Therapeutics," *Investigative Ophthalmology & Visual Science,* vol. 55, no. 13, pp. 6044-6044, 2014.

[168] F. Lasowski and H. Sheardown, "Silicone Hydrogels as Drug Delivery Devices for Various Ocular Therapeutics," *Investigative Ophthalmology & Visual Science,* vol. 56, no. 7, pp. 6072-6072, 2015.

[169] F. Lasowski and H. Sheardown, "Atropine and Roscovitine Release from Model Silicone Hydrogels," *Optometry and Vision Science,* vol. 93, no. 4, pp. 404-411, 2016.

[170] A. Weeks, D. Morrison, J. G. Alauzun, M. A. Brook, L. Jones, and H. Sheardown, "Photocrosslinkable hyaluronic acid as an internal wetting agent in model conventional and silicone hydrogel contact lenses," *Journal of Biomedical Materials Research Part A,* vol. 100A, no. 8, pp. 1972-1982, 2012.

[171] J. N. Demas, B. A. DeGraff, and W. Xu, "Modeling of Luminescence Quenching-Based Sensors: Comparison of Multisite and Nonlinear Gas Solubility Models," *Analytical Chemistry,* vol. 67, no. 8, pp. 1377-1380, 1995.

[172] N. A. Chekina, V. N. Pavlyuchenko, V. F. Danilichev, N. A. Ushakov, S. A. Novikov, and S. S. Ivanchev, "A new polymeric silicone hydrogel for medical applications: synthesis and properties," *Polymers for Advanced Technologies,* vol. 17, no. 11-12, pp. 872-877, 2006.

[173] A. V. Iyer and A. Sahin, "Polymerizable silicone compatibilizers for silicone hydrogels," *Investigative Ophthalmology & Visual Science,* vol. 56, no. 7, pp. 6096-6096, 2015.

[174] T. Matsuda *et al.*, "Yielding Criteria of Double Network Hydrogels," *Macromolecules,* vol. 49, no. 5, pp. 1865-1872, 2016.

[175] E. S. Dragan, "Design and applications of interpenetrating polymer network hydrogels. A review," *Chemical Engineering Journal,* vol. 243, pp. 572-590, 2014.

[176] J. Xu, P. Yang, L. Zhang, and G. Huo, "Radical/Addition polymerization silicone hydrogels with simultaneous interpenetrating hydrophilic/hydrophobic networks," *Journal of Applied Polymer Science,* vol. 132, no. 5, 2015.

[177] J. Wang and X. Li, "Preparation and characterization of interpenetrating polymer network silicone hydrogels with high oxygen permeability," *Journal of Applied Polymer Science,* vol. 116, no. 5, pp. 2749-2757, 2010.

[178] K. Lee, E. A. Silva, and D. J. Mooney, "Growth factor delivery-based tissue engineering: general approaches and a review of recent developments," *Journal of The Royal Society Interface,* vol. 8, no. 55, pp. 153-170, 2011.

[179] L. R. Madden *et al.*, "Proangiogenic scaffolds as functional templates for cardiac tissue engineering," *Proceedings of the National Academy of Sciences,* vol. 107, no. 34, pp. 15211-15216, 2010.

[180] T. J. Long, M. Takeno, C. C. Sprenger, S. R. Plymate, and B. D. Ratner, "Capillary Force Seeding of Sphere-Templated Hydrogels for Tissue-Engineered Prostate Cancer Xenografts," *Tissue Engineering. Part C, Methods,* vol. 19, no. 9, pp. 738-744, 2013.

[181] T. J. Long, C. C. Sprenger, S. R. Plymate, and B. D. Ratner, "Prostate cancer xenografts engineered from 3D precision-porous poly(2-hydroxyethyl methacrylate) hydrogels as models for tumorigenesis and dormancy escape," *Biomaterials,* vol. 35, no. 28, pp. 8164-8174, 2014.

[182] S. I. Somo *et al.*, "Pore interconnectivity influences growth factor-mediated vascularization in sphere-templated hydrogels," *Tissue Engineering Part C: Methods,* vol. 21, no. 8, pp. 773-785, 2015.

[183] R. M. Unruh, J. L. Weaver, and M. J. McShane, "Hydrogel matrix effects on oxygen diffusion: Controlling properties for biosensor applications," in *2015 IEEE SENSORS*, Busan, South Korea, 2015, pp. 1-4: IEEE Xplore, 2015.

[184] S. Loshaek and T. G. Fox, "Cross-linked Polymers. I. Factors Influencing the Efficiency of Cross-linking in Copolymers of Methyl Methacrylate and Glycol Dimethacrylates1," *Journal of the American Chemical Society,* vol. 75, no. 14, pp. 3544-3550, 1953.

[185] C. Esposito Corcione and M. Frigione, "Factors influencing photo curing kinetics of novel UV-cured siloxane-modified acrylic coatings: Oxygen inhibition and composition," *Thermochimica Acta,* vol. 534, pp. 21-27, 2012.

[186] Y. Shi, C. Ma, L. Peng, and G. Yu, "Conductive “Smart” Hybrid Hydrogels with PNIPAM and Nanostructured Conductive Polymers," *Advanced Functional Materials,* vol. 25, no. 8, pp. 1219-1225, 2015.

[187] K. S. Anseth, C. N. Bowman, and L. Brannon-Peppas, "Mechanical properties of hydrogels and their experimental determination," *Biomaterials,* vol. 17, no. 17, pp. 1647-1657, 1996.

[188] J. F. Vincent, *Structural biomaterials,* Third Edition, Princeton University Press, Princeton, NJ, 2012.

[189] K. Haraguchi, R. Farnworth, A. Ohbayashi, and T. Takehisa, "Compositional Effects on Mechanical Properties of Nanocomposite Hydrogels Composed of Poly(N,N-dimethylacrylamide) and Clay," *Macromolecules,* vol. 36, no. 15, pp. 5732-5741, 2003.

[190] N. Wisniewski and M. Reichert, "Methods for reducing biosensor membrane biofouling," *Colloids and Surfaces B: Biointerfaces,* vol. 18, no. 3–4, pp. 197-219, 2000.

[191] H. C. Kolb, M. Finn, and K. B. Sharpless, "Click chemistry: diverse chemical function from a few good reactions," *Angewandte Chemie International Edition,* vol. 40, no. 11, pp. 2004-2021, 2001.

[192] L. M. Campos *et al.*, "Highly Versatile and Robust Materials for Soft Imprint Lithography Based on Thiol-ene Click Chemistry," *Advanced Materials,* vol. 20, no. 19, pp. 3728-3733, 2008.

[193] M. Uygun, M. A. Tasdelen, and Y. Yagci, "Influence of type of initiation on thiol–ene “click” chemistry," *Macromolecular Chemistry and Physics,* vol. 211, no. 1, pp. 103-110, 2010.

[194] L. M. de Espinosa and M. A. Meier, "Plant oils: the perfect renewable resource for polymer science?!," *European Polymer Journal,* vol. 47, no. 5, pp. 837-852, 2011.

[195] M. Firdaus, L. Montero de Espinosa, and M. A. Meier, "Terpene-based renewable monomers and polymers via thiol–ene additions," *Macromolecules,* vol. 44, no. 18, pp. 7253-7262, 2011.

[196] C. Lluch, J. C. Ronda, M. Galià, G. Lligadas, and V. Cádiz, "Rapid Approach to Biobased Telechelics through Two One-Pot Thiol− Ene Click Reactions," *Biomacromolecules,* vol. 11, no. 6, pp. 1646-1653, 2010.

[197] J. A. Carioscia, J. W. Stansbury, and C. N. Bowman, "Evaluation and Control of Thiol-ene/Thiol-epoxy Hybrid Networks," *Polymer,* vol. 48, no. 6, pp. 1526-1532, 2007.

[198] N. B. Cramer *et al.*, "Investigation of thiol-ene and thiol-ene-methacrylate based resins as dental restorative materials," *Dental materials : official publication of the Academy of Dental Materials,* vol. 26, no. 1, pp. 21-28, 2010.

[199] L. Xue, Y. Zhang, Y. Zuo, S. Diao, J. Zhang, and S. Feng, "Preparation and characterization of novel UV-curing silicone rubber via thiol-ene reaction," *Materials Letters,* vol. 106, pp. 425-427, 2013.

[200] H. Lu, J. A. Carioscia, J. W. Stansbury, and C. N. Bowman, "Investigations of step-growth thiol-ene polymerizations for novel dental restoratives," *Dental Materials,* vol. 21, no. 12, pp. 1129-1136, 2005.

[201] J. Fouassier and J. Lalevée, "Photochemical Production of Interpenetrating Polymer Networks; Simultaneous Initiation of Radical and Cationic Polymerization Reactions," *Polymers,* vol. 6, no. 10, p. 2588, 2014.

[202] M. A. Daniele, A. A. Adams, J. Naciri, S. H. North, and F. S. Ligler, "Interpenetrating networks based on gelatin methacrylamide and PEG formed using concurrent thiol click chemistries for hydrogel tissue engineering scaffolds," *Biomaterials,* vol. 35, no. 6, pp. 1845-1856, 2014.

[203] J. J. Wang and F. Liu, "Simultaneous interpenetrating network silicone hydrogels prepared by free radical/cationic hybrid polymerization," *Journal of Applied Polymer Science,* vol. 127, no. 3, pp. 2235-2242, 2013.

[204] J. Xu, L. Zhang, Y. Zhang, T. Li, and G. Huo, "Simultaneous interpenetrating silicone hydrogel based on radical/addition polymerization for extended release of ocular therapeutics," *Journal of Biomaterials Science, Polymer Edition,* vol. 25, no. 2, pp. 121-135, 2014.

[205] K. Eriksson *et al.*, "Application of high-performance chromatographic and electrophoretic methods to the purification and characterization of glucose oxidase and catalase from penicillium chrysogenum," *Journal of Chromatography A,* vol. 397, pp. 239-249, 1987.

[206] A. Biswas, A. T. Nagaraja, and M. J. McShane, "Fabrication of Nanocapsule Carriers from Multilayer-Coated Vaterite Calcium Carbonate Nanoparticles," *ACS Applied Materials & Interfaces,* vol. 6, no. 23, pp. 21193-21201, 2014.

[207] A. Biswas, A. T. Nagaraja, Y.-H. You, J. R. Roberts, and M. J. McShane, "Cross-linked nanofilms for tunable permeability control in a composite microdomain system," *RSC Advances,* vol. 6, no. 75, pp. 71781-71790, 2016.

[208] Y. H. You, A. T. Nagaraja, A. Biswas, J. H. Hwang, G. L. Coté, and M. J. McShane, "SERS-Active Smart Hydrogels With Modular Microdomains: From pH to Glucose Sensing," *IEEE Sensors Journal,* vol. 17, no. 4, pp. 941-950, 2017.

APPENDIX

MATLAB Code for Extracting Time and Lifetime Arrays from *In Vivo* Oxygen Modulation Data Spreadsheets

```
clear all
close all
clc

%load data
file = 'C:\Users\Rachel Unruh\OneDrive\Documents\Lab
Docs\Kiwi\07072016\pHEMA\';
fn = 'Experiment160707105458_07072016_ReaderData_Channel1_WL1';
data = importdata([file '\' fn '.csv'],',',7);
%step response - find response time
time = data.textdata(:,1)';
time = time(:,8:length(time));
time=datenum(time)*24*60*60;
starttime=time(1,1);
for i=1:length(time)
time(i,1)=time(i,1)-starttime;
end
time = time./3600;
l1 = data.data(:,3)';
%i1 = data.data(:,2)'
t=0;

figure()
hold on
plot(time, l1)
xlabel('Time (hrs)')
ylabel('Lifetime (\mus)')

Lifetime_Transposed = l1'
```

MATLAB Code for Baseline and Peak Signal Analysis of *In Vivo* Oxygen Modulation Data

```
clear all
close all
clc

%Creates raw data variable arrays
time = input ('Enter timepont values as a matrix: ');
lifetime = input('Enter lifetime values as a matrix: ');

%makes lifetime vs. time plot
plot(time, lifetime);

%enter how many times you changed the oxygen concentration in vivo
N_peaks = input('Enter concentration number: ');

%enter sequence of oxygen concentrations during oxygen modulation(s)
%conc = input('Enter concentrations: ');

%determines steady-state lifetime value ranges
for i=1:N_peaks
start(i)=input('Enter start time: ');
done(i)=input('Enter end time: ');
index=find(time>=start(i));
index1(i)=index(1);
index=find(time<=done(i));
index2(i)=index(length(index));

h=line([start(i) start(i)],[min(lifetime) max(lifetime)]);
set(h,'Color','g');
h=line([done(i) done(i)],[min(lifetime) max(lifetime)]);
set(h,'Color','r');
x = (time(index1(i))+time(index2(i)))/2;
%text(x, max(lifetime), num2str(conc(i)), 'HorizontalAlignment',
'center', 'VerticalAlignment', 'bottom');
end

%finds average lifetime value for each steady-state interval
j=1;
values = lifetime(index1(1): index2(1));
for i=1:N_peaks
%if(conc(i)==conc(i+1))
%values = [values lifetime(index1(i+1):index2(i+1))];
%else
m(j)=mean(values);
n(j)=length(values);
st(j)=std(values);
e(j)=st(j)/sqrt(n(j));
```

```
confidence(j)=1.96*st(j)/sqrt(n(j));
p(j)=(m(j)-m(1))/m(1)*100;
pst(j) = ((st(j)+m(j))-m(1))/m(1)*100-p(j);
values = lifetime(index1(i+1):index2(i+1));
j=j+1;
%end
end
m(j)=mean(values);
n(j)=length(values);
st(j)=std(values);
e(j)=st(j)/sqrt(n(j));
p(j)=(m(j)-m(1))/m(1)*100;
pst(j) = ((st(j)+m(j))-m(1))/m(1)*100-p(j);
```